Control and Commissioning of a Hot-Gas Bypass Compressor Load Stand for Testing Light-Commercial Compressors Using Low-GWP Refrigerants

By

Jake M Singleton

Bachelor of Science in Mechanical Engineering.
Oklahoma State University
Stillwater, OK
2018

Submitted to the Faculty of the
Graduate College of
Oklahoma State University
in partial fulfillment of
the requirements for
the Degree of
Master of Science
July, 2020

Control and Commissioning of a Hot-Gas Bypass Compressor Load Stand for Testing Light-Commercial Compressors Using Low-GWP Refrigerants

Thesis Approved:

Dr. Craig Bradshaw

Thesis Advisor

Dr. Christian Bach

Dr. Jeffrey Spitler

ACKNOWLEDGMENTS

I feel very blessed to have had so much support throughout the duration of this project. So many people have come to my aid, in many ways, as I have been working on this project. I would like to thank everyone who has been there for me during this period of my life.

First, I would like to thank my parents for supporting me throughout my entire education, and for always being there when I needed them. I would also like to thank my better half and my best friend, Brooke. Without her unwavering love and support, I would not have been able to do any of this.

I would like to thank Dr. Craig Bradshaw for giving me this opportunity. I have learned so much and have gained so much confidence in myself as a professional, and I attribute that to his constant support and guidance. He was always very patient and encouraging when I was struggling or when I made mistakes. I am very grateful to have him as an advisor.

I am incredibly thankful to Gary Thacker for his willingness to help support the operation of the load stand. His help with any electrical work and many other aspects of building and running the load stand is a huge reason I was able to complete my project. I greatly enjoyed working by his side. In doing so, I gained a large amount of incredibly useful knowledge.

All of the students within the BETSRG research group have helped me at some point during this project, and I am very grateful to them, specifically to the undergraduate assistants that helped me: Caleb Bengs, Jeff Huizenga, and Sammy Willhoite.

There are many people who I received support from, with regard to different aspects of the load stand, who I am very grateful to. To Joe Orosz, for his insight on several different problems that I was trying to solve. To Shahebaz Malik and Dennis Harrington who answered so many questions about the screw compressor. And to Eric Parent, who gave me several ideas on how to improve the load stand.

I would also like to thank Seth Yarborough for working alongside me for much of this project. His assistance, mechanical expertise, and calm presence helped me to solve many problems and to finish my project. I would have struggled to complete this project without his help. It was a privilege to work alongside such a good friend.

Finally, I would like to thank Torad and JCI for allowing me to test their compressors and for sponsoring parts of this project. They were incredibly gracious with their time and energy, which allowed me to successfully complete this project.

Acknowledgments reflect the views of the author and are not endorsed by committee members or Oklahoma State University.

Name: Jake M Singleton

Date of Degree: July, 2020

Title of Study: Control and Commissioning of a Hot-Gas Bypass Compressor Load Stand for Testing Light-Commercial Compressors Using Low-GWP Refrigerants

Major Field: Mechanical and Aerospace Engineering

Abstract: As a result of changing efficiency standards for HVAC&R equipment, hydrofluorocarbon refrigerants such as R134a and R410A are in the process of being phased out because of their high Global Warming Potential (GWP). Many low-GWP refrigerants, such as R1234yf, R1234ze(E), R1234ze(D), R32, and several blends of these, are being considered as replacements. This creates a need for design changes to compressors. Recent work by Schmidt et al. (2019) presented a hot-gas bypass compressor load stand constructed at Oklahoma State University to facilitate testing of compressors deployed with these refrigerants ranging in capacity from 10-80 tons.

This work extends the previous by developing a comprehensive controls package to maintain stability and control over the wide range of capacities and operating conditions. This controls package, implemented in LabVIEW^{TM} (Elliott et al., 2007), allows independent control over the compressor suction pressure and temperature and discharge pressure, simultaneously, using Proportional-Integral (PI) controllers. The controllers were tuned to maintain a set point as well as minimize the random uncertainty of the measurements.

A series of control validation tests were performed, using a 40 ton scroll compressor, to validate the control scheme, and to evaluate the resulting quality of primary measurements. The initial results suggested that the load stand was able to minimize the contribution of the random uncertainty to the total over the duration of the test. Upon further investigation, it was found that the time required for testing could be reduced by three times, with the optimization of the control strategy.

A 30 ton spool compressor and a 75 ton screw compressor were used perform commissioning tests on the load stand. The results of the commissioning tests showed that the load stand is capable of collecting valid test data, in accordance with the compressor testing standards set by ASHRAE-23.1 (2010). A comparative analysis of the data to data provided by the manufacturers of each of these compressors suggested that the load stand is capable of measuring accurate performance data. The results suggest that the load stand is considered a fully commissioned compressor testing facility.

TABLE OF CONTENTS

Chapter Page

LIST OF TABLES

LIST OF FIGURES

Figure Page

ABBREVIATIONS

GWP	Gloabal Warming Potential
PID	Proportional Integral Derivative
PI	Proportional Integral
PV	Process Variable
VI	Virtual Instrument

NOMENCLATURE

VARIABLES	UNITS	DESCRIPTION
$s_{\bar{x}}$	-	Random Uncertainty of Sample
s_x	-	Sample Standard Deviation
N	-	Sample Length
x_j	-	Measurement value
$\bar{x}$	-	Sample mean
$b_{\bar{x}}$	-	Systematic Uncertainty
$u_{\bar{x}}$	-	Total Uncertainty
$P_{suc,range}$	kPa	Range of pressures within specified threshold
$P_{suc,setpoint}$	kPa	Suction pressure set point
$P_{suc,threshold}$	kPa	Suction pressure threshold
$\dot{Q}$	watt	Heat transfer rate
$\dot{m}_w$	kg/s	Mass flow rate of water
c_p	J kg K	Specific heat
$T_{w,exit}$	°C	Exiting water temperature
$T_{w,in}$	°C	Inlet water temperature
u	-	Control Process variable
e	-	Control set point error
K_p	-	Proportional gain
K_i	-	Integral gain
K_d	-	Derivative gain
T_i	min	Integral time constant

$K_{p,u}$	-	Critical proportional gain
T_u	min	Critical integral time constant

CHAPTER 1

Introduction

In support of a global effort to reduce the environmental impact of HVAC&R equipment, lowering the global warning potential (GWP) of refrigerants was introduced in the Kigali Amendment of the Montreal Protocol, which requires countries to reduce the use of HFCs by 85 percent between 2019 and 2036. As a result, Schmidt et al. (2019) developed a hot-gas bypass compressor load stand for the purpose of testing the effect of low-GWP refrigerants on compressor performance, for which the controls and commissioning is being addressed in this project. The objective is to develop a control strategy to quickly collect compressor performance data and to use this to compare the results to the already verified performance data of two different compressors. These tests would validate the load stand at two different nominal capacities, thus verifying the operating envelope that the load stand was designed for.

1.1 Literature Review

1.1.1 Compressor Testing

Compressor testing procedures have been outlined in two standards, ASHRAE-23.1 (2010) and ASHRAE-23.2 (2014), for subcritical and transcritical cycles, respectively. These standards outline the required measurement uncertainties, as well as the required measurement results that are to be recorded. The standards also define what is required for a condition to be determined steady state so that performance data may be collected. They also define the two main types of compressor testing, the flow meter type and the calorimeter type. These two compressor testing methods

primarily differ in the way that they determine mass flow rate. The flowmeter type uses direct measurements of refrigerant mass flow rate while the calorimeter type uses heat balances on one of the heat exchangers to determine the flow rate.

The calorimeter type of compressor test stand is commonly used in the HVAC&R industry. Moesch et al. (2016) used a modified calorimeter to test performance characteristics of a scroll compressor with economized vapor injection. Salts et al. (2019) tested the performance of a scroll and a dual rotary compressor, using a calorimeter load stand and found comparable results to performance tests done on a heat pump system.

The flow meter type of compressor load stand is also a quite common compressor testing method. The hot-gas bypass load stand falls into this category, which was introduced by McGovern (1984) as a potentially advantageous system because its design requires that an excess of liquid always be present in the system, meaning that amount of charge in the system does not need to be changed with changing conditions. McGovern (1984) also discusses that, because of its design, there is a small amount of thermal inertia within the condenser, which allows for fast response to changing operating conditions.

Since its introduction, the hot-gas bypass compressor load stand has been a popular method for testing compressors. Hubacher et al. (2002) developed a hot-gas bypass stand for the purposes of measuring the performance of CO_2 compressors, Bradshaw et al. (2011) used this type of test stand to validate a model of a miniature-scale linear compressor, and Orosz et al. (2014) used a hot-gas bypass stand to determine performance characteristics of a novel spool compressor. Its advantages make it a desirable method for testing compressors.

1.1.2 Control

The control of compressor test stands and thermal systems, in general, have been widely researched to find ways to more efficiently operate and to more quickly reach steady state. Sathe et al. (2008) explain how the hot-gas bypass stand moves between test conditions faster than a calorimeter, because it directly controls the three operating conditions (suction pressure, discharge pressure, and suction superheat). Another difference they observed is that hot-gas bypass stands require much less condenser cooling capacity than calorimeters because a majority of the discharge gas is bypassed, so the amount of refrigerant flowing through the condenser is lower.

Marriott (1973) also explains that typical calorimeters have slow response times and are not effective at stabilizing quickly, making them less efficient at collecting numerous data points. Marriott et al. (1974) then built a hot-gas bypass style load stand to take advantage of its low thermal inertia to accelerate the compressor testing process. A three stage approach to starting the compressor and reaching a steady state condition, using automatic controls, was defined. The results of this approach showed that a steady state condition could be reached within 17 minutes of start-up.

Proportional Integral Derivative (PID) control, and many of its forms are widely used for the control of vapor compression cycles. Marcinichen et al. (2008) describe that PI control is often optimal, because of its simplicity, ability to have zero offset, and its disturbance rejection. They developed a dual single input single output (SISO) controller to control the suction superheat and the capacity by simultaneously modulating an electronic expansion valve and the speed of the compressor, respectively. They found that the PI controllers worked optimally, with a low settling time and a good ability reject disturbances. They were also able to optimize the system performance with this type of controller.

Salazar and Méndez (2014) also used PID control on a vapor compression cycle. For a transcritical CO_2 cycle, they were able to compare the conventional PID control,

a linear controller, to a nonlinear PID controller. They found that, when implemented correctly, a nonlinear PID controller can lead to lower amounts of overshoot and faster settling times, leading to a shorter amount of time it takes to reach steady state.

Many other control theories exist and have been implemented in different thermal systems. For example, Singh et al. (2000) developed an adaptive controls scheme based on Linear Quadratic Regulator theory. Another such example is Flesch and Normey-Rico (2010), who implemented a dead-time compensator controller on a calorimeter load stand.

1.1.3 Commissioning

To determine if a compressor test stand produces reliable performance data, it must go through a commissioning process. During that process, the load stand must produce results in accordance with each of the guidelines set by ASHRAE-23.1 (2010). However, to extend this, it is a common practice to test equipment which has existing performance data. This gives further confirmation that the results are valid. Wenzel et al. (2016) provides an example of a comparative analysis to catalog data as a way of validating the design of a refrigeration test facility. AHRI-Standard-540-2015 (2015) also gives guidance on how to validate performance data. The standard gives a method for verifying published ratings of compressors using data from a single compressor. It gives acceptable amounts for minimum mass flow rate, minimum capacity, and maximum power input. If the performance data has already been verified by a manufacturer, the same criteria can be used to verify the performance data collected on a new test facility.

The literature gives a clear definition of how to adequately test compressor performance. It also gives several examples of different methods of compressor testing and the advantages and disadvantages that go along with each method. Ultimately, the advantages of testing time and ease of control were the deciding factors for the

development of a hot-gas bypass compressor load stand. The literature also provides several examples of control strategies that can be used for compressor test stands and for thermal systems, in general. Because of its simplicity and ease of implementation, standard PID control was used as the main control strategy for this load stand. The literature does, however, lack information about the commissioning of compressor testing facilities. This project will address that issue, and will give a clear definition of how the performance data collected from the load stand was validated and how it was commissioned as a reliable compressor testing facility.

1.2 OSU Load Stand

The design of the compressor load stand was presented by Schmidt et al. (2019) and operates on the principle of a hot-gas bypass cycle. The hot-gas bypass cycle operates similarly to a normal vapor compression cycle, except at the exit of the compressor, refrigerant vapor is separated into two flow paths. The majority of the refrigerant vapor is part of the bypass line that will be used to heat the remaining amount of refrigerant to a specified compressor inlet temperature, after the smaller portion passes through the condenser and is expanded to suction pressure in the liquid expansion valve.

There are a minimum of three parameters that are required to be manipulated during compressor testing to gather performance data over the full range of the compressor's operating capabilities. These include, a simulated evaporating temperature, the condensing temperature, and the suction temperature (*i.e.* the suction superheat of the compressor).

The simulated evaporating temperature is the saturation temperature at the suction pressure, which represents the pressure a compressor would be exposed to at a particular evaporating temperature. Control of the simulated evaporating temperature is achieved through manipulation of the suction pressure (P01). This is

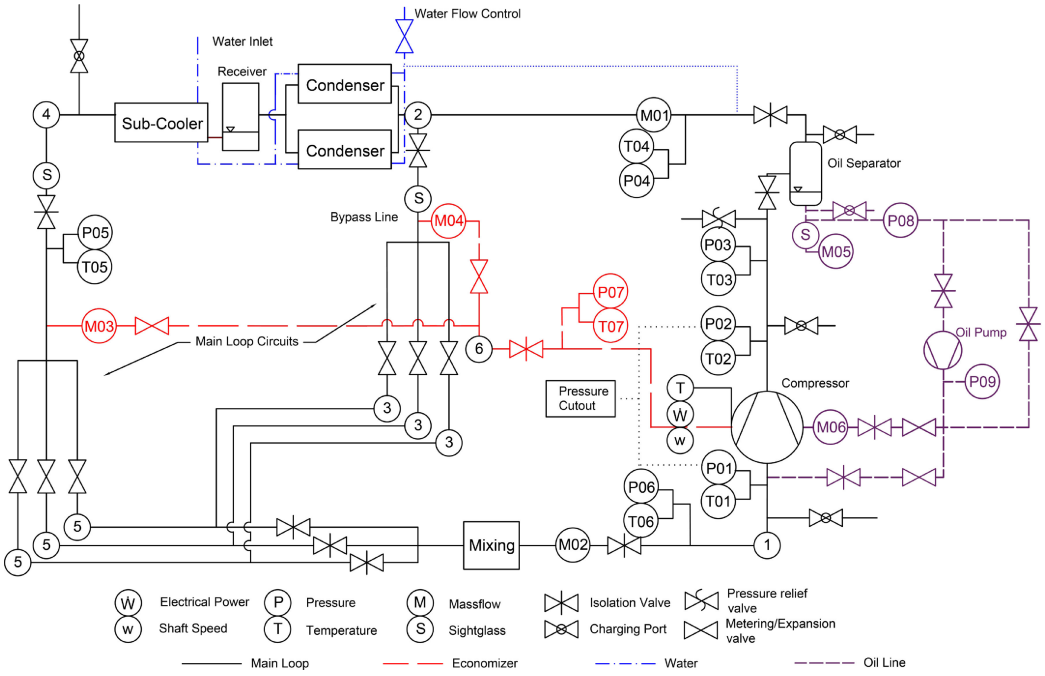

Figure 1.1: Load Stand Schematic (Schmidt et al., 2019)

accomplished by adjusting the expansion valves on the gas bypass line. Figure 1.1 shows a schematic of the load stand and all of its control mechanisms, the gas bypass valves operating between state 2 and 3. These valves directly control P01.

The condensing temperature is the saturation temperature at the discharge pressure of the compressor, which is controlled to set the desired condensing temperature. The compressor discharge pressure is manipulated through the control of the cooling water provided to the condensers shown in Figure 1.1. The flowrate of water going through the condensers will cause a change in the discharge pressure (P02) of the refrigerant.

Finally, the amount of superheat desired will affect the suction temperature of the compressor. The suction temperature can be controlled by three liquid expansion valves, which operate between state 4 and 5, where T01 is the suction temperature being measured.

The desired operating ability of the load stand, as presented in Schmidt et al. (2019), is to be able to move rapidly between operating conditions, so that a matrix

of conditions can be tested quickly, with little down time between test points. This operating ability should be achieved across a range of compressor capacities from 10-80 tons and a system pressure up to 4500 kPa. However, in order to achieve that ability, a controls scheme had to be developed that would allow for automatic movement between points and stabilization, to greatly reduce the amount of time required for each test.

Additionally, the load stand must also produce reliable and accurate results. To accommodate this, the controls scheme was also designed to reduce the amount of random uncertainty of the measurements enough, such that systematic uncertainty is effectively the only source of uncertainty affecting the results.

The load stand and the controls algorithms are implemented and a control validation test was performed to verify that the load stand controls program reaches operating conditions with a total uncertainty that approaches the systematic (sensor) uncertainty, effectively eliminating the random measurement uncertainty. This level of uncertainty is well below what is required in ASHRAE-23.1 (2010), which is a defining feature of this test environment. The total uncertainty ($u_{\bar{x}}$) is outlined in ASME PTC 19.1 (Abernethy et al., 1985) and is calculated in Equation 1.1 as the root-sum-square of the random uncertainty ($s_{\bar{x}}$) and the systematic uncertainty ($b_{\bar{x}}$), which is defined as the uncertainty associated with the measurement devices.

$$u_{\bar{x}} = \sqrt{(b_{\bar{x}})^2 + (s_{\bar{x}})^2} \tag{1.1}$$

1.3 Project Overview

The objective of this project was to first develop a control strategy using LabVIEW^{TM} (Elliott et al., 2007) so that compressors could be tested at different operating conditions, quickly and accurately. After this, the load stand was to be commissioned with two different compressors. A 30 ton spool compressor and a 75 ton screw compres-

sor. This would provide evidence that the load stand is a reliable compressor testing facility, ranging from the middle of its designed capacity range to its upper limit.

The first commissioning activity of the load stand was to develop and test the control strategy. Before being used to test compressors, the load stand must be able to reliably reach steady state. To test the control strategy, a 40 ton scroll compressor was tested. During this testing, improvements were made to the control strategy, to more easily reach steady state. Once these improvements were made, commissioning tests could be performed on the load stand.

The first commissioning test was performed on a 30 ton spool compressor, which served to show the ability of the load stand to collect reliable data at a capacity in the middle of its designed range. During these tests, some modifications and improvements were made to the stand so that the load stand could collect more accurate data. After these modifications, the final tests of this commissioning procedure were performed.

After commissioning at 30 tons, the load stand was commissioned with a 75 ton screw compressor, to show the load stand's ability to collect reliable data at the upper end of its designed capacity range. During this time, the load stand was, again, modified to overcome some inefficiencies that were observed during the 30 ton commissioning, and to obtain more accurate results. After this, the load stand was tested across a range of operating conditions to be commissioned at 75 tons.

CHAPTER 2

Preliminary Load Stand Control Scheme

The load stand is equipped with a comprehensive data collection and controls scheme, shown in Figure 2.1, that uses a variety of sensors to measure the desired variables. These sensors record data for the sake of characterizing compressor performance as well as to be process variables in the control scheme.

The load stand uses gauge pressure transducers as well as T-type thermocouples and RTDs for measurements of pressures and temperatures. It also uses Coriolis mass flow meters for high-accuracy mass flow measurements on the suction, discharge, economizer gas and liquid lines, and the oil line. An accelerometer measures the frequency response of the compressor motor to infer rotational speed. Finally, a watt transducer is used to measure the power used by the compressor during a test. To improve the accuracy of the temperature and pressure measurements, the thermocouples, RTDs, and pressure transducers have been calibrated using high accuracy calibration equipment. The temperature devices are calibrated in an IsoTemp calibration bath, where the measured temperatures are compared to a high accuracy reference thermometer, a ThermoProbe TL1-A. The pressure devices are calibrated using a Druck DPI 612 pressure calibrator. The specific models of instruments and their systematic uncertainty have been previously reported by Schmidt et al. (2019), who also conducted an uncertainty analysis to quantify the systematic uncertainty propagated to the calculation of both the isentropic and volumetric efficiencies. Schmidt et al. (2019) concluded that the systematic uncertainty propagated to these metrics is acceptable for testing, but assumes a negligible contribution of random uncertainty.

The three load stand control variables previously discussed (suction temperature and pressure, discharge pressure) are controlled using a Proportional-Integral (PI) controller for each control variable using feedback from the on-board instruments. The control scheme is executed by code developed in LabVIEW™ (Elliott et al., 2007), where measurements are taken from the load stand and the PI controller loops create changes to control variable set points by user input. In order to accurately determine performance metrics, the load stand must be operating at steady-state, meaning there is no significant change of any of the control variables over the length of the testing period. According to ASHRAE-23.2 (2014), steady-state operation requires that the data points collected must not be successively increasing or decreasing and must be within the specified tolerances of ±1% on the suction and discharge pressure and ±1 °C (2 °F) on the suction temperature, when testing at supercritical pressures. Additionally, ASHRAE-23.1 (2010) specifies the same required tolerances for testing compressors, when testing at subcritical pressures. The target tolerance for this load stand is within the range of uncertainty of the measurement devices (*i.e.* systematic uncertainty). The systematic uncertainty of the load stand equates to ±0.689 kPa (0.1 psia) on the suction pressure, ±0.11 K (0.2°R) on the suction temperature, and ±2.59 kPa (0.375 psia) on discharge pressure. To achieve this, the random uncertainty must be minimized for the testing period. Using PI controllers, the system is able to reach steady-state, with minimal amounts of random uncertainty for a wide range of operating conditions.

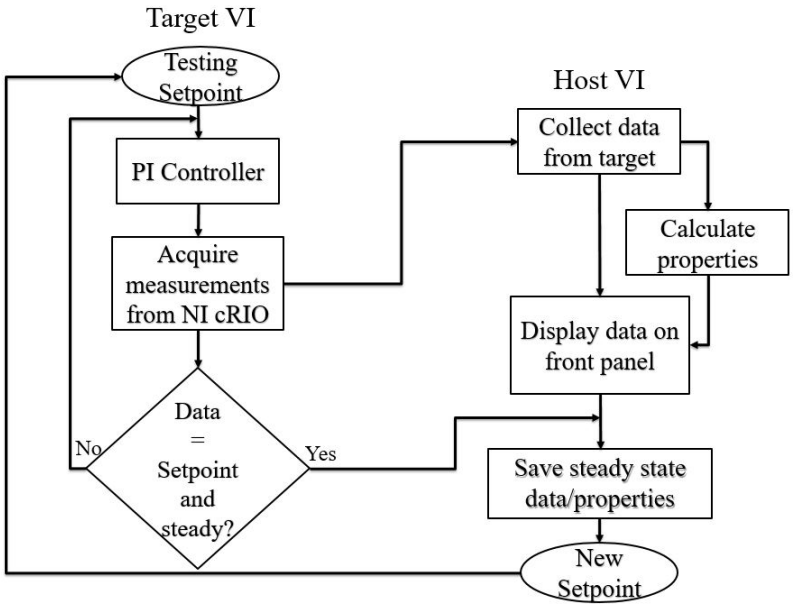

Figure 2.1: Flow chart of data acquisition and controls.

2.1 Suction Pressure Control Mechanism

The suction pressure is controlled by three gas expansion valves. The large range of desired operational capacities (10-80 tons) necessitates three parallel expansion valves that can be used to make large, medium, and small adjustments. During operation, only one valve is controlled at a time, and the decision of what valve to use is decided by a threshold logic that utilizes the nominal capacity of the compressor and how far away the measured suction pressure is from the set point. If the nominal capacity is above or below the set threshold (40 tons), the smallest and largest valves, respectively, can be eliminated from use. Then, to determine which of the remaining two valves to use, measured suction pressure plus a range dictated by a threshold value of 34.5 kPa (5 psia) is calculated as,

$$P_{suc,range} = P_{suc,setpoint} \pm P_{suc,threshold}. \tag{2.1}$$

If the suction pressure is outside of the range given by $P_{suc,range}$ then the larger valve is used, and the smaller valve if less than the range. Each of these valves has its

own PI controller, with independent gains, which adjusts the suction pressure toward the set point.

2.2 Suction Temperature Control Mechanism

Similar to the suction pressure, the suction temperature is controlled using three liquid expansion valves on the liquid line that exits the condenser. Adjusting the amount of liquid that mixes with the bypassed discharge gas will have the greatest effect on the suction temperature (*i.e.* superheat), therefore, the liquid expansion valves were selected to control this process variable. Because there are three liquid lines to control the capacity of the compressor load stand, the selection process for which expansion valve to use is the same thresholding procedure as the suction pressure with a threshold of 2 °C (3.6 °F).

2.3 Discharge Pressure Control Mechanism

The discharge pressure is controlled by adjusting the flow of water through the condensers. The PI controller adjusts the flow rate of water to meet the desired condition by adjusting two devices: a bypass valve and the rotational speed of a pump. A schematic of this setup is shown in Figure 3. The condensers of the load stand are connected to an intermediate cooling water supply line, which then interact with two intermediate heat exchangers that are subsequently connected to the building chilled water supply. The amount of heat transfer within the condensers is dependent on the mass flow rate of water, seen in Equation 2.2.

$$\dot{Q} = \dot{m}_w c_p (T_{w,exit} - T_{w,in}). \tag{2.2}$$

This expression suggests, as more water is bypassed, less heat will be transferred from the load stand to the cooling water, thus increasing the condensing temperature

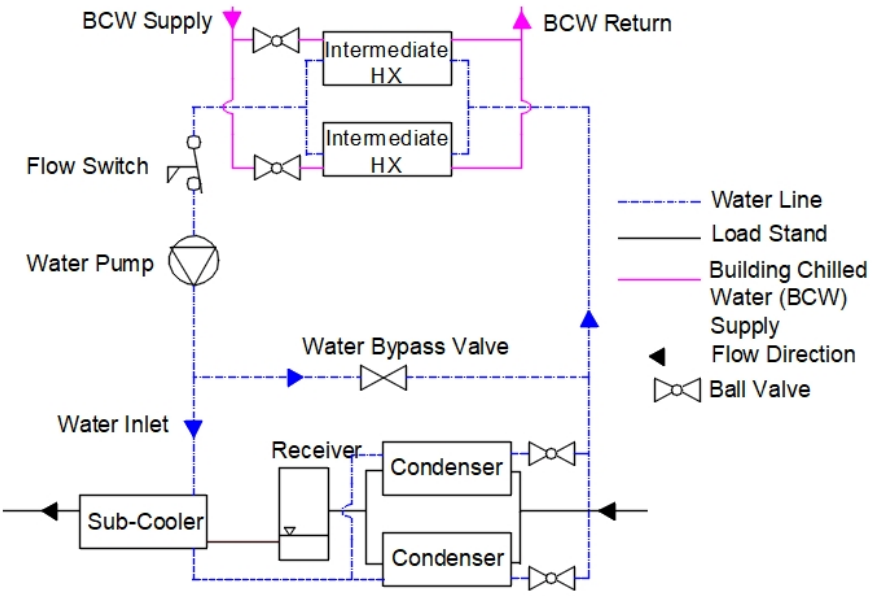

Figure 2.2: Schematic of cooling water loop

of the load stand, which in turn increases the discharge pressure.

The bypass valve acts as the coarse adjustment of the flow rate and the pump speed is used to fine-tune the water flow. The bypass valve position is adjusted from fully closed to fully open. The pump acts as fine adjustment because changes in the rotational speed of the pump tend to create smaller changes in the system than the bypass valve. By increasing the rotational speed of the pump, the flow rate of water will increase, which will cause an increased amount of heat transferred from the refrigerant to the cooling water in the condensers. Therefore, the pump speed is inversely proportional to the condensing temperature.

The purpose of having two intermediate heat exchangers and two condensers is to be able to control within the range of capacities. By using only one of the condensers or intermediate heat exchangers, the size of compressor that can be supported by the load stand is reduced, which is beneficial for testing smaller compressors that have a lower capacity rating.

The process for selecting which of these devices, the water pump or bypass valve, to use is similar to that of the expansion valves. A threshold is set at 34.47 kPa (5 psia), which defines when the controller switches from coarse to fine control. Then, by setting correct proportional and integral gains, all of the controllers move their respective devices to bring the system to a desired set point.

2.4 PI Controller Tuning

To adequately control the three parameters of the load stand automatically, the controllers are tuned with appropriate gains so that the control variable, $u(t)$, in Equation 2.3 would converge to the desired set point by minimizing the error, $e(t)$, the difference between the set point and the current value of the process variable.

$$u(t) = K_p e(t) + K_i \int_0^t e(t')dt' + K_d \frac{de(t)}{dt} \tag{2.3}$$

The controllers do not use the derivative gain, K_d because, if not very precisely tuned, the derivative gain can cause large amounts of instability. To avoid this, the controllers only use proportion and integral gains, K_p and T_i respectively, where

$$K_i = \frac{K_p}{T_i}. \tag{2.4}$$

Proportional and integral gains were found using the tuning method described by Ziegler and Nichols (1985). During this method the controllers started with initial values of $K_p = 0$ and $T_i = \infty$, while the system was stabilized at some arbitrary point. Then the value of the controller was increased by 10 percent and the proportional gain, K_p was changed until the critical gain, $K_{p,u}$, was reached, where sustained oscillations were observed. The period of oscillation at this point, T_u, was found for each of the controllers separately. The method for finding these values can be better visualized in Figure 2.3. After finding these values, Ziegler and Nichols (1985) determined that

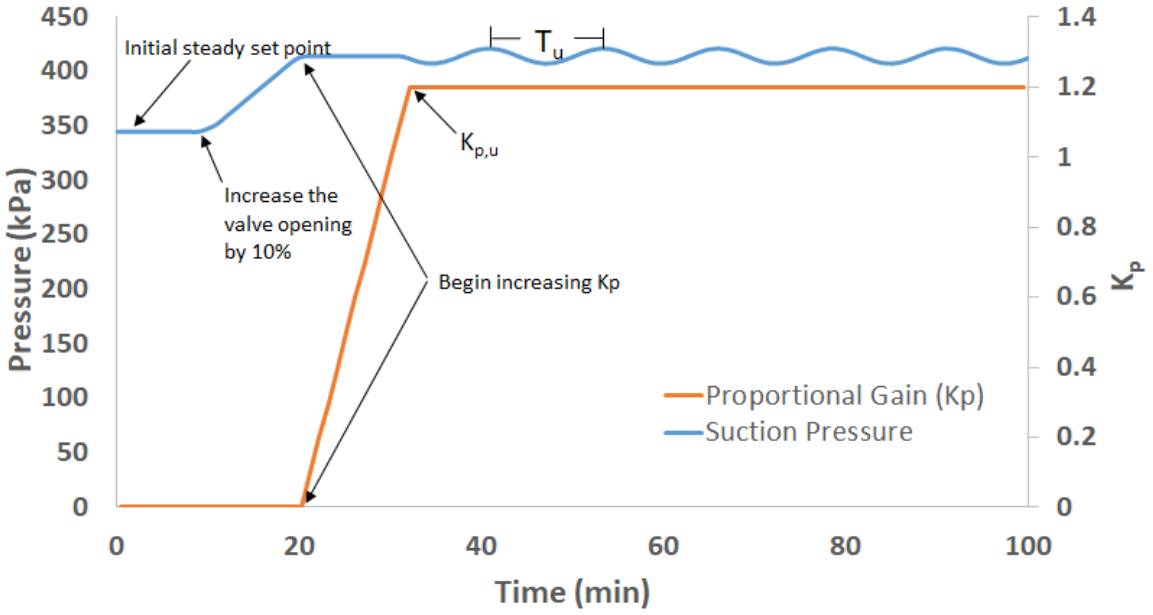

Figure 2.3: Example of finding the critical proportional and integral gains.

the optimum values for the proportional and integral gains, respectively, are

$$K_p = 0.45K_{p,u} \tag{2.5}$$

and

$$T_i = \frac{1.2}{T_u}. \tag{2.6}$$

The results of the tuning process can be seen in Table 2.1, where the proportional and integral gains for each controller are listed. It should be noted that the compressor used for initial commissioning tests was a lower capacity compressor, thus the large gas and liquid valves were not used.

Table 2.1: List of values for K_p and T_i

	K_p	T_i (min)
Medium Gas Valve	0.542	2.03
Small Gas Valve	0.173	0.636
Medium Liquid Valve	-0.22	2.9
Small Liquid Valve	-0.0413	12.063
Water Bypass Valve	0.081	6.75
Water Pump	-0.161	1.936

CHAPTER 3

Initial Control Testing

To test the efficacy of the control strategy a series of preliminary tests were performed using a Bitzer GSD80485VAB4-1 40-ton scroll compressor as a way to verify that all of the equipment works properly and that steady-state conditions can be reached using the controllers, within a reasonable degree of accuracy. According to ASHRAE-23.1 (2010), the suction and discharge pressures must be maintained within ±1% of the absolute pressure that is specified and the suction temperature must be maintained within ±1 K (±2 °R) of its specified value. This is the maximum error that can be allowed for each set point when testing. However, the instrumentation selected for the load stand is capable of significantly better systematic uncertainty than this requirement (±0.05% of full-scale for pressures and ±0.11 K for the suction temperature). Thus, to meet standard 23.1 requirements the controllers need to only reduce the random uncertainty such that it does not add significantly to the instrumentation systematic uncertainty. Using the methods described in ASME PTC 19.1 (Abernethy et al., 1985) the random uncertainty ($s_{\bar{x}}$) for each operating condition was calculated using Equation 3.1.

$$s_{\bar{x}} = \frac{s_x}{\sqrt{N}} \tag{3.1}$$

where s_x is the sample standard deviation over the sample length, N (1000 points), given by Equation 3.2, in which x_j is the measurement value and $\bar{x}$ is the sample

mean.

$$s_x = \sqrt{\sum_{j=1}^{N} \frac{(x_j - \bar{x})^2}{N-1}} \tag{3.2}$$

After the effectiveness of the control strategy was established, preliminary commissioning tests were performed on a 30-ton spool compressor to determine the reliability and accuracy of the performance results gathered from the load stand. These preliminary commissioning tests demonstrated the capability of the load stand at, roughly, a mid-range capacity of the load stand and were able to point out some issues that needed to be addressed before the final commissioning tests.

3.1 Control Strategies for Resolving Instability

Because the control variables for the compressor load stand are connected, it is challenging to control each variable independently because a change in one variable causes changes in the others as well. Throughout the preliminary testing process a couple of issues were experienced that provided unsatisfactory results. The first is the coupling between suction temperature and pressure and the second is the control over cooling water flow. Mechanisms to address these challenges are presented after which it was possible to collect steady-state data with an acceptable set point error and minimized random uncertainty.

3.1.1 Coupling of suction temperature and pressure.

One of the difficulties in maintaining steady data throughout the duration of the test was the connection between suction temperature and pressure. As the liquid line valves are adjusted to change the suction temperature, a significant change in the suction pressure can be observed as well. As a result, rapid changes in the temperature cause the pressure to change rapidly, to which the suction pressure controller responds, creating a cycle of one controller responding to the other. This creates periodic instability, where the values start near the set point but diverge as the controllers

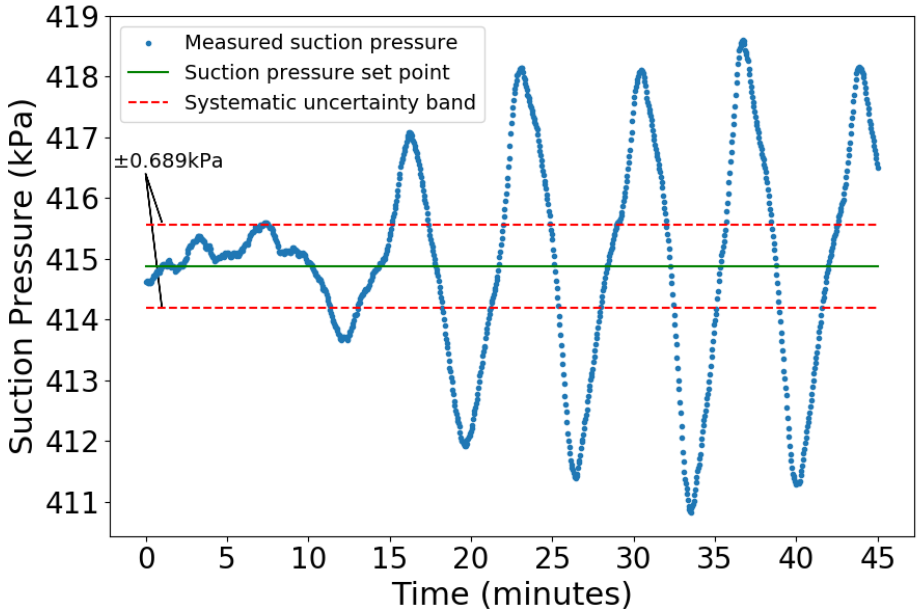

Figure 3.1: Instability in suction pressure caused by controller over-correction

fight each other. This is visualized in Figure 3.1 which shows the suction pressure response at a desired set point of 10 °C (50 °F) evaporating temperature, 32.2 °C (90 °F) condensing temperature, and 11.1 K (20 °R) superheat. At roughly 10 minutes into the test the controller instability is observed and the data quickly extends beyond the systematic uncertainty bands that are the objective to control within.

This behavior resulted in an aborted test and a post-test evaluation that led to corrective action. To correct this instability, the PI gains for the suction temperature controller were lowered below that of the suction pressure by roughly an order of magnitude. The objective of this change is to control the temperature very gradually so that the pressure response is not large enough to cause over-correcting by its controller. The resulting adjustments to the PI gains resulted in the data presented in Figure 3.2.

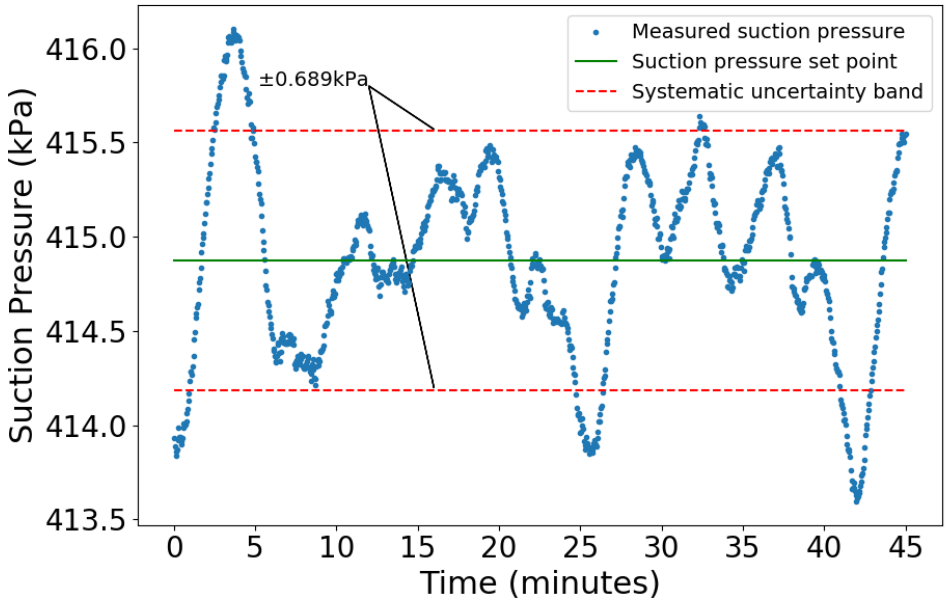

Figure 3.2: Suction Pressure at 414.9 kPa with corrected PI gains

3.1.2 Sensitivity of discharge pressure to cooling water temperature.

Another element of instability in the load stand during the preliminary test phase was the sensitivity of the discharge pressure to changes in the cooling water temperature. Initial tests recorded a large difference in the condenser water inlet and exit temperature. The test shown in Figure 3.3 had an average entering water temperature of 13.5 °C (56.3°F) and an exiting water temperature of 28.17 °C (82.7°F). Referencing Equation 2.2, it is observed that a large temperature difference will result in higher heat transfer per unit mass flow rate of water. Because of this, small changes in the flow rate of water will have a large effect on the heat transfer rate. This causes large, rapid changes in the discharge pressure, which the controllers respond to, creating larger changes. As a result, the system never completely stabilizes. As Figure 3.3 shows, the system had an undesirable, large oscillatory behavior because of this large temperature difference of water across the condenser. The steady-state set point error was negligible and the random uncertainty was 0.067 kPa (0.0097 psia).

To resolve this issue, the flow rate of chilled water from the building through

the intermediate heat exchangers in Figure 2.2 needed to be reduced significantly, to increase the temperature of water entering the condensers. One of the intermediate heat exchangers was shut off entirely from the building chilled water supply and the other had its chilled water supply choked by partially closing the shutoff valve. With the flow rate of chilled water decreased, the amount of heat dissipated from the load stand's water supply decreased, which increased the water temperature at the inlet of the condensers to 23.89 °C (75 °F) and changed the temperature at the exit of the condensers to 27.7 °C (81.9 °F). Doing this led to increased stability of the discharge pressure, which yielded better steady state results as shown in Figure 3.4. By using only one of the intermediate heat exchangers, the capacity of the condenser is decreased, which is advantageous when using smaller capacity compressors. If the cooling load of the condensers to the load stand is too high, changes in the mass flow rate of water can significantly affect the changes in the discharge pressure. Therefore, it is most effective to have a condenser capacity that is not over-sized for the compressor. Another issue that was observed was, the temperature of the building chilled water could change unexpectedly, which cannot be controlled. This would have an effect on the intermediate water loop, causing unexpected changes. Another objective of this controls scheme is to be able to respond to these changes quickly enough to maintain stability. Having a smaller cooling load in the intermediate heat exchangers helps to mitigate this issue.

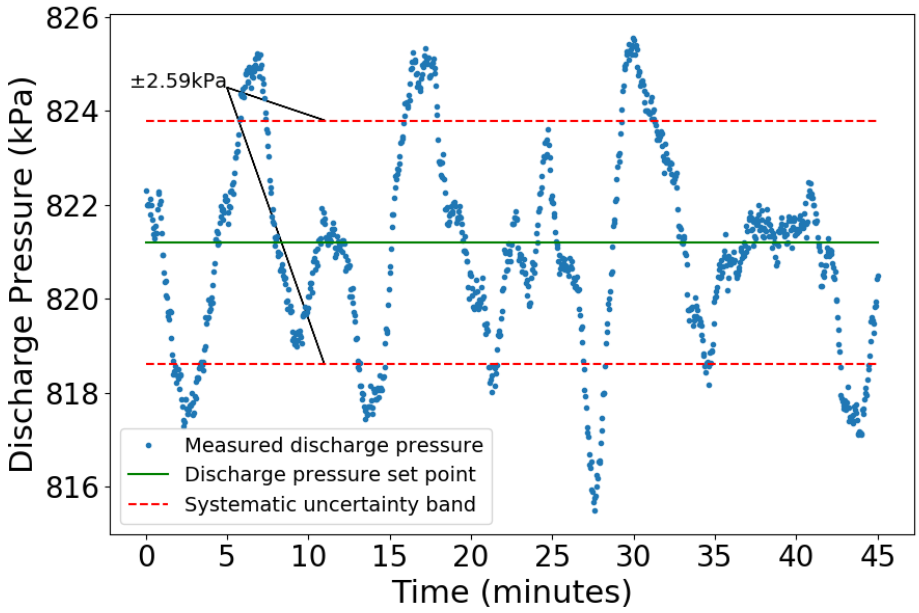

Figure 3.3: Discharge pressure of a system with a large condenser water temperature difference.

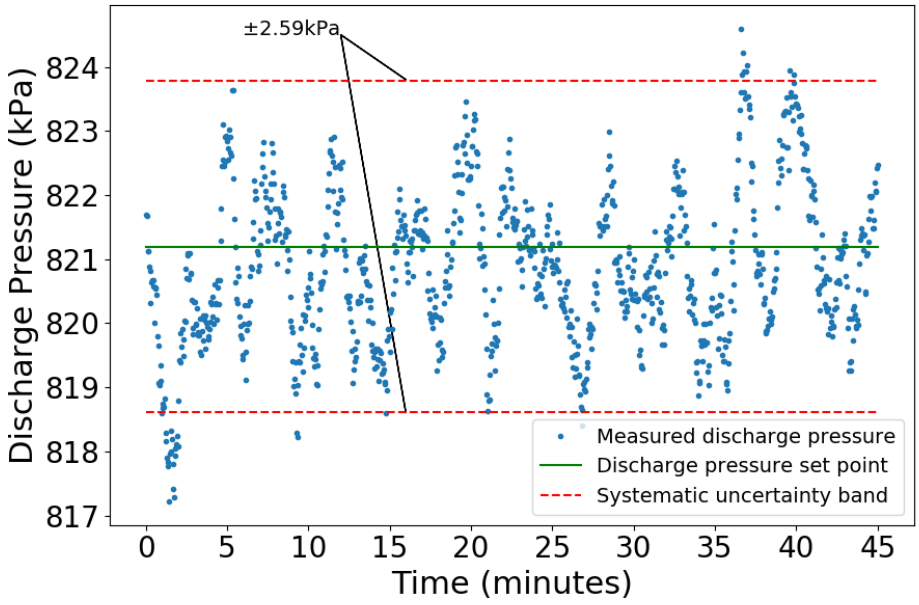

Figure 3.4: Discharge pressure at 821 kPa

3.2 Steady-State Results

A matrix of data was tested on the compressor to validate that the load stand can provide control of the testing conditions using R134a as the working fluid. Figures 3.2, 3.4, and3.5 show one such condition that was tested, 10°C (50 °F) evaporating temperature, 32.2°C (90 °F) condensing temperature, and 11.1 K (20 °R) of superheat at the inlet of the compressor. From this condition, the suction pressure set point is 414.9 kPa (60.17 psia), the discharge pressure set point is 821 kPa (119.1 psia), and the suction temperature set point is 21.1 °C (70°F). The figures show how the data compares to the set point over the test length of 1000 samples at 0.37 samples/second sample rate. The green line represents the set point and the red lines represent the systematic error for the instruments associated with each measurement. Along with these figures, the random uncertainty was calculated.

Figure 3.2 shows that the suction pressure holds well within the error range of ±0.689 psia for the duration of the test, with an average value of 414.9 kPa (60.17 psia) (zero error relative to the set point). The calculated random uncertainty for this test is 0.016 kPa (0.0023 psia). This provides verification that the suction pressure can be precisely controlled.

The discharge pressure, with small exceptions, stays within the desired error range of ±2.59 kPa for the 1000 samples tested as seen in Figure 3.4. It had an average value of 820.8 kPa (119.05 psia) with a random uncertainty of 0.038 kPa (0.0055 psia). A 0.2 kPa (0.05 psia) set point error is well within the desired range of acceptable values and the random uncertainty does not add significantly to the systematic uncertainty.

Likewise, the suction temperature maintains a reasonable amount of steadiness throughout the duration of the test. The suction temperature was more difficult to control because of its connection with suction pressure. Temperature changes are very

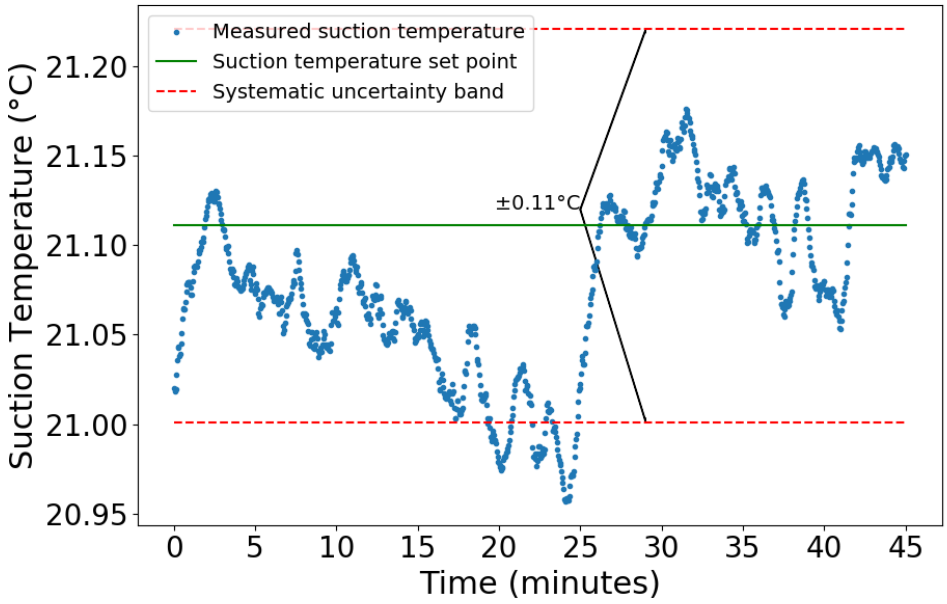

Figure 3.5: Suction Temperature at 21.22°C

sensitive to changes in the pressure, so as the controllers for suction pressure change, they can cause undesirable large changes in the suction temperature. However, as is seen in Figure 3.5, the control scheme keeps the temperature for the current test at the set point within a reasonable degree of error. The average suction temperature for the test was 21.08 °C (69.94°F). Compared to the desired temperature of 21.1 °C (70°F) the load stand is able to test within the desired parameters with an error of 0.09 percent and a random uncertainty of 0.0016 °C (0.0028 °F).

The quantification of the steadiness of the data is completed by a comparison of the random uncertainty relative to the systematic uncertainty of the specific measurement. The target metric is 5 percent of the total uncertainty as this will sufficiently reduce the influence of random uncertainty on the net result of the test, and maintain total uncertainty to well within the ranges dictated by standards (ASHRAE 23.1/2).

By resolving the issues that lead to instability, the amount of random uncertainty was reduced to within that 5 percent target as is evident in Figures 3.6 and 3.7, which present the relative random uncertainty of the suction pressure at the set point

presented previously compared to total uncertainty with the target line of 5% shown for reference. Figure 3.6 presents the relative random uncertainty for the unstable case presented in Figure 3.1. It can be observed over the course of 1000 samples (roughly 45 minutes of test time) that this test resulted in the system being unable to stabilize, thus, being unable to minimize random uncertainty. In contrast to this, Figure 3.7 shows how the total uncertainty approaches the systematic uncertainty over the length of the test period, minimizing at just above 2% relative random uncertainty. This provides validation that after correcting the instability, the control scheme is able to produce accurate steady-state results.

This result of being able to minimize the random uncertainty also suggests that testing length can be optimized. In the test presented in Figure 3.7, the random uncertainty reaches the target uncertainty of 5% of the total uncertainty at about 275 samples (roughly 12 minutes). Being able to know when the uncertainty reaches this point could significantly decrease the amount of time that it takes to collect a steady-state condition. It is also noted that similar results are found for both discharge pressure and suction temperature but only suction pressure is presented for brevity. This analysis shows that the control development and tuning produced a minimized random uncertainty at a single operating condition. This analysis will be further extended in the following section to explore the influence of the operating condition itself.

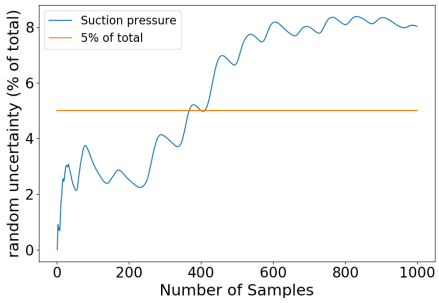

Figure 3.6: Random uncertainty of suction pressure before resolving instability.

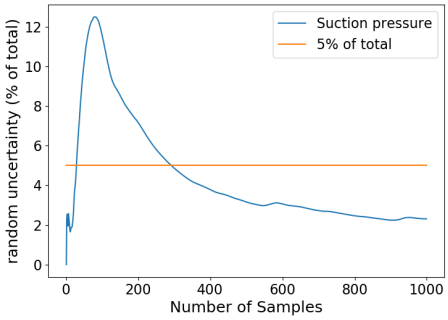

Figure 3.7: Random uncertainty of suction pressure after resolving instability.

3.3 Investigation of Random Uncertainty Sources

The following section extends the uncertainty analysis to explore the influence of operating conditions on the ability of the load stand to control random uncertainty, given a specific set of control algorithm gains. To facilitate this, the same scroll compressor was tested at 12 different operating conditions (with some repeat tests, totaling 17 test points), with varying suction and discharge pressures at a fixed superheat of 11.1 °C (20 °F) as presented in Table 3.1. The relative random uncertainty of these results are presented as a function of various control variables. Similar to previous results, each data point presented is the average of 1000 samples at the most stable conditions possible within the limits of controller oscillation (*i.e.* any oscillations present were allowed to stabilize as much as possible without adjusting the controller gains).

As previously mentioned, the target amount of uncertainty was 5% of the total uncertainty. Each of the operating conditions tested were analyzed for the amount of uncertainty. The minimum, maximum, and average amount of random uncertainty for each control variable is shown in Table 3.2. The results show that the suction temperature and discharge pressure, on average, have random uncertainty contributions of less than 5 % of the total uncertainty, and the suction pressure is closely above. These results are promising but do show that improvements can still be made.

Table 3.1: Matrix of operating conditions for testing uncertainty sources

	Evaporating Temp (°C)	Condensing Temp (°C)	Runs
1	7.22	21.11	1
2	7.22	26.67	2
3	7.22	32.22	1
4	7.22	37.78	4
5	7.22	43.33	2
6	7.22	48.89	1
7	7.22	54.44	1
8	-12.22	37.78	1
9	-6.67	37.78	1
10	-1.11	37.78	1
11	4.44	37.78	1
12	10	37.78	1

Table 3.2: Range of random uncertainties as a percentage of total uncertainty

	Min	Max	Average
Suction Pressure	2.28%	9.48%	5.52%
Suction Temperature	1.47%	9.73%	4.76%
Discharge Pressure	0.92%	6.45%	2.71%

As such, further investigation into what factors influence the amount of random uncertainty was performed in an attempt to increase the stability of the steady-state conditions.

The conditions that were tested were held at a constant superheat, meaning that the test matrix only varied the evaporating and condensing temperatures. It could be surmised that, because these are the two main variables being changed, there would be a correlation between evaporating/condensing temperature and the amount of random uncertainty at each condition. This hypothesis was evaluated, using regression analysis, and the results of the correlations are shown in Table 3.3, with their respective regression coefficients (R^2) listed. Furthermore, as previously discussed, the evaporating and condensing temperatures are controlled by a variety of different devices. By tracking the average position of each of these devices for the duration of the test (for example, the average speed of the water circulating pump), correlation

Table 3.3: Table of weakly correlating suction/discharge pressure uncertainties with varying test conditions

Condition	R^2	
	Suction	Discharge
Condensing Temperature	0.792	0.815
Evaporating Temperature	0.134	0.082
Water Pump Speed	0.816	0.755
Condenser Water Inlet Temperature	0.848	0.795
Water Bypass Valve Position	0.331	0.256
Sub-cooling	0.776	0.705
Medium Gas Expansion Valve Position	0.631	0.485
Small Gas Expansion Valve Position	0.746	0.674
Medium Liquid Expansion Valve Position	0.805	0.736
Small Liquid Exapnsion Valve Position	0.791	0.796

coefficients between the average controller positions and the random uncertainty were found and analyzed with their results shown in Table 3.3.

The analysis shows that the evaporating and condensing temperatures do not have a particularly strong correlation to the suction or discharge pressure random uncertainty. In addition, the extension of this analysis to the average position of the devices controlling the conditions found that none of these variables strongly correlated to the amount of random uncertainty associated with the tests.

The analyses performed yielded inconclusive results as to which variables had the greatest affect to the amount of random uncertainty within the control variables. This gives evidence that there is no single control parameter to adjust to achieve improved control. This also shows that there are not any systematic issues with the control scheme, as there are no major conflicts with any of the various control variables. This narrowed the source of any instability to the controllers themselves, which meant that the control strategy could be re-evaluated to yield better results.

CHAPTER 4

Improved Load Stand Control Scheme

The analyses of the previous chapter concluded that to more consistently achieve the random uncertainty goal of 5% of the total uncertainty, an improved control strategy needed to be implemented. The implementation of a new strategy could significantly improve the accuracy of the results collected on the load stand and could improve the time required to collect a steady state condition. The following section will discuss the improvements made to the control strategy and will demonstrate how it contributes to the overall objective of the project: to develop a control strategy that allows for the quick testing of compressors with a minimal amount of time between test conditions.

4.1 Improved PI Tuning

Section 2.4 discussed how the controllers were tuned using the Ziegler Nichols method of PI tuning. The proportional and integral gains that were found were often not optimal for the testing being performed. With these gains, the testing time for each condition was often quite long. As previously discussed, the tests that were performed took on the order of 45 minutes to collect a steady state condition, which is not optimal, as the desired operating ability of the hot-gas bypass stand is to test conditions rapidly. Therefore, new PI gains needed to be found to achieve the desired ability of the load stand.

The Ziegler Nichols method of tuning is often too aggressive for most control systems, making large oscillations in the process variable, which is not desirable (Skogestad, 2004). Because of this, Tyreus and Luyben (1992) offer a modified Ziegler

Nichols tuning method for slower responding systems and systems with a larger dead time. Referring to Section 2.4, once sustained oscillations have been reached and the critical proportional gain ($K_{p,u}$) and critical time constant (T_u) have been found, the proportional and integral gain, respectively, are

$$K_p = 0.313 K_{p,u} \tag{4.1}$$

and

$$T_i = 2.2 T_u. \tag{4.2}$$

It is important to note that each of the controllers was tuned independently, meaning no other controllers were turned on during the tuning process. This is important because the optimal gains will change with different testing conditions and with other controllers making changes to the system. It is often necessary to modify the gains during the testing process to achieve optimal control. Nevertheless, the above tuning parameters, provided by Tyreus and Luyben (1992) give a close estimation of what the optimal gains should be, meaning a minimal amount of change is needed to achieve optimal control. These tuning parameters led to the new PI gains shown in Table 4.1.

Table 4.1: List of improved values for K_p and T_i

	K_p	T_i (min)
Medium Gas Valve	0.77	5.63
Small Gas Valve	0.0912	0.879
Medium Liquid Valve	-0.153	7.656
Small Liquid Valve	-0.287	0.5
Water Bypass Valve	0.15	1.2
Water Pump	-0.161	0.35

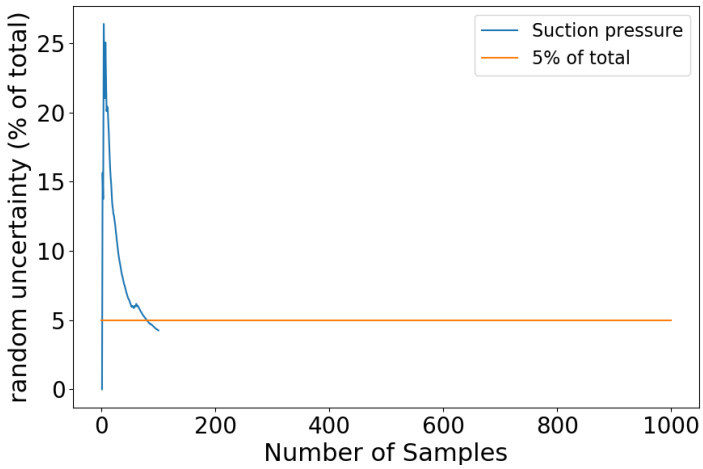

Figure 4.1: Example of suction pressure random uncertainty minimized in 100 samples

The implementation of these new gains resulted in better control of the load stand. The stand was able to reach steady state much quicker than before, and was able to quickly move between test conditions, which it was unable to do previously. This greatly reduced the amount of time it took to collect test conditions and increased the number of tests that were able to be performed in a day. For example, Figures 4.1 - 4.3 show one such test, where the random uncertainty of each of the three process variables was minimized to the target of 5% of the overall uncertainty in about 100 samples, which is equivalent to about 4.5 minutes.

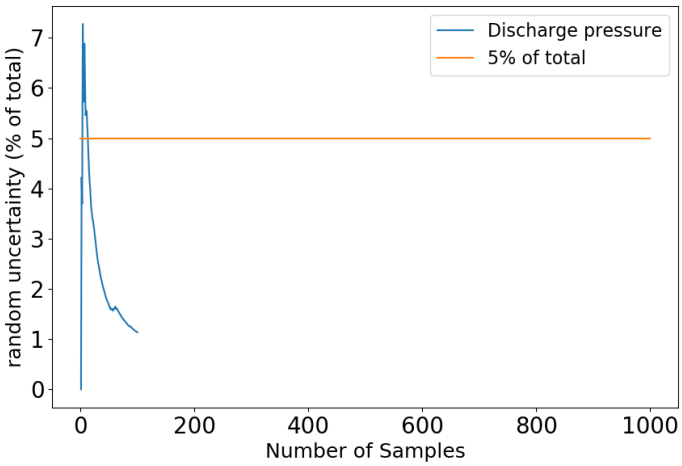

Figure 4.2: Example of discharge pressure random uncertainty minimized in 100 samples

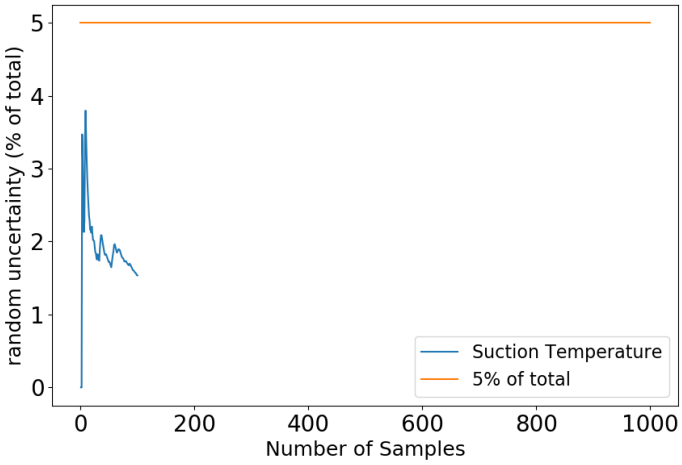

Figure 4.3: Example of suction temperature random uncertainty minimized in 100 samples

4.2 Strategy for Keeping Controllers in their Optimal Ranges

Process controllers are typically treated as if they have a linear relationship between the controller position and its desired output value. For example, it would be expected for the position of a valve to be exactly where the controller tells it to be. Valves operate between 0 and 100% open. If a linear relationship exists between input and output, then at an input of, for example, of 5%, it would be expected that the valve would be 5% open. If the input was 95%, it would be expected that the valve would be 95% open. However, this relationship does not typically exist in the ranges outside of 10-90%. Below 10% and above 90%, the relationship is highly non-linear. When the control valves are within these non-linear ranges, control is difficult to maintain. This led to the implementation of a scheme to keep the controller within the 10-90% range.

As discussed in Section 2.1, only one valve is being controlled at a time. The others can be set manually, but are not under influence of the controller. In order to limit the controllers to the 10-90% range, the controllers are stopped whenever they reach the upper or lower limit, and one of the other valves is slowly incremented toward the set point. This ultimately will cause an overshoot of the process variable, but that will cause the controller to respond, moving away from the 10 or 90% limit and toward the middle of its range, where it controls optimally.

The result of the implementation of this scheme helped the load stand to control better under automatic control, thus requiring less interference by the operator.

4.3 Automatic Determination of Steady-State and Saving

To further reduce the amount of operator intervention when controlling the load stand, the control logic was modified to automatically determine when a test has reached steady state and to save the test when that condition has been satisfied. To do this, the program creates a data queue when all three of the process variables are within

the ASHRAE-23.1 (2010) tolerances (± 1% on suction and discharge pressure, ± 1 K on suction temperature), then saves that data queue when the random uncertainty of each process variable has minimized to below 5% of the total uncertainty and the data has been queuing for 9 minutes. ASHRAE-23.2 (2014) states that a steady state condition is a test where for three consecutive data points, collected three minutes apart, the process variables are neither successively increasing nor successively decreasing. Because the load stand samples test data more frequently than every three minutes, a nine minute test sample is used to determine when the test is at steady state. When this criteria has been met, the program will save the data and will send a text message to the operators, telling them that the point has been saved. Figure 4.4 shows a diagram of how the new controls scheme was implemented to allow for less operator intervention.

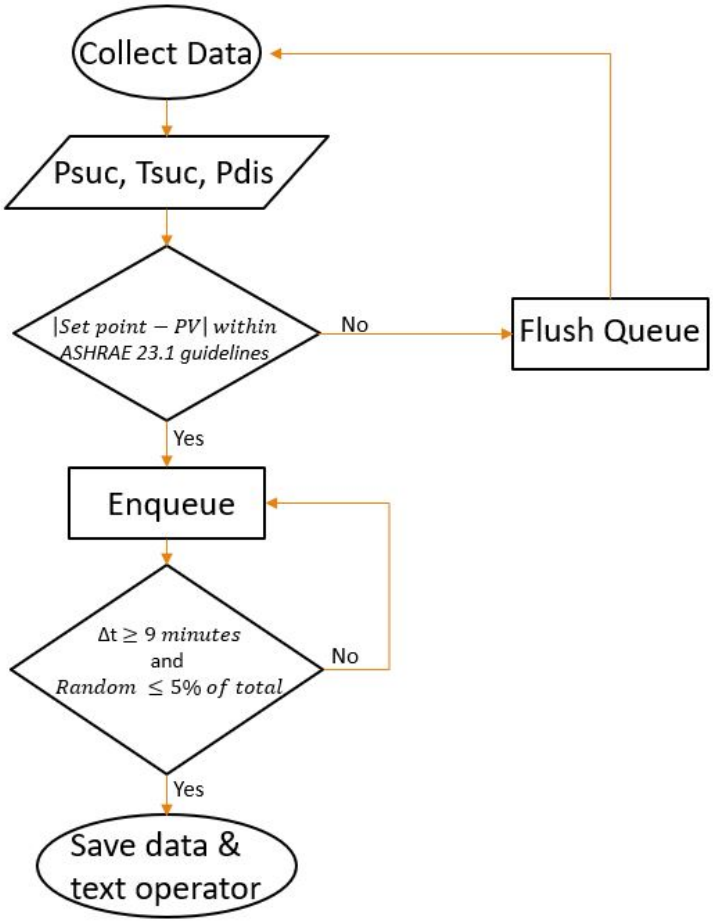

Figure 4.4: Flow chart of improved controls scheme with automatic determination of steady state.

CHAPTER 5

Preliminary Commissioning Tests

To determine the reliability of the load stand at a mid-range capacity of the stand, a 30-ton spool compressor was tested across a wide range of conditions. The purpose of these tests was to, again, show the effectiveness of the control strategy, to verify that the mass flow measurements agree with their redundant sensors within ± 3%, as is specified by ASHRAE-23.1 (2010), and to show that the performance data collected matches that collected by the manufacturer, with a reasonable degree of accuracy. These tests also served to highlight any issues with the load stand that needed to be addressed before it was to undergo final commissioning tests.

5.1 Oil Separation

Initial tests of the 30-ton spool compressor showed that the mass flow rates recorded on the load stand were significantly higher than the values recorded by the manufacturer. This led to artificially high values of volumetric efficiency, which would read over 100% at low pressure ratios. This phenomenon, shown in Figure 5.2, indicated that the mass flow values of the load stand were incorrect and needed to be resolved.

When viewing the sight glass directly downstream of the discharge mass flow meter, a significant amount of oil could be seen moving through the load stand. It was hypothesized that the oil being carried over was being measured by the mass flow meters, which caused those readings to be artificially high. To resolve this issue, a conventional oil separator, as seen in Figure 5.1, was installed in series with the coalescing oil separator. This would allow the majority of the oil to be filtered by the

Figure 5.1: Image of the secondary oil separator used with the 30-ton spool compressor

conventional separator, while the coalescing separator would catch the rest of the oil that is carried over.

The results of the additional separator can be seen in Figure 5.2. These results show that the addition of the second oil separator helped to decrease the mass flow rate measurements, which, in turn, lowered the volumetric efficiencies to more consistently realistic values. These results also more closely match the performance data that was collected by the manufacturer, providing confidence that the load stand is capable of collecting data that is accurate and reliable.

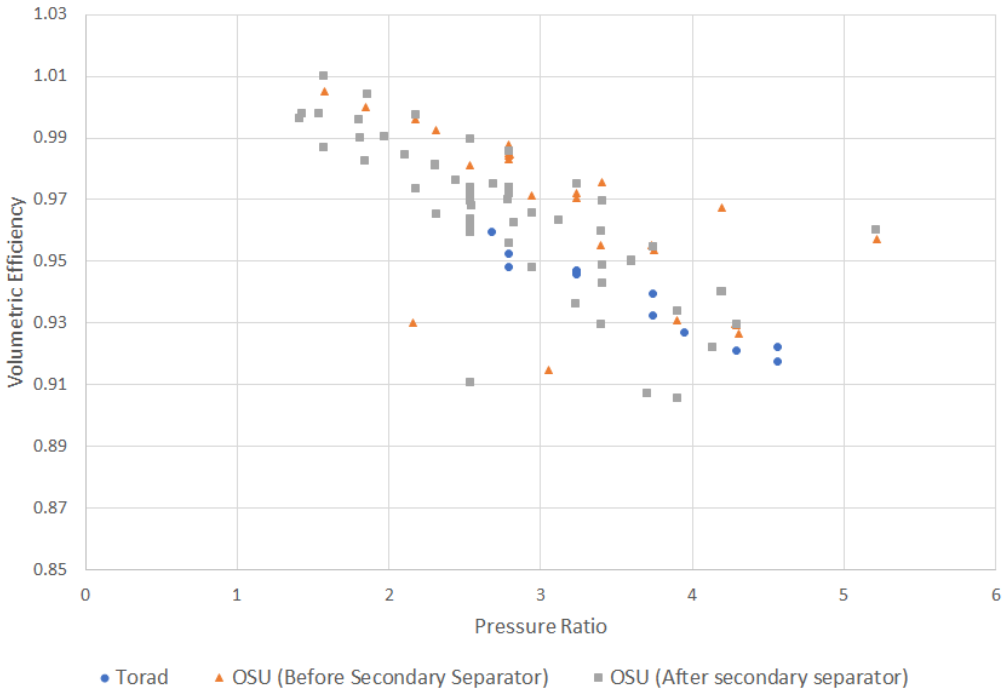

Figure 5.2: Comparison of OSU and Torad volumetric efficiencies

5.2 Modification of Mixing Sections

As a hot-gas bypass type of compressor testing facility, the load stand was designed to utilize the mixing of the bypassed gas with the liquid exiting the condensers to create the suction condition, rather than through the use of an evaporator. The method of doing this is simple, with the adjustments of valves, as described in Chapter 2. However, there is a caveat to this: the liquid and gas refrigerant must be well mixed and entirely in a vapor form by the time it passes through the suction mass flow meter. This is because the mass flow meters used on the stand are Coriolis type flow meters. They are very accurate but very sensitive to the density of the refrigerant. If a two phase mixture enters a vapor reading Coriolis meter, the measurement can be affected significantly, which causes disagreement between the suction and discharge flow meters. According to ASHRAE 23.1 (ASHRAE-23.1, 2010), for compressor testing, the primary and secondary measurements must be within 3% of each other, at steady state, to collect a valid test point. Figure 5.3 shows several data points that

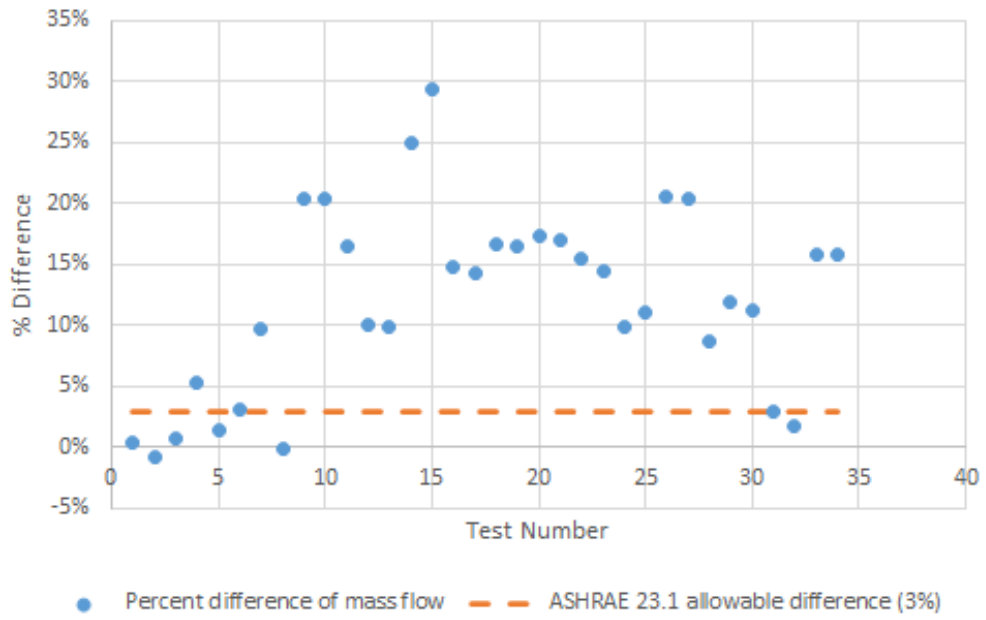

Figure 5.3: Percentage difference of suction and discharge mass flow measurements prior to resolving mixing issues

were collected during the testing of the 30 ton spool compressor, and compares the suction and discharge mass flow measurements. As the figure shows, except for a few outliers, the suction and discharge mass flow measurements never show agreement. This is because two-phase refrigerant was entering the suction mass flow meter, giving elevated readings compared to the discharge flow meter.

There are two factors that affect the quality of mixing of gas and liquid refrigerant: the length of time the two are mixing, and the amount of turbulence in the mixing section. The longer the gas and liquid are mixing, more heat is transferred to the liquid, thus giving more time to vaporize the liquid refrigerant. Along with this, higher turbulence encourages more mixing to occur and improves the heat transfer to the liquid. This, again, will help the liquid to vaporize more easily. Because of the poor ability of the load stand to mix entirely, it was decided that the mixing sections of the load stand be extended, to add length, and objects be placed in the tubing to encourage mixing.

Before the modifications to the mixing sections of the load stand, the mixing

Figure 5.4: Original load stand mixing section

sections were comprised of three vertical lengths of tubing which joined with the suction tube where the mixing was completed. This is shown in Figure 5.4. However, this being inadequate to properly mix the gas and liquid refrigerant, each of the three sections were increased in length with the addition of a "U" bend, as is shown in Figure 5.5. Additionally, in each side of each fitting of the mixing sections, two pieces of 1/2" raised expanded metal were brazed into place, shown in Figure 5.6. The expanded metal was brazed to the female fittings as a method of inducing as much turbulence as possible into the flow of the mixing sections, thus encouraging the fluid to become entirely vapor.

The results of these modifications show a significant improvement in the mixing of the gas and liquid refrigerant. The percent difference between the suction and discharge mass flow measurements show a much better agreement (3-4%), as seen in

Figure 5.5: Load stand mixing section after modifications

Figure 5.6: Example of expanded metal brazed into a copper elbow

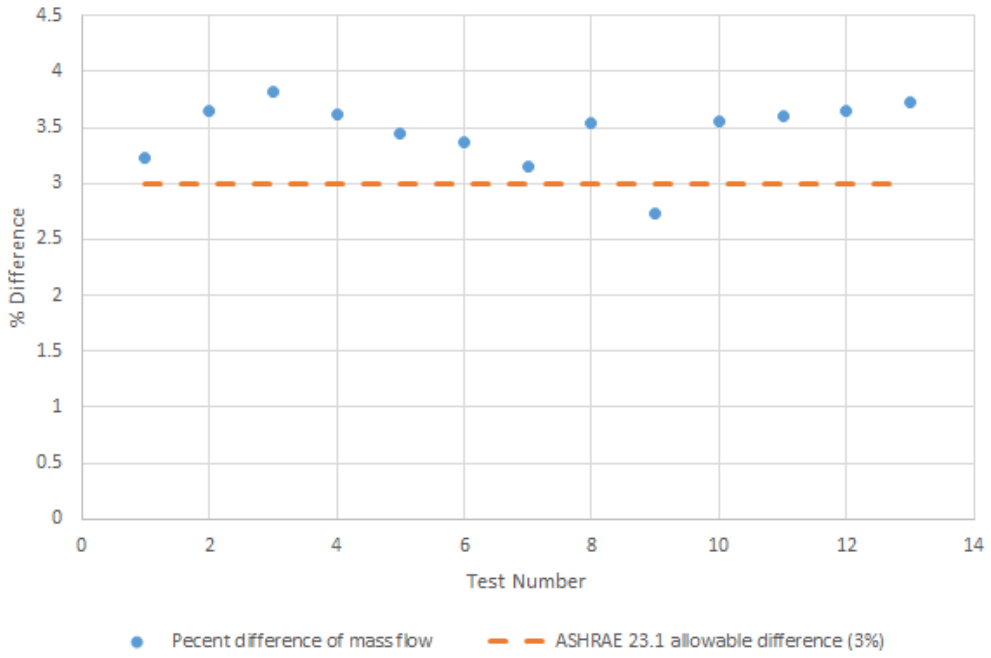

Figure 5.7: Percentage difference of suction and discharge mass flow measurements after resolving mixing issues

Figure 5.7. However, not all of the data collected quite reached the 3% threshold that is required by ASHRAE 23.1 (ASHRAE-23.1, 2010). This suggests that more modifications may need to be made in order to fully achieve the desired mixing. This will be especially true for compressors at the low end of load stand's capacity range. With compressors with a lower mass flow rate, the velocity through the gas bypass lines will be lower, which will result in less heat transferred to the liquid refrigerant.

5.3 Final Results of Preliminary Commissioning Tests

After resolving the issues of oil carryover and the mixing of the hot-gas and liquid lines, the compressor load stand was much better able to collect valid performance data. When compared to the manufacturer's data, the load stand was able to measure very similar results, with only a few percent of variation, as seen in Table 5.1. With these results, the load stand could be considered commissioned at 30 tons and could undergo the final commissioning tests.

Table 5.1: 30-ton spool compressor comparison of performance data to the manufacturer

		OSU	**Torad**	**% diff**
Psuc	psia	49.77	49.80	**-0.060%**
		49.79	49.78	**0.026%**
Tsuc	F	60.03	59.66	**0.624%**
		59.84	60.09	**-0.407%**
Pdis	psia	138.85	138.86	**-0.004%**
		161.18	161.19	**-0.007%**
Tdis	F	144.18	142.34	**1.293%**
		155.60	153.94	**1.080%**
Msuc	lbm/min	101.82	96.23	**5.810%**
		99.33	95.17	**4.374%**
Mdis	lbm/min	98.84	94.94	**4.110%**
		97.63	94.18	**3.664%**
Speed	Hz	29.16	29.29	**-0.007%**
		29.09	29.16	**-0.004%**

CHAPTER 6

Final Commissioning Tests

After the preliminary commissioning tests, performed with the 30-ton spool compressor, the load stand was to undergo final commissioning tests with a York CTS24DAAD-460/200 75-ton screw compressor, provided by Johnson Controls Inc. This would serve to verify that the load stand can collect valid data at the upper end of the designed capacity range. It would also serve to define the limitations of the load stand.

6.1 Modifications Needed for Final Commissioning Tests

During the testing of the 30 ton spool compressor and before the final commissioning tests that were performed on the 75 ton screw compressor, it was found that the load stand, while being able to achieve steady state, did not perform optimally in many cases. The discharge pressure was often very difficult to maintain control of and the automatic control valves and the pump on the oil line needed to be re-sized for the larger screw compressor, to accommodate its oil flow rate. Along with this, it was found that the strategy for oil separation was insufficient for the amount of oil that circulates within the screw compressor.

6.1.1 Water Line Modifications

After initial tests were performed on the load stand, it was determined that more fidelity was needed on the water line, to better control the discharge pressure. Previously, the main controllers for the discharge pressure were the condenser bypass valve and the water pump. However, the water pump, being a centrifugal pump, operates

very inefficiently at lower speeds. Because of this, the pump must be operated at or near its full speed or the risk of the pump overheating and triggering a thermal cutout becomes much greater. When this happens, the pump shuts off, which, in turn, trips the load stand safety circuit and shuts down the compressor. To ensure that the pump stays near its full speed, a valve was placed in line with the condensers as a way to vary the flow rate that passes through the condensers without having to vary the pump speed too much. Additionally, a bypass valve to the intermediate heat exchangers was installed. This provides extra fidelity in control, when needed, but is mostly used as a coarse adjustment of the water flow to account for different sized compressors. As larger compressors will reject a greater amount of heat to the water line, the intermediate bypass valve will be closed to provide more cooling to the condensers.

6.1.2 Oil Line Modifications

During the initial design of the load stand, an oil pump was selected based on a few assumptions of the flow rate of oil. However, during the operation of the load stand, it was found that the oil pump could not function properly for two reasons. One being that the magnetic coupling that motor and pump shafts was not strong enough to keep the motor and pump connected with the system pressure drop. According to the pump manufacturer, the pump requires a rare earth magnet type coupling when operating with higher viscosity fluids, such as oil, because the torque requirement becomes too great for traditional magnets to stay connected. The second reason the pump could not function properly was because it was designed around the assumption that the maximum flow rate of oil would be around 3% of the maximum compressor mass flow rate (Schmidt et al., 2019). However, the 75 ton screw compressor that was tested required a flow rate of oil of about 13% of the compressor flow rate. This was 29.7 lbm/min at a compressor flow rate of 230 lbm/min. Therefore, the pump

was undersized for the compressor that was to be tested.

To determine to what degree the oil pump was undersized, and to appropriately size a new pump, an estimation of the system pressure drop was made for the length of tubing used and the number and type of fittings as well as the density and viscosity of the fluid that was used. Figure 6.1 shows the system pressure drop as it varies with the flow rate of oil and the capabilities of the original pump that was installed on the oil line of the load stand. As the figure shows, the pump can only supply a maximum of about 2 gpm (15.58 lbm/min) of oil. Therefore, the system requires a much larger pump to supply the flow rate of oil that was needed for the 75 ton screw compressor.

It was decided that a Haight model 10U pump would be a sufficient replacement for the oil pump that was originally installed on the load stand. It is able to supply up to 10 gpm of flow of the oil at a pressure drop of 50 psi, well sufficient to overcome the system pressure drop at the design flow rate of oil of the 75 ton screw compressor. Additionally, the new pump is mechanically coupled to the motor, rather than magnetically as was the case with the original oil pump. This means the pump will no longer decouple from the high pressure of the system.

6.1.3 Oil Separation for 75 Ton Screw Compressor

The 75 ton screw compressor was tested on the load stand as a means finalizing the commissioning of the load stand. However, during initial testing of this compressor, it was discovered that the oil separation scheme of the load stand was inadequate for the screw compressor that was being tested. It was observed that large amounts of oil were being carried over past the oil separator, which affected the measurements taken on the load stand. The most affected was the refrigerant mass flow rate, which, with the addition of large amounts of oil, was substantially higher than what was indicated by the measurements taken by JCI. This, in turn, affected the calculation of volumetric

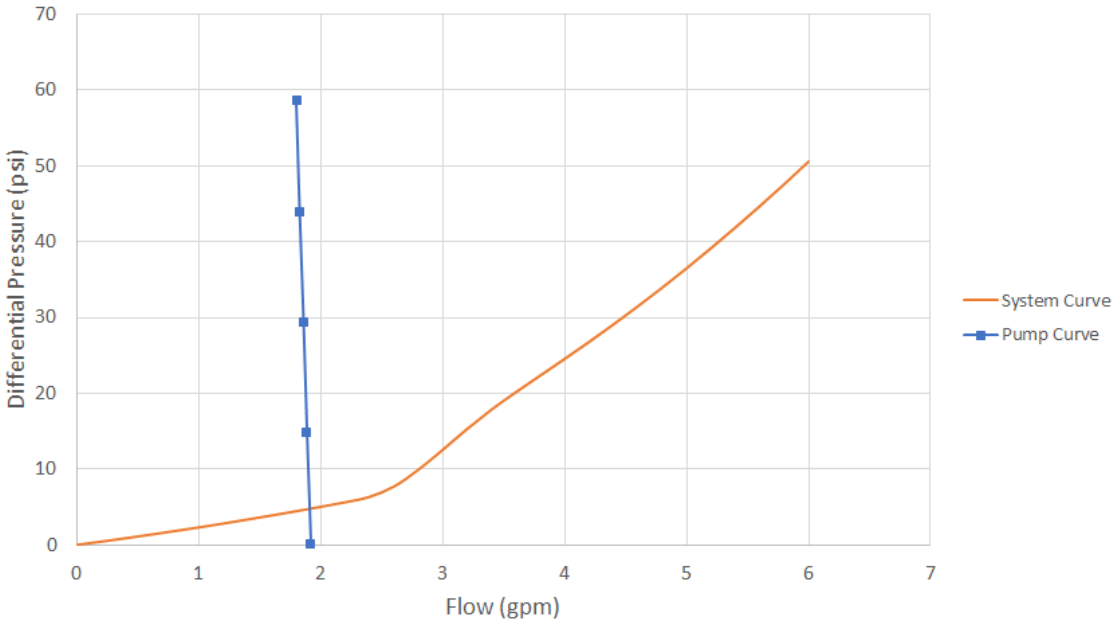

Figure 6.1: Oil line pressure drop with originally installed oil pump

efficiency, making the value appear significantly higher than was expected. Figure 6.5 shows a percentage difference between the initial measurements collected for a speed curve and the data provided by JCI.

The oil separator that the load stand is equipped with is a Temprite coalescing style separator, model 930R, as was selected by Schmidt et al. (2019), who determined that the separator should sufficiently separate oil for a 143.4 tons capacity using R134a at 40 °F evaporating and 100 °F condensing. However, it cannot separate oil at that capacity for compressors which do not have internal oil separation. Many compressors hold oil in a sump, where it collects after passing through an oil separation mechanism held within the compressor. As a result of this internal separation, the amount of oil leaving through the discharge of the compressor – the oil carryover – is a relatively low percentage of the total mass flow (about 1%). The 75 ton screw compressor that was tested, however, did not have any internal oil separation, and as such, had an oil carryover rate of about 10-30%. This is far too much for any coalescing style separator to work effectively.

Figure 6.2: Coalescing filter after a blow out caused by too high of an oil carryover rate.

A coalescing oil separator works by using a glass fiber filter media which refrigerant passes through, but collects small droplets of oil, which collide to form larger droplets, which are gravity-fed to a drain. This is a very effective form of oil separation for scenarios when the oil carryover rate from the separator is relatively small. However, when the oil carryover rate is high, as was the case with the 75 ton screw compressor, the oil overwhelms the filter media, creating a layer of oil along the media which causes a large pressure drop of refrigerant across the filter. When the pressure drop becomes too high, the filter gasket, or worse, the filter itself can blow out. During initial testing of the 75 ton screw compressor, the coalescing separator did suffer from a filter blow out seen in Figure 6.2. Issues such as this created a need to re-evaluate the oil separation scheme for the compressor load stand.

To overcome the inability to effectively separate oil, a Bitzer OA4188US separator,

capable of handling up to 29.72 GPM of oil flow, was installed upstream of the coalescing separator, which is seen in Figure 6.3. This is a centrifugal style separator, specifically designed for screw compressors. In order to get the oil circulation rate through the compressor load stand to a minimum, the coalescing and centrifugal separators were used in series such that the centrifugal separator would remove a majority of the oil to a level that would not overwhelm the coalescing separator, which would in turn remove the small amount of oil that was still carried over. An updated schematic can be seen in Figure 6.4, which shows how the new oil separation strategy is used with the load stand. Since the centrifugal separator is rated for 400 psi, while the discharge line of the load stand is rated for pressures up to 650 psi, it could not be a permanent addition to the load stand. Therefore, it was installed with flanges within the manifold section of the load stand. As a result of this installation, the oil circulation rate within the load stand was minimized, which caused the measurements to much better agree with the data that was provided by JCI as seen in Figure 6.5.

Figure 6.3: Bitzer OA4188US centrifugal separator installed upstream of the coalescing separator.

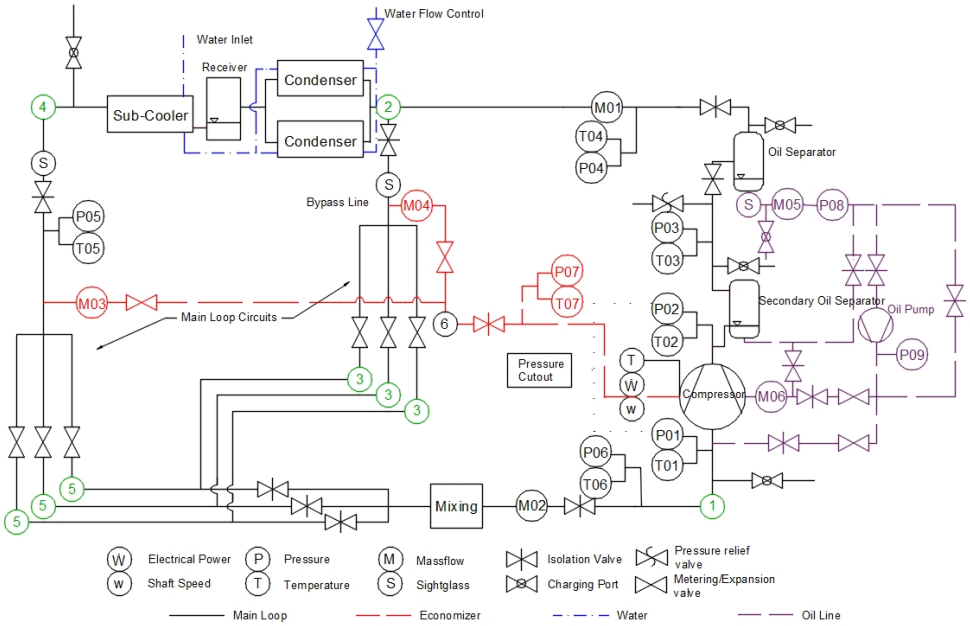

Figure 6.4: Updated load stand schematic showing new oil separation strategy

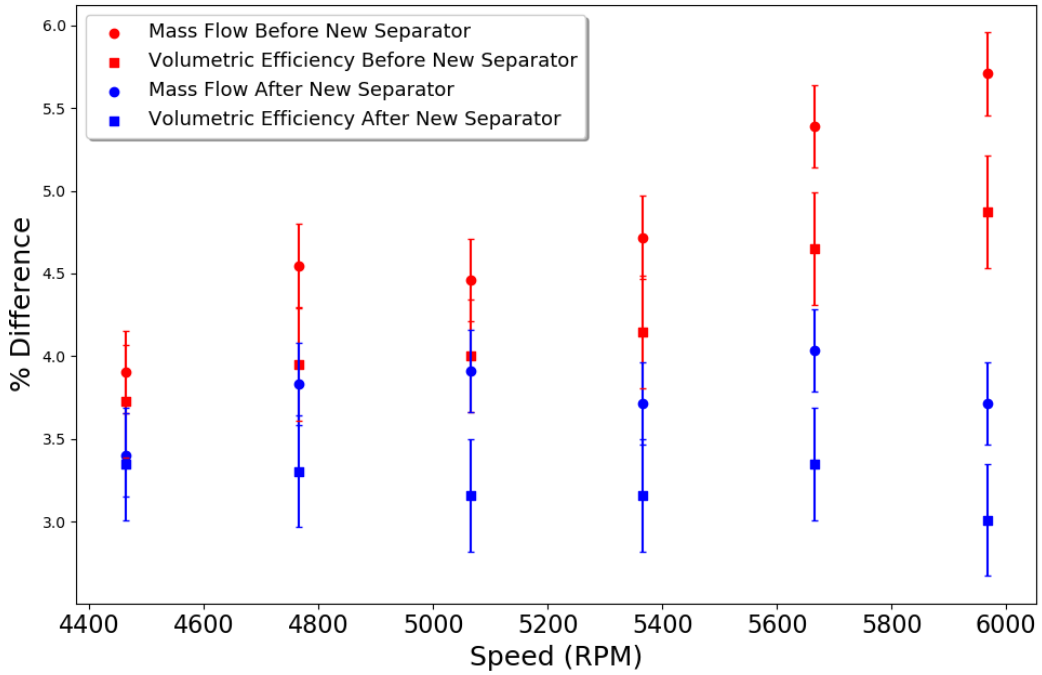

Figure 6.5: Comparison of percentage difference between mass flow and volumetric efficiency collected by OSU and JCI with errorbars representing total uncertainty

6.2 Results of Final Commissioning Tests

After the final modifications to the load stand were made, a series of tests were run on the 75 ton screw compressor, across a spectrum of operating conditions for which the performance results were directly compared to data provided by JCI. The entire test matrix can be found in Table 6.1. With the ability to minimize the uncertainty of the control variables (suction pressure/temperature, discharge pressure) and the ability to have matching primary and secondary measurements, the objective of the final commissioning tests was to replicate JCI's data as closely as possible. This would ensure that the verification of the performance data collected would be as accurate as possible. By precisely controlling to the specified suction pressure/temperature, discharge pressure, and compressor speed, the output variables (*i.e.* discharge temperature, mass flow, power, etc.) would, ideally, match those measured by JCI.

As Figure 6.6 shows, the load stand was controlled to the conditions at which JCI

Table 6.1: Test matrix for 75 ton screw compressor

	Evaporating Temp (°F)	Condensing Temp (°F)	Superheat (°R)	Speed (RPM)
1	40.07	125.04	9.03	4460
2	40.12	124.96	9.01	4760
3	40.09	124.95	9.12	5060
4	40.01	124.98	9.11	5360
5	39.96	125.00	9.16	5660
6	40.04	125.00	8.92	5960
7	39.95	124.95	8.97	6256
8	40.04	109.91	9.18	6058
9	40.05	120.01	8.92	6053
10	40.00	129.87	9.04	6047
11	39.96	139.95	9.18	6041
12	39.04	126.92	9.06	6048
13	39.96	105.97	8.90	4318

tested the compressor. With the exception of five outlying speed points, the total uncertainty of the control variables was within ± 0.5% of the value that JCI tested, with a few outlying conditions, confirming that the load stand is closely replicating the conditions that were tested by JCI. Additionally, the operating conditions that were tested can only be considered valid if the primary and secondary mass flow measurements are within ± 3% of each other (ASHRAE-23.1, 2010). For all operating conditions, the mass flow measurements were within the allowable tolerance, as is seen in Figure 6.7.

With each condition being precisely replicated, the output measurements and performance characteristics of the compressor could be measured and compared to JCI's data, as a way of confirming the results that are collected on the load stand. The most important output variables are those that directly affect the performance data of the compressor. These are: discharge temperature, mass flow, and motor power consumption. As Figure 6.8 shows, the values of the output variables are reasonably close to the same variables collected by JCI, with a small amount of uncertainty.

The data collected with the 75 ton screw compressor matches the data that was previously collected by JCI for this machine with, typically, less than 5% error. This,

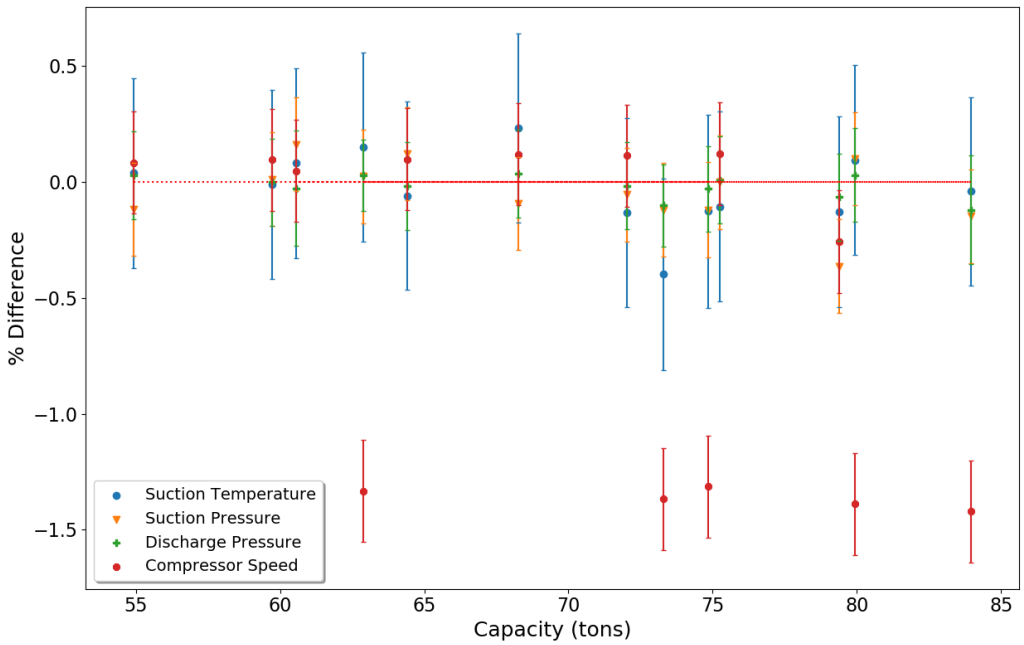

Figure 6.6: Comparison of control variables collected on the load stand to those collected by JCI with error bars representing total uncertainty

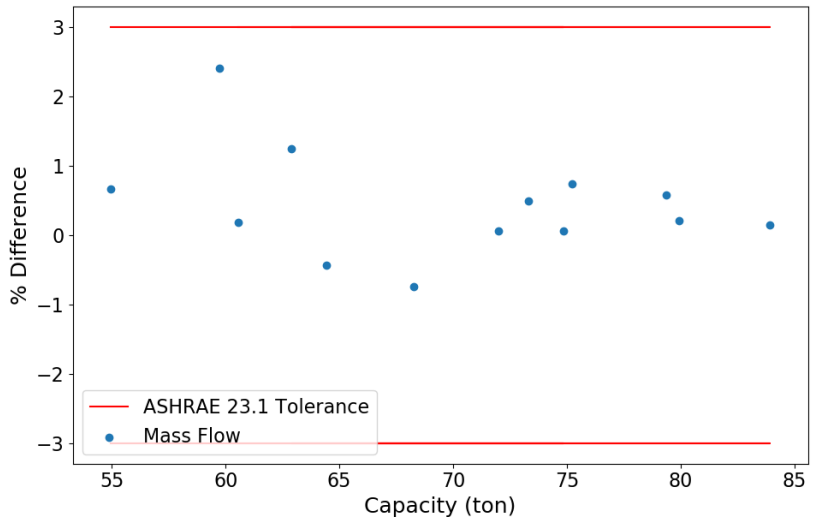

Figure 6.7: Percent difference of the primary and confirming mass flow rates for each testing condition

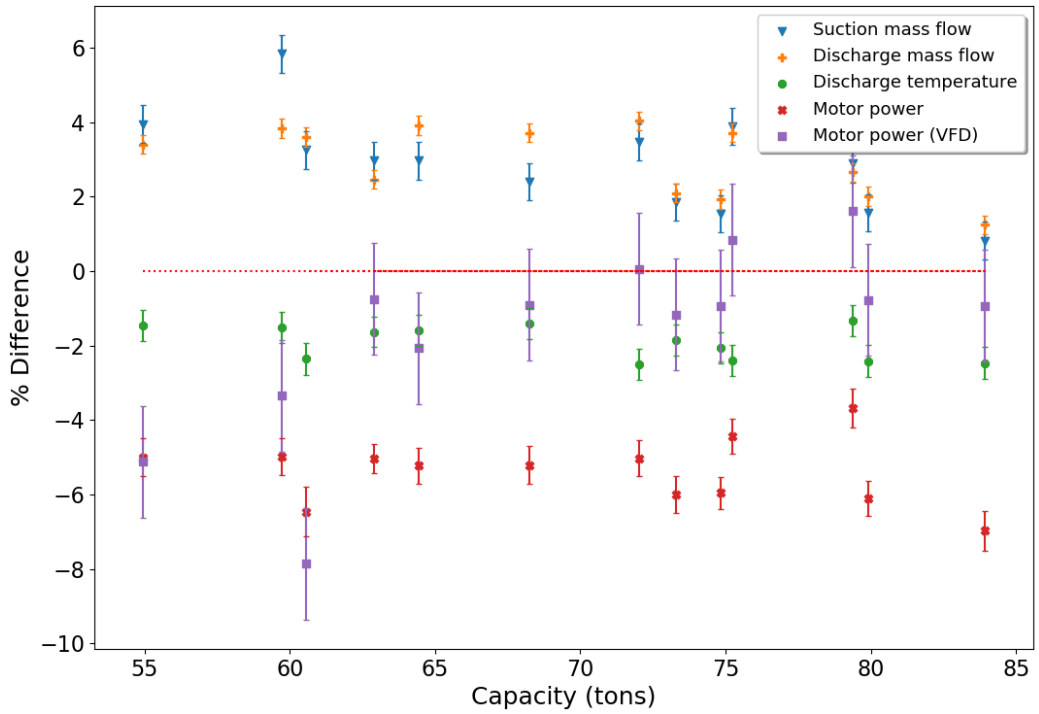

Figure 6.8: Comparison of output variables collected on the load stand to those collected by the JCI with error bars representing total uncertainty

combined with achieving the measurement tolerances, specified by ASHRAE-23.1 (2010), gives significant confidence to the data that is collected on the compressor load stand. Additionally, AHRI-Standard-540-2015 (2015) gives guidance to verifying data collected with a single compressor. This was intended to be used for verification of published compressor performance, but using the same guidelines on data used to commission the load stand will provide the same level of confidence to the load stand as data that is published by a manufacturer. For the conditions that were tested, AHRI-Standard-540-2015 (2015) gives an uncertainty limit of 5%. The performance data that was collected on the load stand does fall within this uncertainty limit. As such, the performance data collected by the load stand is considered verified and the commissioning of the load stand, at its full capacity, is considered successfully completed.

6.2.1 Initial Testing of Compressor Load Stand with Economizer Circuit

The compressor load stand was designed and built to accommodate compressors that have the capability of economization, as discussed by Schmidt et al. (2019). The 75 ton screw compressor was the first compressor tested on the load stand which had that capability. JCI, however, did not provide data that performance characteristics could be validated with. As such, it was used to verify the functionality of the economizer and to provide new performance data of the compressor with an economizer circuit.

A compressor operating with an economizer cycle typically has decreased power consumption, because the economizer provides cooling to the compressor at an intermediate stage of the compression process. This leads to an increased isentropic efficiency. As described by Schmidt et al. (2019), the economizer circuit of the load stand mixes a portion of the subcooled liquid and a portion of the discharge gas to create an injection condition at an intermediate pressure and temperature. During the testing of the economizer loop, the intermediate pressure set points were set at

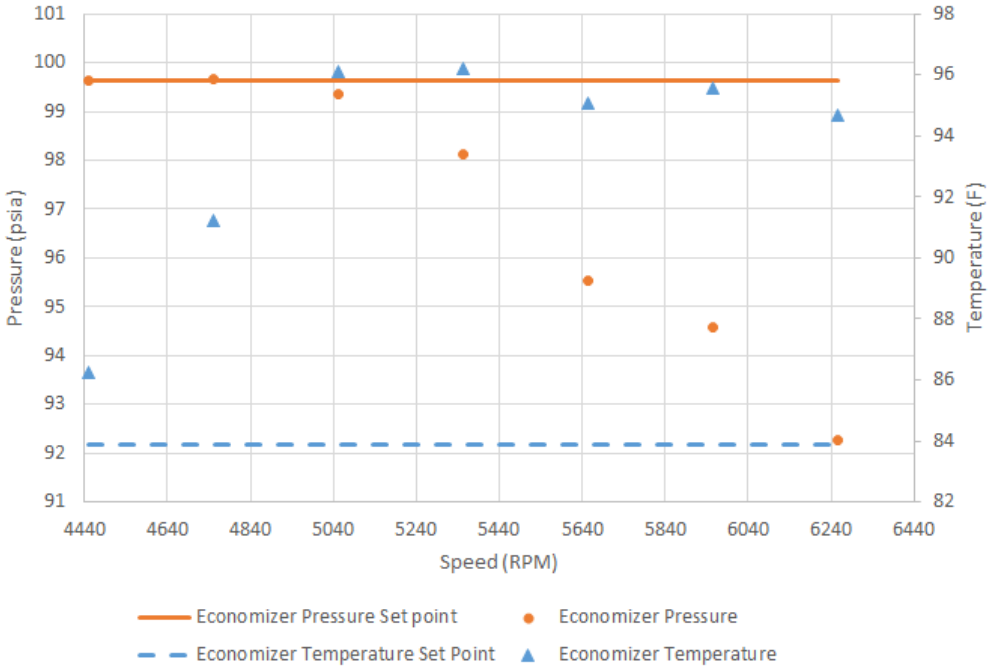

Figure 6.9: Economizer temperature and pressure with respect to their set points across a speed curve

the square root of the product of the suction and discharge pressure, while the temperature set points were chosen to have 5 °R of superheat. The initial tests were performed across a range of compressor speeds at a constant evaporating and condensing temperature. The results of these tests showed that the economizer line was inadequately sized to accommodate the 75 ton screw compressor. Across the entire range of compressor speeds, the injection temperature was always much higher than its set point. At a compressor speed of 170 Hz and above, the economizer pressure could not be increased to the desired set point, regardless of valve positions. This can be visualized in Figure 6.9.

The economizer line was originally sized with the assumption that it would be, at most, 15% of the total volume of the load stand. The original model showed that the total mass flow of the economizer should be, at most, 45 lbm/min. However, it was found, during testing, that the minimum economizer flow rate needed for this compressor was over 70 lbm/min. So, by removing this assumption and solving for

the percentage of total volume that is used for economizing, it is found that the economizer circuit should be sized to be at least 31% of the total volume of the load stand.

CHAPTER 7

LabVIEW Operation

As discussed in Chapter 2, the compressor load stand is equipped with a comprehensive data acquisition and controls system, which is executed by code developed in LabVIEW^{TM} (Elliott et al., 2007). The code collects raw data, uses the controls algorithm to make adjustments, and performs post-processing of the data to determine performance metrics. It performs these tasks through the use of two virtual instruments (VIs), a target and a host. The target VI is uploaded to and runs on the data acquisition system (NI CompactRIO-9035) and interfaces with all of the measurement and control devices. It can read data from the measurement devices and can write to each of the controllers. The host VI, on the other hand, runs on the computer and can only read data that the target VI sends to it. It is responsible for displaying the data and for performing calculations for things such as efficiency or state properties. The two VIs communicate through shared variables, which are able to be transmitted from one VI to the other. This chapter will describe the components of each of these VIs to explain how to operate them, as well as to explain how the code was written.

7.1 Target VI

The target VI, which is responsible for the data acquisition and control, will look similar to Figure 7.1 when the VI opens on the computer. From here the user will be able to view different pages to control different aspects of the of the load stand. Each page of the target is used to control a different aspect of the load stand. For example, the suction pressure and temperature are controlled on a single page. The

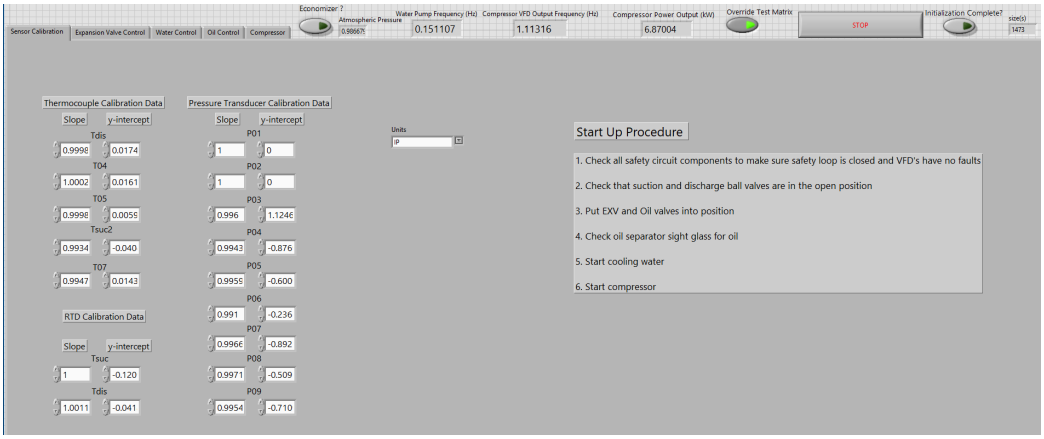

Figure 7.1: Screen shot of the target VI on start-up

adjustments made on this screen are communicated through various sub VIs to ultimately be transmitted to the valves via the output signals. Figure 7.2 shows the path of communication between the various sub VIs that will communicate with the valve controllers to make physical changes to the operating condition of the load stand.

7.1.1 Data Collection

The first page that is viewed when the target VI opens is called "Sensor Calibration", as can be seen in Figure 7.1. Here the user can input the calibration information for all of the pressure and temperature sensors. Rather than using the factory calibration, these sensors are calibrated in the lab, using the calibration devices mentioned in Chapter 2, to ensure that they have the best accuracy. This is done by comparing the sensor data to the calibration device at several points across the span of the sensor, and applying a linear equation fit, so that the sensor data matches the calibration device closely. The calibration information on this page corresponds to the slope and y-intercept of these curve fits.

To perform the data acquisition, an array is initialized for each measurement type (temperature, pressure, etc.) and the data that is collected populates those arrays at a rate of 1 sample/second. Figure 7.3 shows an example of this process with a block of code that samples the RTD measurements. In this code, an empty array is

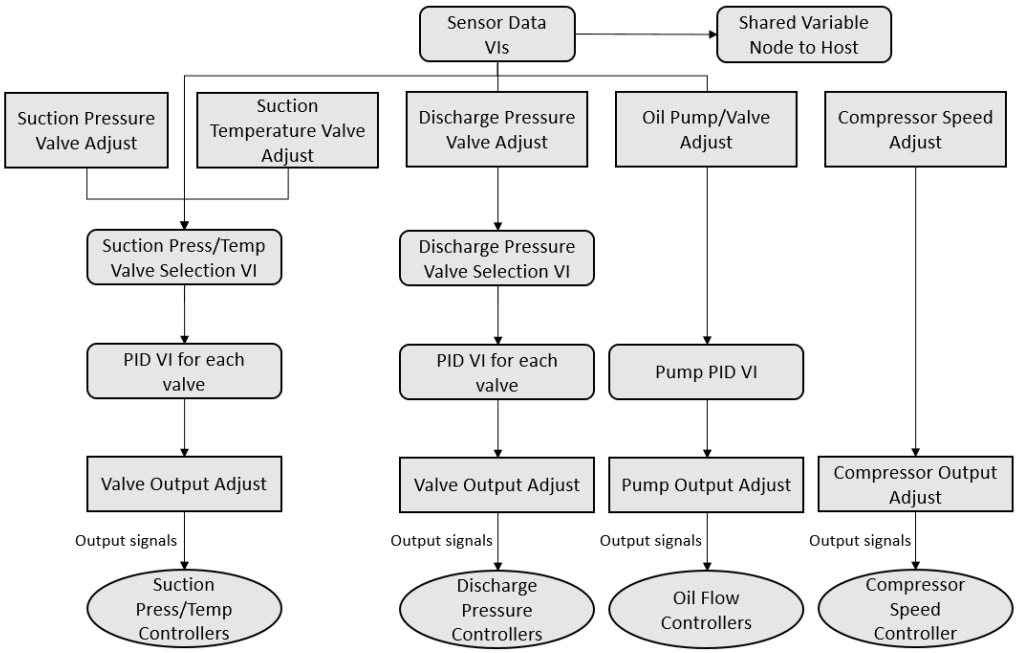

Figure 7.2: Visualization of how the data flows through VIs within the target

initialized, then each RTD measurement is read and has the calibration correction factors applied to it. Then each RTD measurement is inserted into the array.

For each sample, all of the data that is measured is inserted into their respective arrays, which are subsequently bundled together to form a cluster. This cluster is set up as a shared variable. This allows all of the data that is collected on the target to be transmitted to the host, where calculations can be performed and the data is displayed. Figure 7.4 shows the operation of bundling all of the data arrays together to create a cluster that is sent to the host.

7.1.2 Expansion Valve Controls

The page following the "Sensor Calibration" page is used to control the gas bypass and liquid expansion valves as well as the economizer gas and liquid valves. It is called "Expansion Valve Control" and will look similar to Figure 7.5. Each set of valves will have three pages for monitoring and controlling.

Page one shows the position of the valves and allows the user to manually set

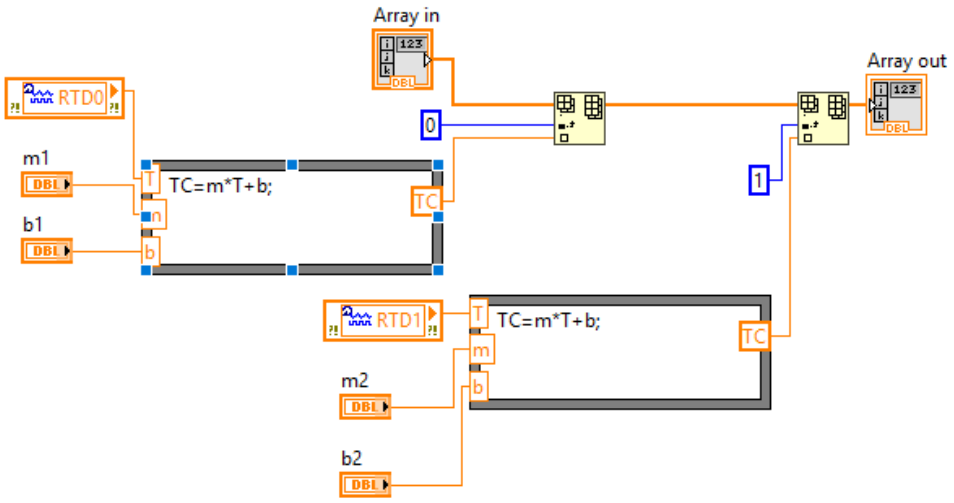

Figure 7.3: Example of data collection code with RTD measurements

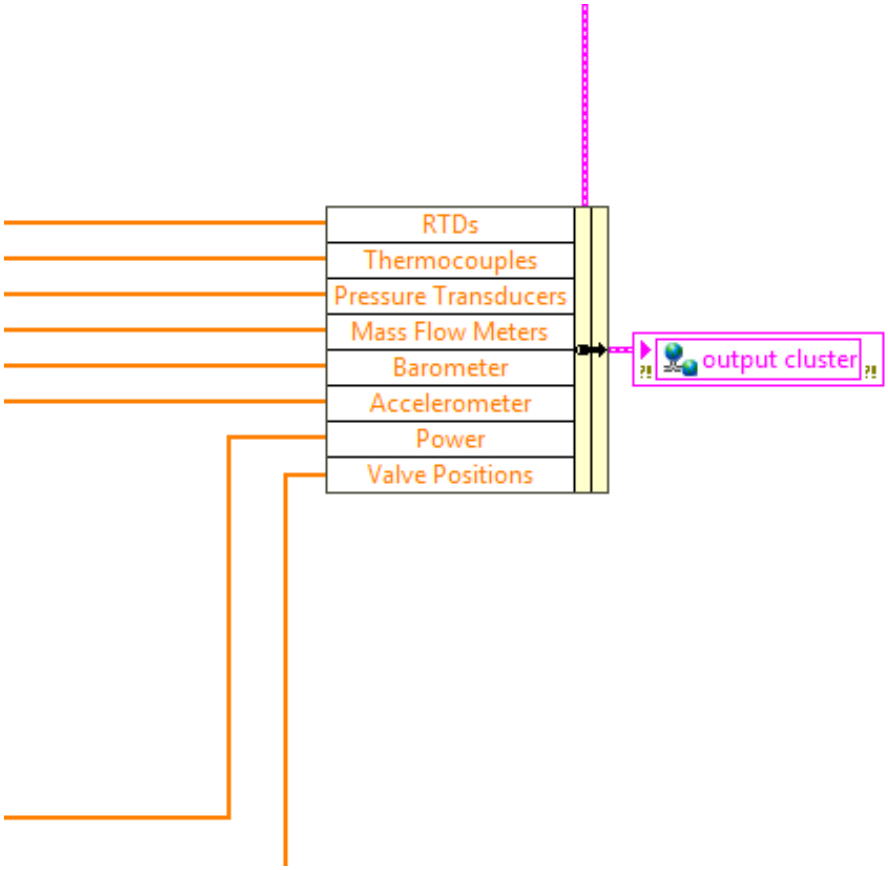

Figure 7.4: All measurement arrays creating one output cluster

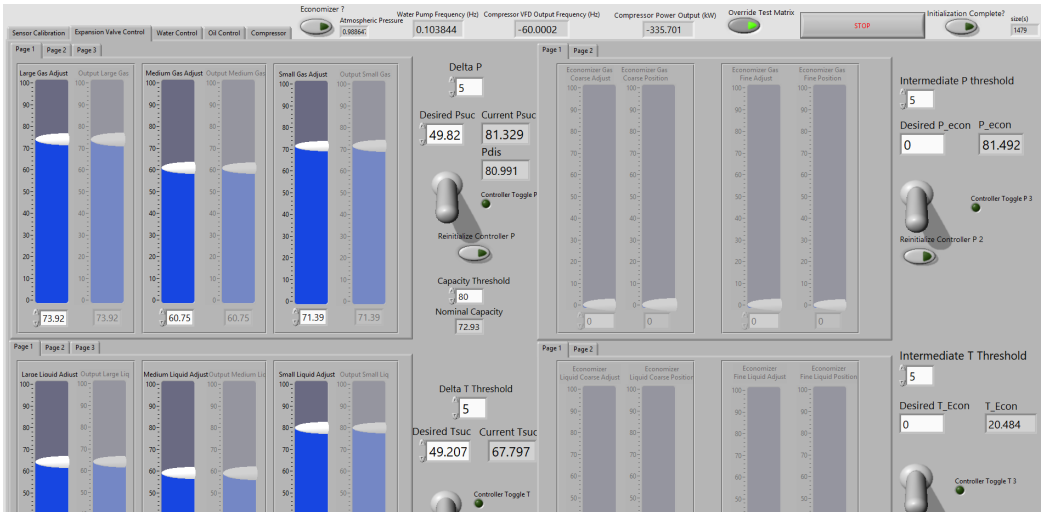

Figure 7.5: Sceenshot of the "Expansion Valve Control" LabVIEW screen

the position of each valve. Figure 7.6 shows an example of this with the gas bypass valves, which control the suction pressure.

Page two allows the user to input the PID gains for each of the valves, shown in Figure 7.7, which is the PID gain page for the gas bypass valves. For each valve, the PID gains can be manipulated independently in real time. This allows the user to adjust the level of control easily. This page also has an autotune feature, which will automatically find the PID gains for each valve, using the Ziegler Nichols method of controller tuning discussed in 2.4. To autotune the gains of a controller, the load stand must be operating at an arbitrary steady state condition, with all other controllers placed in manual. Then, the user presses "Autotune" button and waits until the "tuning completed?" light turns on. Once this light turns on, the user presses the "Accept Autotune" button to use the tuned PID gains.

Page three shows the user the current value for the process variable, compared to the set point. Figure 7.8 shows this page for the suction pressure. It shows the current position of the suction pressure, the set point, and the error band above and below the set point. This gives the user a good idea of how the load stand is controlling. The goal is to get the control variable to match the set point line as closely as possible.

To the right of each set of controllers is a switch that allows the operator to

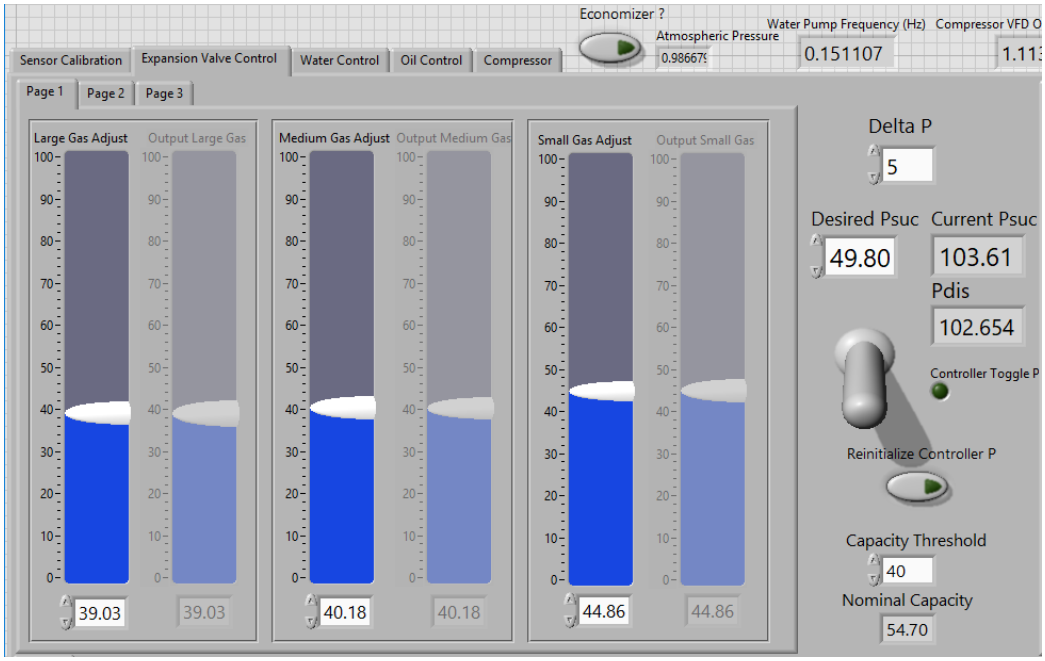

Figure 7.6: Suction pressure control - page one - valve position

Figure 7.7: Suction pressure control - page two - PID gains

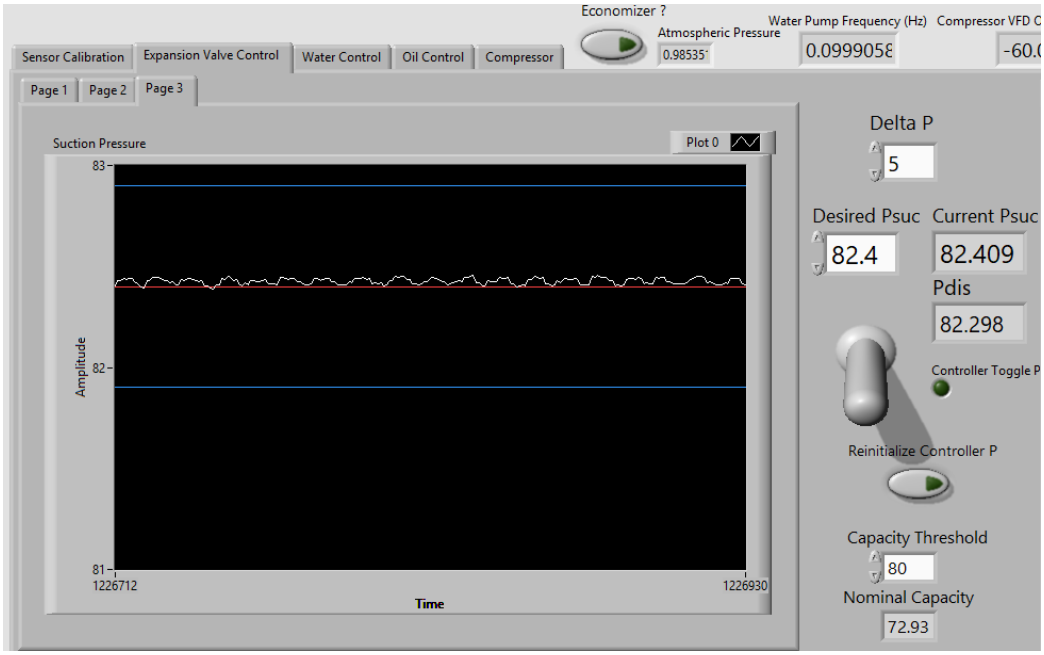

Figure 7.8: Suction pressure control - page three - Suction pressure plot

switch the control mode to manual or auto. When the switch is in the downward position, the controllers are in manual mode and changes to the process variable are only made by adjusting the position of the sliders on page one. When the switch is in the upward position, the controllers will operate automatically, using their PID tuning parameters to make adjustments. When the controllers are in auto mode, a "Controller Toggle" light will turn on. Figures 7.9 and 7.10 show the controller auto switch in both the "off" and "on" position. These figures also show the inputs to the valve selection scheme that is discussed in 2.1. "Capacity Threshold" is the nominal capacity that determines if the largest or smallest valve will be eliminated from use, while "Delta P" is the pressure threshold that determines which of the two remaining valves will be used.

The automatic control functionality starts in a VI that performs the valve selection process described in Section 2.1. Here, by using the compressor's operating capacity and by comparing the current value of the process variable to the set point, the code determines which valve is to be adjusted for optimal control. An example of this is

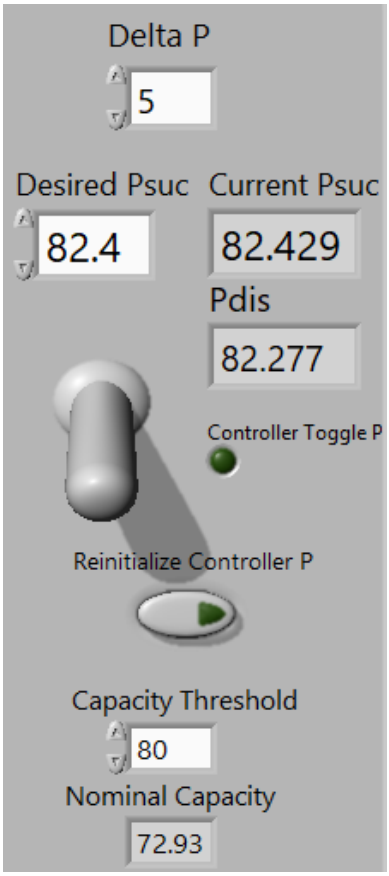

Figure 7.9: Suction pressure controller auto switch turned off

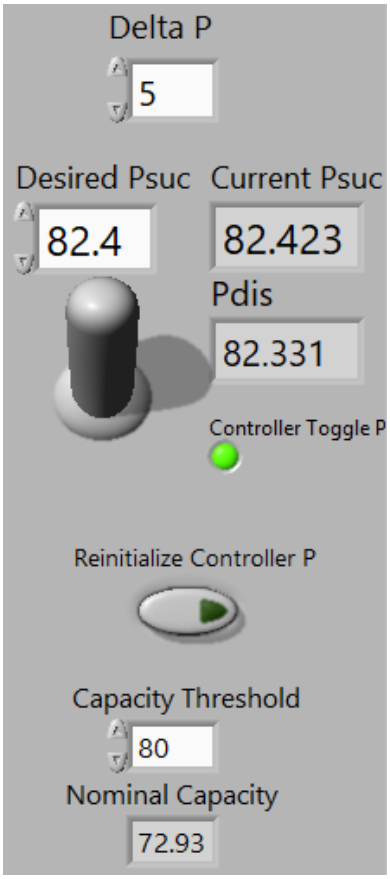

Figure 7.10: Suction pressure controller auto switch turned on

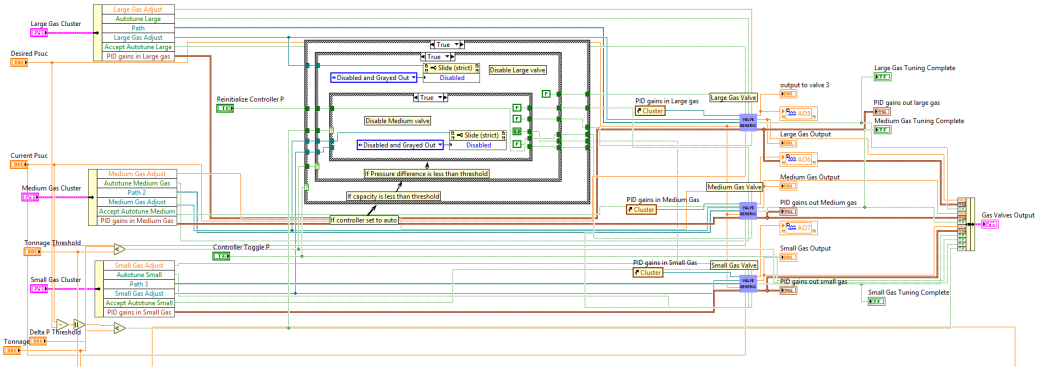

Figure 7.11: Suction pressure valve selection code

shown in Figure 7.11, where inputs are given for the gas bypass valves, and the code automatically selects which valve to adjust.

After the selection process, there is another sub VI, for each individual valve, where the valve position, process variable, set point, and PID gains are input into the built in PID LabVIEW function. In this VI, the current valve position (0-100%) is converted to an analog output (4-20 mA). To automatically control the valve, the PID function adjusts the analog output to open or close the valve. After the valves have been adjusted, the new analog output gets converted back to a valve position, between 0-100%, to be reflected on the valve output slider (the grayed out slider in Figure 7.6). An example of this sub VI can be seen in Figure 7.12. This VI was modified from its original format to solve an issue that was noticed during initial testing, which was that the automatic control did not work when the process variable was far away from its set point. The PID gains were tuned such that they were much too fast to allow the system to respond to large changes. This would cause scenarios where the valves would open or close entirely, creating very large spikes, or in the case of the gas bypass valves closing, would cause the flow to drop to a point that triggered a low pressure cutout. Figure 7.13 gives an example of the pressure response when the controller reacts of a value that is far from the set point. As such, an element was added to automatically lower the proportional gains, so that the controller would respond slower, allowing the system to react to its changes.

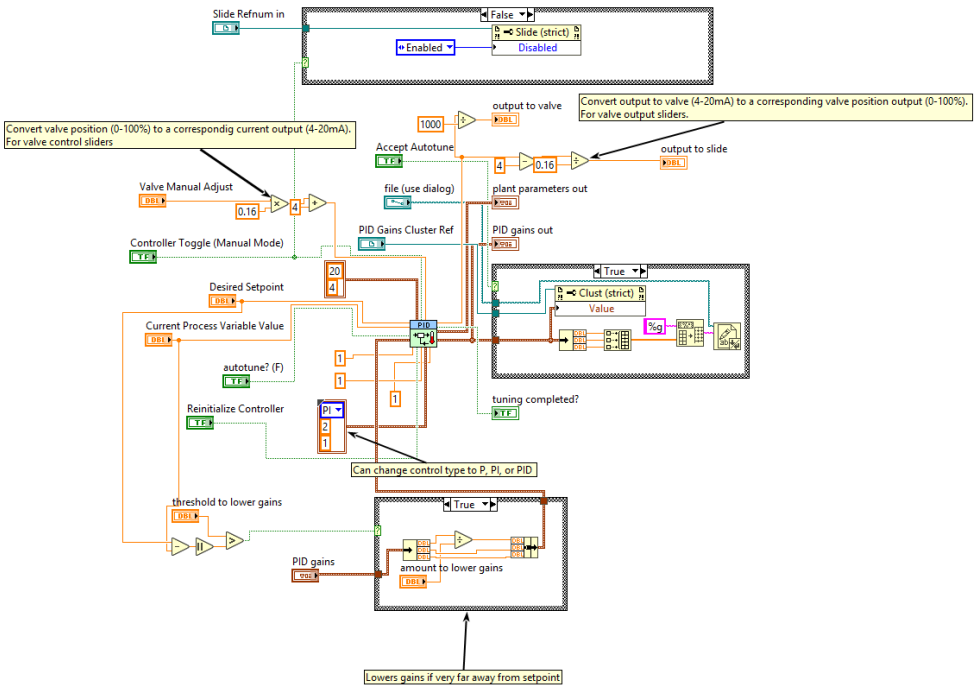

Figure 7.12: Suction pressure valve control code

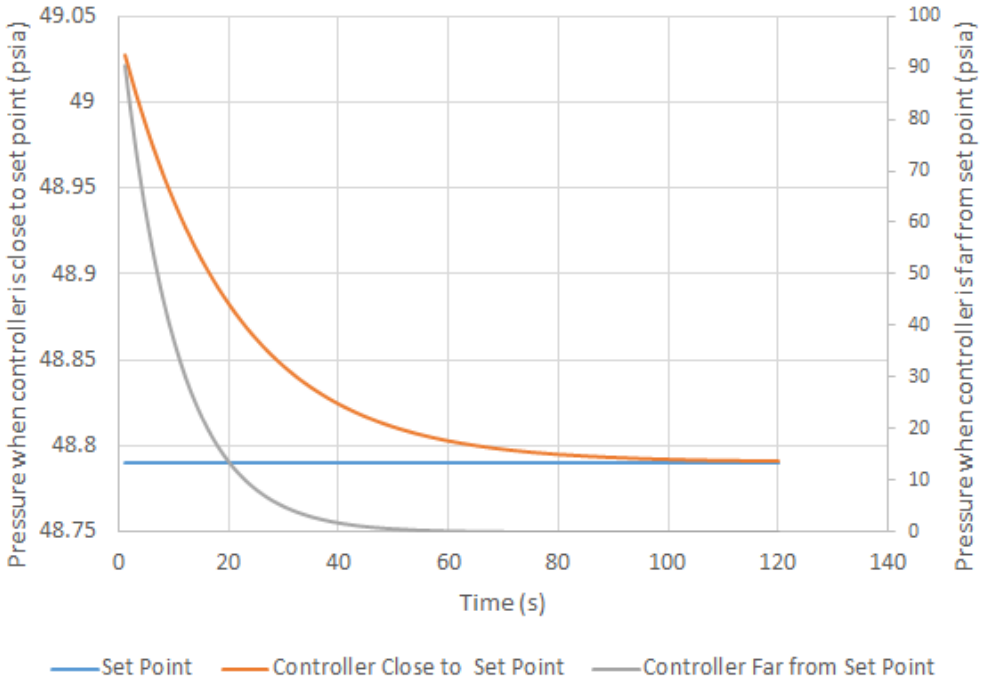

Figure 7.13: Illustration of response of gas valves when the pressure is too far from the set point, causing the pressure to drop too low

7.1.3 Use of bumpless transfer with controllers

Another important part of the control logic that was implemented was the use of bumpless transfer. When the controller is in manual mode, the analog output that controls the valve position will match what is input by the operator. This is the reason why each of the three valves in Figure 7.6 has two slide adjustments. The one on the left is the user input and the one on the right is the controller output. When the input is changed the output should be changed as well, and they should always match. However, if the controller is put into auto mode, the output will change while the input remains the same and there is a mismatch between the two. This becomes a problem when the controller is changed from auto to manual. In manual mode, the controller will be placed in the position that the input slider is in. Therefore, if the controller is changed from auto to manual, the valve position will simply revert back to its original position that is dictated by the input slider position. In order to avoid this, a bumpless transfer system must be implemented so that the output value is written to the input value so that the input value will change as the PID controller changes the output. To do this in LabVIEW, a Value Property Node created for the controller input is created, which reads the controller output data and writes that data to the valve adjust sliders. Figure 7.14 is an example of this being implemented with the automatic control of the small gas valve.

7.1.4 Water Line Controls

The next page on the Target VI is called "Water Control" and is where the adjustments to the water flow rate through the condensers are made. Figure 7.15 shows that there are four controllers on the water line. The furthest left in the figure is the bypass valve to the condensers. The second is an inline water valve to the condensers. The third is the water pump, and the fourth is a valve that acts as a bypass to the intermediate heat exchangers.

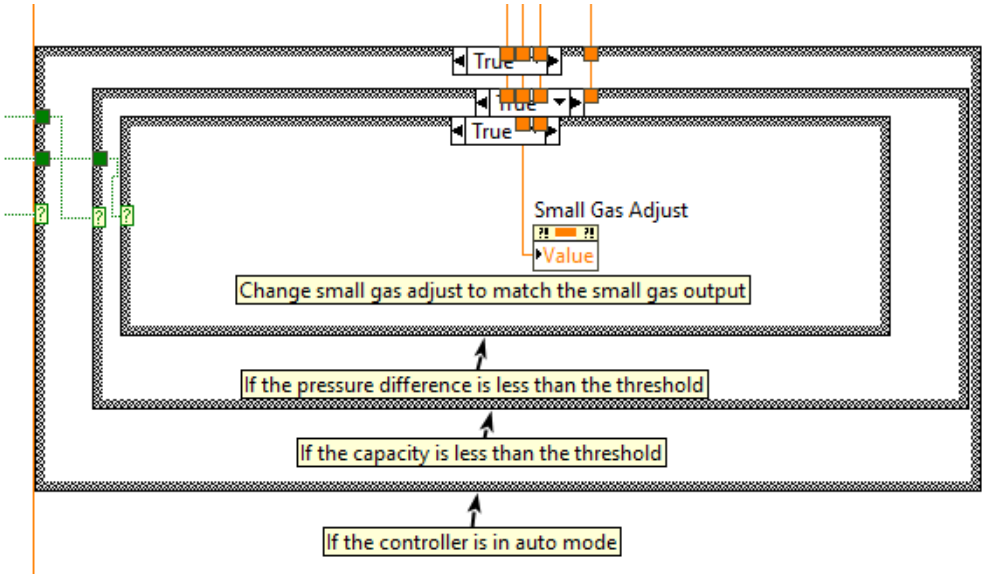

Figure 7.14: Example of bumpless transfer being implemented in LabVIEW

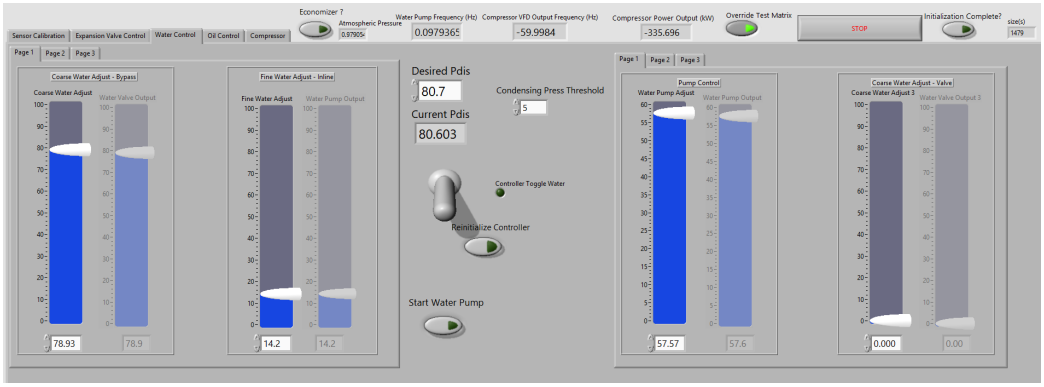

Figure 7.15: "Water Control" LabVIEW page

The condenser bypass and inline valves operate on PID control, in a similar manner to the gas bypass and liquid expansion valves do. The valve selection criteria for this is discussed in Section 2.3, with the only difference being the inline valve to the condensers now acts as the fine control, rather than the pump. An example of the bumpless transfer system on these valve can be seen in Appendix C.

7.1.5 Oil Line Controls

Figure 7.16 shows the next page on the Target VI, which is called "Oil Control" and is where the flow rate of return oil to the compressor is controlled. There are three

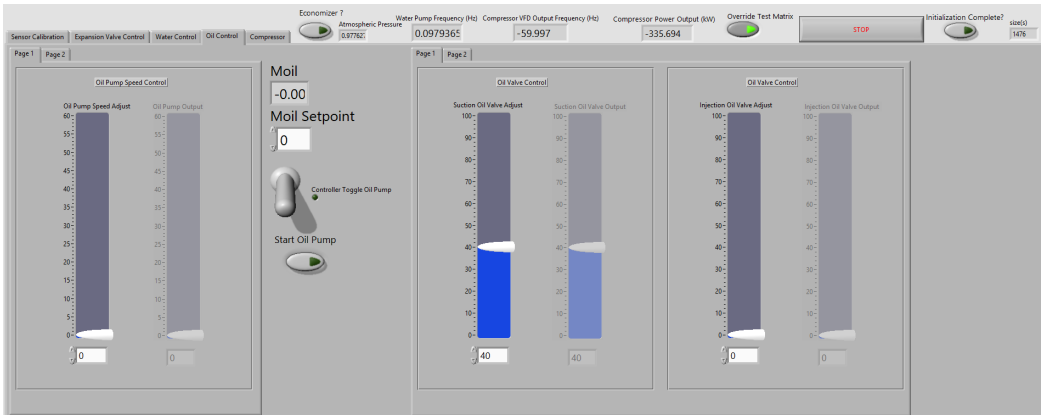

Figure 7.16: "Oil Control" LabVIEW page

different ways that the flow rate of oil can be controlled: through the changing of the oil pump speed when the oil pump is used, the use of a metering valve to control the flow rate into the suction line, and the use of another metering valve that controls the flow rate of oil injected into the compressor, if the compressor has an injection port.

All three methods of oil flow control are operated similarly to the previously discussed controllers. Generally, these controllers are only operated in manual mode, because oil return rates are typically not controlled as precisely as other process variables, so coarse adjustments will be sufficient to control the oil flow rate.

7.1.6 Compressor Control

The last page of the Target VI is where the speed of the compressor is controlled. It can be seen in Figure 7.17. On this page, the operator simply changes the output frequency of the VFD, which changes the rotational speed of the compressor. To start the compressor, place the speed adjustment slider into the desired position and press the "Start Compressor" button.

Because the compressor frequency, which is a controlled test condition, only relies on the VFD output, PID control is not used with the compressor. Any changes to the frequency are manual and will remain constant for the duration of each test condition.

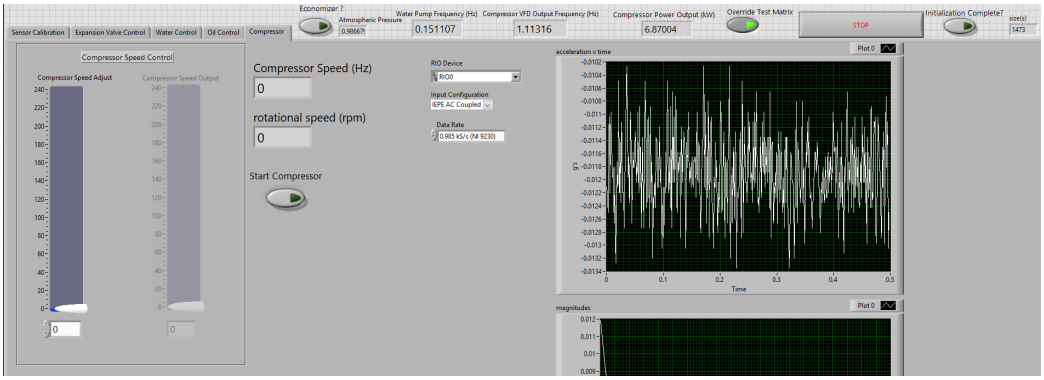

Figure 7.17: "Compressor" LabVIEW page

Some compressors will operate at a different range of speeds or input frequencies. Most compressors operate from 0-60 Hz. However, the 75 ton screw compressor that was tested operated, nominally, at 200 Hz. Thus, for different compressors, it may be necessary to change the range of compressor operating frequencies. Changing this range of frequencies requires that scaling factor of the 4-20mA signal that communicates with the VFD be changed as well. To change this scaling factor, the user can change the minimum and maximum speeds on the "Compressor Speed Adjust" slider and the code will automatically adjust the 4-20mA scaling factor. For the mA signal to correctly set the desired compressor speed, the VFD must be programmed to have the same range of speeds.

7.2 Host VI

The Host VI, seen in Figure 7.18, is where the data visualization and calculations take place. There are two pages on the Host VI: one that contains all the necessary information to record and save data, and one that displays all data and calculated values so the user can visualize the current conditions of the compressor load stand. The flow of data through the various VIs within the host can be visualized by Figure 7.19

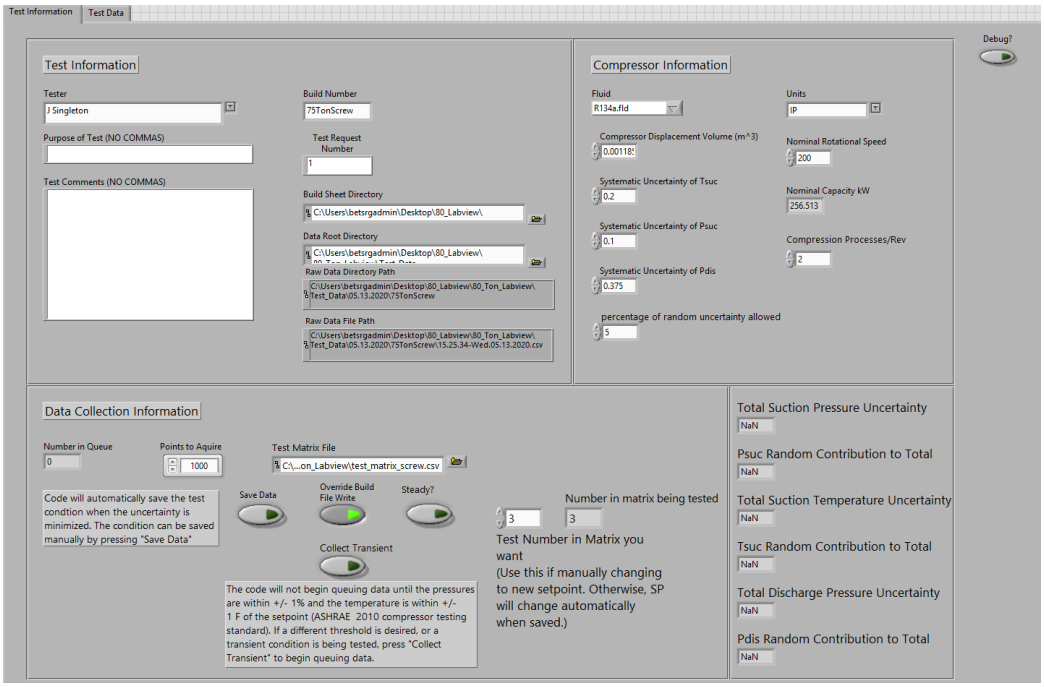

Figure 7.18: Host VI front page

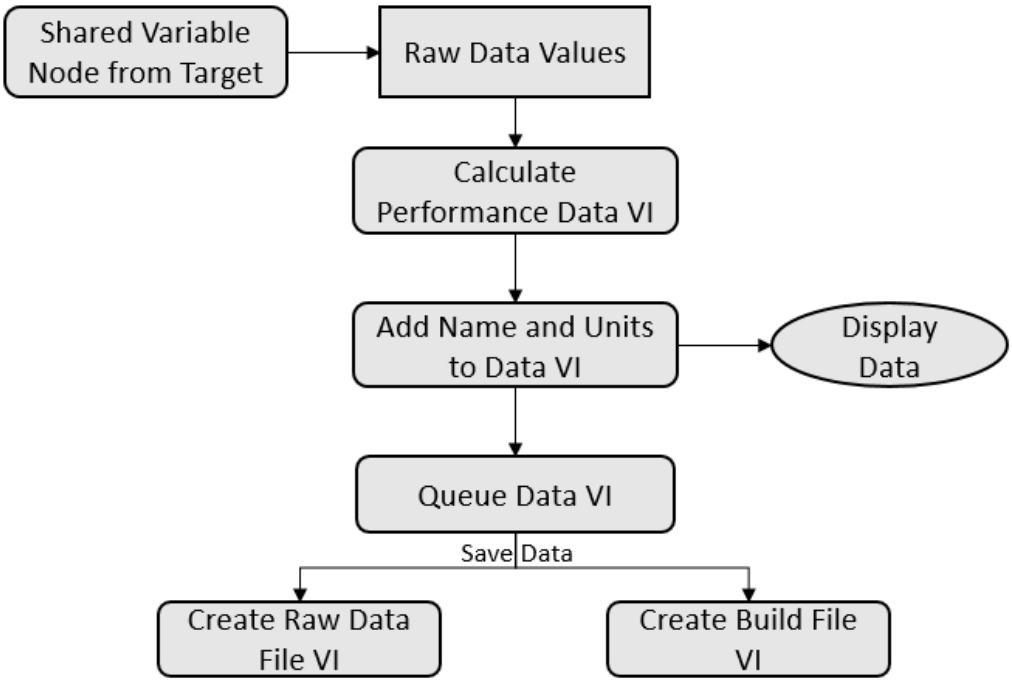

Figure 7.19: Flow of data through host VIs

7.2.1 Test Information

The "Test Information" page is the first page of the Host VI. On this page, the user can input and view the test information, the information about the compressor, the data collection information, and the total uncertainty of each process variable, as well as the amount of that which is random uncertainty.

In the upper left quadrant of the "Test Information" page, the user can input information about the test that will create and write to the raw data file and the build file. Figure 7.20 shows how the build files and raw data files are created from a saved test condition. A new raw data file is created each time a steady state condition is saved and contains every data point in the data queue, or every data point that was collected during the test. The build file contains the average values for each raw data file. There is one build file for each build number, which will contain a set of tests for a specific compressor. On this page of the VI the user can specify the paths for both the build file and the raw data file to be saved in. The user can also specify who is testing the compressor and for what purposes, as well as add any comments that are necessary, all of which will be added to the data files.

The upper right quadrant of this page contains information about the compressor. Here, the user can specify the fluid that is being used, which is necessary for calculating efficiency, superheat, subcooling, etc. The compressor displacement volume, which is needed for calculating volumetric efficiency can also be input. The nominal rotational speed of the compressor can be specified, as well, which will be used in a nominal capacity calculation. The systematic uncertainty of each of the three primary sensors is also specified here. These values should not change unless the sensor is replaced or re-calibrated for a different span.

In the lower left quadrant there is information about the points being tested. For each test condition, the maximum number of points that can be held in the data queue is specified. This number is typically set at 1000, but can be increased or decreased

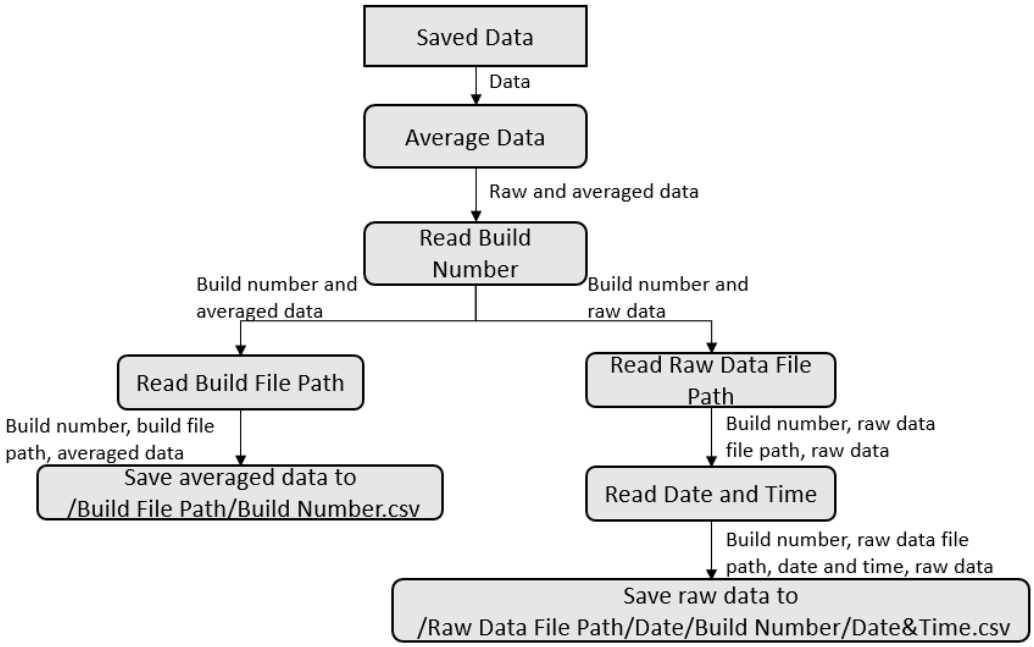

Figure 7.20: Flow chart of data flow of a saved test condition

as needed. Because the saving criteria is that all three of the primary variables have minimized random uncertainties, the data queue will often not be filled with all 1000 data points. The user can also select the file that in which the test matrix is found. The test matrix file contains the suction pressure, suction temperature, discharge pressure, and compressor speed for each test condition. For each condition, the Host VI will send those values to the Target VI and will automatically write them as the set points. When a condition is saved, the new set points will automatically become the values on the next line of the test matrix file. The operator can manually choose which point in the test matrix to run or can entirely override the test matrix by pressing the "Override Test Matrix" button located on the Target VI.

The lower right quadrant of this page shows the total uncertainty and the random uncertainty contribution for each of the primary variables in the data queue. The VI will not begin queuing the data until all three of the measurements are within the ASHRAE 23.1 specified ranges, unless the "Collect Transient" button has been pressed. Once the data begins queuing, the operators can watch the percentage of

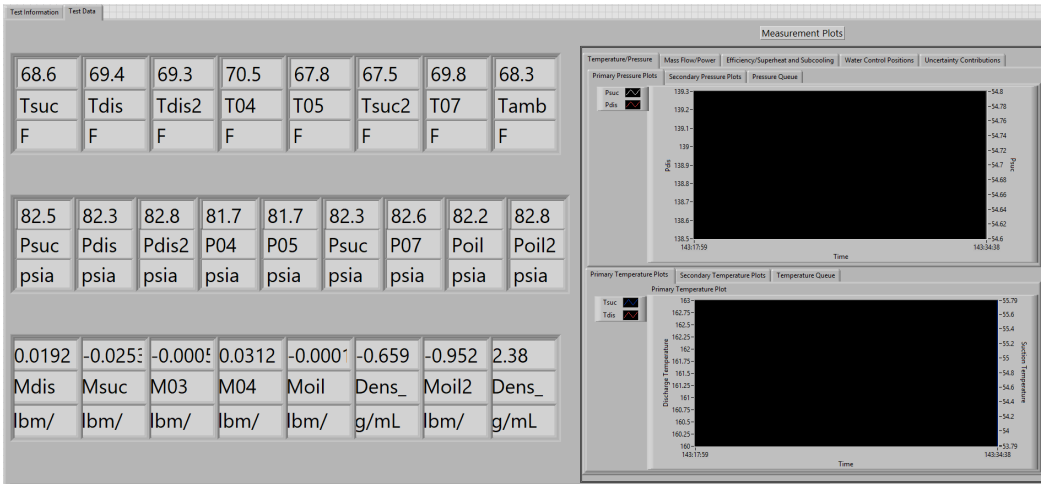

Figure 7.21: Host VI "Test Data" page

total uncertainty that is random and can save the data when they are satisfied with the results, or the VI will automatically save when all three variables have reached a random uncertainty contribution to total of 5% or less.

7.2.2 Test Data

The second page of the Host VI, seen in Figure 7.21 is called "Test Data". Here the raw data, as well as the calculated values are displayed numerically and graphically. The user can view all of the test data and can see how it changes over time. The plots are formatted to show every data point in the queue, so that the operator can visually determine if the test is reaching steady state or not.

7.3 Testing Best Practices

Over the course of the commissioning process of the compressor load stand, some best practices for testing have been identified, which will be useful for future operators to know. This section will discuss those practices and will give a general overview of how to run the compressor load stand.

7.3.1 Start-up

Before starting the compressor, it is always necessary to do a safety check on the load stand to ensure that it can run without any potential issues. Below is a checklist that should be followed before each time the load stand is started.

- Check all safety circuit components to make sure the safety loop is closed and the VFD's have no faults
- Check that all necessary ball valves are open. Make sure that there is a path for refrigerant to flow
- Check that there is oil in the sight glass of the separator
- Check that there is a path for oil to flow back to the compressor
- Put EXV and oil valves into position
- Make sure the water line has a path to circulate water

After each of these items has been checked off, the operator should start the water pump. Once the pump ramps up to its set speed, the compressor can be turned on.

While the compressor is ramping up to its set speed, the suction pressure will drop significantly. If the gas bypass valves are not opened enough, the pressure will drop too low, triggering a low pressure cutout. Because of this, the gas bypass valves should be set to a more open position. However, there does need to be some restriction in the bypass lines to create a pressure difference between the suction and discharge. With many compressors, the flow of oil is dependent on this pressure difference and it is necessary to start the flow of oil immediately. With these two factors affecting the start-up of the compressor, the gas bypass valves should be set at about 60-70% when the compressor is starting, until the initial pressure drop has ceased.

7.3.2 Reaching Steady State

After the initial rapid changes, upon start-up, the temperatures and pressures of the load stand will begin to level out. It is best to wait for this to occur before attempting to reach the set points. The most effective way to reach steady state quickly is to control the discharge pressure close to its set point first, so that the controller can be placed in auto. After the controller is in auto, the suction pressure and the suction temperature should be adjusted.

As previously discussed, the controllers have mechanisms that help to slow their response when far away from the set point. However, it is often much easier and quicker to adjust the temperature and pressures manually, initially, until the process variables are closer to their set points. When just one controller is far away from its set point, the automatic control can be relied on, more often. This is generally the case when the load stand is transitioning between conditions. However, when all three process variables are far away from their set points, the automatic control tends to work poorly.

There are some conditions at which the controllers do not reach the set point easily. They will rapidly oscillate around the set point, or will tend to stay a constant amount above or below the set point, the latter being the most common case. In these scenarios, the PID gains can be changed to help encourage the controllers to reach their set points. In general, adjusting the integral gain has been observed to be the most effective at enhancing the control of the load stand. In the case where the controller is oscillating about the set point, the integral term (T_i) should be increased. If the controller has a steady state error and holds at a position away from the set point, T_i should be decreased. The load stand can be sensitive to these changes, so adjustments should be small.

CHAPTER 8

Conclusions and Future Work

8.1 Conclusions

A controls system for a hot-gas bypass compressor load stand was created in order to quickly and accurately move between design conditions. Using a range of controls from coarse to fine, the stand is able to automatically reach test conditions for compressor capacities from 10-80 tons. A series of valves and pumps are controlled with an array of PI controllers, which were tuned during preliminary testing on a 40 ton scroll compressor with R134a as the working fluid. Initial tests were done with the load stand to determine its ability to maintain control over specified set points. It was found that accurate steady-state data was unobtainable without further tuning of controllers and resolving other reasons for instability, such as sensitivity of the conditions to changes caused by a cooling water temperature that was too low. By resolving the issues of instability, the system was able to significantly improve the testing time by minimizing random uncertainty to 5% of the total uncertainty in 275 samples, whereas previously, it was unable to reach that amount of uncertainty over a 1000 sample test period.

Furthermore, analysis was performed to determine which variables affected the amount of random uncertainty the most. The results of this analysis showed no strong correlation between any of the conditions and the amount of random uncertainty in the control variables, suggesting that improvements should be made to the PI controllers.

Additional tuning to the PI controllers was performed using tuning parameters

better suited for control of thermal systems. The results of this additional tuning yielded a much better ability to achieve accurate steady state results and a much faster testing time. With the new control strategy, the load stand is able to minimize steady state uncertainty in as little as 4.5 minutes and can transition between points rapidly.

With an optimized control strategy, the load stand was able to undergo commissioning tests with a 30 ton spool compressor and a 75 ton screw compressor. In the case of the 30 ton spool compressor, mixing of the gas and liquid proved to be insufficient. Modifications were made to the load stand which significantly improved the quality of mixing. In both cases, oil separation was a barrier to collecting good data, as it would artificially increase the measured mass flow rates. Upon addressing that issue, the load stand was able to collect data consistent with data that was provided by the manufacturers, for both compressors.

The results of these tests show that the load stand has been commissioned at 30 tons and at 75 tons. The load stand operates optimally and is able to produce accurate, reliable results.

8.2 Future Work

In the immediate future, the load stand will be used to test a 40 ton spool compressor which will be the first compressor that will be independently tested with the load stand to determine its performance metrics. In the future, the load stand will be used to test compressors with low-GWP refrigerants to test which, if any, can be a suitable drop-in replacement for the current HFCs, which are being phased out.

The load stand will likely need further modification to test compressors across its entire range of capacities and to properly utilize its capabilities. With the modifications to the mixing section that were already made, the quality of mixing was significantly improved. However, with compressors at lower capacities, the mixing is

likely to worsen. Even after the mixing sections were modified, there was significant difficulty in achieving a matching suction and discharge mass flow when testing the 30 ton spool compressor. It is unlikely that the load stand will be able to perform optimally with a compressor smaller than 30 tons. As such, new strategies to mitigate the problem should be investigated. One possible solution is to test at 40°R of superheat, or above. This would decrease the amount of liquid needed to mix with the bypassed gas, and would improve mixing. However, since this is not likely to be feasible for all scenarios, a different solution is to move the suction flow meter to just downstream of the discharge flow meter, where the flow is still entirely vapor. Another option is to replace the Coriolis meter with a turbine flow meter, which would be able to measure accurate volume flow rates even if the flow is two-phase. The mass flow, then, could be calculated with the density at suction, which is found based on the temperature and pressure measurements.

The next modification to be made is to rebuild the economizer line. After initial testing of the economizer and upon investigating the model on which the line sizing was based, it appears that significantly more mass flow is needed for economization than originally anticipated. Because of this, the economizer line tubing and valves should be rebuilt at a bigger size, to allow more mass flow through that circuit. The initial testing of the economizer line showed that the maximum flow through the economizer gas was about 80 lbm/min, which was not enough to reach the economizer pressure set point. The tubing and valves should be sized so that it can handle close to 100 lbm/min. Likewise, the economizer liquid line only allowed for a maximum of about 12 lbm/min of flow, which was not nearly enough to reach the temperature set point. This being the case, the tubing and valves on the economizer liquid line should be sized to handle about 20 lbm/min of flow.

References

Abernethy, R. B., Benedict, R. P., and Dowdell, R. B. (1985). ASME measurement uncertainty. *Journal of Fluids Engineering, Transactions of the ASME*, 107(2):161–164.

AHRI-Standard-540-2015 (2015). Performance rating of positive displacement refrigerant compressors and compressor units.

ASHRAE-23.1 (2010). Methods of Testing for Rating the Performance of Positive Displacement Refrigerant Compressors and Condensing Units That Operate at Subcritical Temperatures. Technical report, American Society of Heating, Refrigeration, and Air Conditioning Engineers.

ASHRAE-23.2 (2014). Methods of Test for Rating the Performance of Positive Displacement Compressors that Operate at Supercritical Pressures of the Refrigerant. Technical report.

Bradshaw, C. R., Groll, E. A., and Garimella, S. V. (2011). A comprehensive model of a miniature-scale linear compressor for electronics cooling. *International Journal of Refrigeration*, 34(1):63 – 73.

Elliott, C., Vijayakumar, V., Zink, W., and Hansen, R. (2007). National Instruments LabVIEW: A Programming Environment for Laboratory Automation and Measurement. *Journal of Laboratory Automation*, 12(1):17–24.

Flesch, R. C. and Normey-Rico, J. E. (2010). Modelling, identification and control of a calorimeter used for performance evaluation of refrigerant compressors. *Control Engineering Practice*, 18(3):254 – 261.

Hubacher, B., Groll, E., and Hoffinger, C. (2002). Performance measurements of a semi-hermetic carbon dioxide compressor.

Marcinichen, J. B., Holanda, T. N. d., and Melo, C. (2008). A dual siso controller for a vapor compression refrigeration system.

Marriott, L., Lady, E., and Evans, L. (1974). Accelerated test for rating positive displacement refrigeration compressors using computer control.

Marriott, L. W. (1973). *Control of a Refrigeration Compressor Calorimeter for Minimum Testing Time*. Phd dissertation, University of Michigan.

McGovern, J. (1984). Analysis of a refrigerant compressor load stand incorporating hot gas bypass and a single full condensation heat exchanger.

Moesch, T. W., Bahman, A. M., and Groll, E. A. (2016). Performance testing of a vapor injection scroll compressor with r407c.

Orosz, J., Bradshaw, C. R., Kemp, G., and Groll, E. A. (2014). An update on the performance and operating characteristics of a novel rotating spool compressor.

Salazar, M. and Méndez, F. (2014). Pid control for a single-stage transcritical co2 refrigeration cycle. *Applied Thermal Engineering*, 67(1):429 – 438.

Salts, N. P., Rohleder, C., Groll, E. A., Chretien, L., Yang, B., and Becerra, R. (2019). Performance testing of a dual rotary compressor with a variable speed PSC motor. *IOP Conference Series: Materials Science and Engineering*, 604:012058.

Sathe, A., Groll, E., and Garimella, S. (2008). Experimental Evaluation of a Miniature Rotary Compressor for Application in Electronics Cooling. Technical report.

Schmidt, D., Singleton, J., and Bradshaw, C. (2019). Development of a light-commercial compressor load stand to measure compressor performance using low-GWP refrigerants. *International Journal of Refrigeration*, 100.

Singh, G., Zaheer-uddin, M., and Patel, R. (2000). Adaptive control of multivariable thermal processes in hvac systems. *Energy Conversion and Management*, 41(15):1671 – 1685.

Skogestad, S. (2004). Simple Analytic Rules for Model Reduction and PID Controller Tuning Simple analytic rules for model reduction and PID. *Journal of Process Control*, 14(4).

Tyreus, B. D. and Luyben, W. L. (1992). Tuning PI Controllers for Integrator/Dead Time Processes. *Industrial and Engineering Chemistry Research*, 31(11):2625–2628.

Wenzel, M., Elbel, S., and Hrnjak, P. (2016). Design, build-up, and commissioning of 350 kw refrigeration test facility for experimental investigation of large cold chain equipment.

Ziegler, J. G. and Nichols, N. B. (1985). Optimum Settings for Automatic Controllers. *Journal of Dynamic Systems, Measurement, and Control*, 115(2B):220.

APPENDIX A

Python Single Test Condition Analysis Code

```
# -*- coding: utf-8 -*-
import numpy as np
import pandas as pd
import matplotlib.pyplot as plt
import csv
import glob2
from matplotlib.backends.backend_pdf import PdfPages
import os
for name in glob2.glob('*.csv'):
    print(name)
    x,y=[[],[]]
    file1, ext=os.path.splitext(name)
    Filename=str(file1)+'.csv'
    df=pd.read_csv(Filename,skiprows=12)
    columns=df.dtypes.index
    Psuc=np.array(df[columns[0]])*6.895
    Tsuc=(np.array(df[columns[1]])-32)*(5/9)
    Pdis=np.array(df[columns[2]])*6.895
    Tdis=np.array(df[columns[3]])
    DT_sup=np.array(df[columns[28]])
    DT_sub=np.array(df[columns[29]])
    w=np.array(df[columns[6]])

    t=np.arange(1,1000)
    P_s=np.ones(999)*60.17*6.895     # *6.895 to convert psi to kPa
    P_d=np.ones(999)*119.1*6.895     # *6.895 to convert psi to kPa
    T_s=((np.ones(999)*70)-32)*(5/9)  # (T-32)*(5/9) to convert F to C
    DT_s=np.ones(999)*20
    ti=t/(0.37*60)

    plt.figure(figsize=(10,6.5))
    plt.plot(ti,Psuc, '.', label = 'Measured suction pressure')
    plt.plot(ti,P_s,'g', label = 'Suction pressure set point')
    plt.plot(ti,P_s+(0.1*6.895),'r--',
             label = 'Systematic uncertainty band')
    plt.plot(ti,P_s-(0.1*6.895),'r--')
    plt.xlabel('Time (minutes)', fontsize=22)
```

```
plt.ylabel('Suction Pressure (kPa)', fontsize=22)
#plt.title('Suction Pressure')
plt.xticks(np.arange(min(ti)-0.045, max(ti)+1, 5))
plt.xticks(fontsize = 20)
plt.yticks(fontsize = 20)
plt.legend(fontsize = 14)
plt.text(12, 415.8, '+/-0.689kPa', horizontalalignment='right',
        fontsize = 14)
plt.arrow(12, 415.8, 4, -.23)
plt.arrow(12, 415.8, 4, -1.6)
plt.show()

plt.figure(figsize=(10,6.5))
plt.plot(ti,Tsuc, '.', label = 'Measured suction temperature')
plt.plot(ti,T_s,'g', label = 'Suction temperature set point')
plt.plot(ti,T_s+0.11,'r--', label = 'Systematic uncertainty band')
plt.plot(ti,T_s-0.11,'r--')
plt.xlabel('Time (minutes)', fontsize=22)
plt.ylabel('Suction Temperature (C)', fontsize=22)
#plt.title('Suction Temperature')
plt.xticks(np.arange(min(ti)-0.045, max(ti)+1, 5))
plt.xticks(fontsize = 20)
plt.yticks(fontsize = 20)
plt.legend(fontsize = 14)
plt.text(25, 21.12, '+/-0.11C', horizontalalignment='right',
        fontsize = 14)
plt.arrow(25, 21.12, 4, .1)
plt.arrow(25, 21.12, 4, -.118)
plt.show()

plt.figure(figsize=(10,6.5))
plt.plot(ti,Pdis, '.', label = 'Measured discharge pressure')
plt.plot(ti,P_d,'g', label = 'Discharge pressure set point')
plt.plot(ti,P_d+(0.375*6.895),'r--',
        label = 'Systematic uncertainty band')
plt.plot(ti,P_d-(0.375*6.895),'r--')
plt.xlabel('Time (minutes)', fontsize=22)
plt.ylabel('Discharge Pressure (kPa)', fontsize=22)
#plt.title('Suction Pressure')
plt.xticks(np.arange(min(ti)-0.045, max(ti)+1, 5))
plt.xticks(fontsize = 20)
plt.yticks(fontsize = 20)
plt.legend(fontsize = 14)
plt.text(12, 824.5, '+/-2.59kPa', horizontalalignment='right',
        fontsize = 14)
```

```
plt.arrow(12, 824.5, 6, -.7)
plt.arrow(12, 824.5, 6, -5.9)
plt.show()

with PdfPages('50E-90C-20S.pdf') as pdf:
    plt.figure(1)
    plt.plot(t,Psuc)
    plt.plot(t,P_s)
    plt.plot(t,P_s+0.1,'r')
    plt.plot(t,P_s-0.1,'r')
    plt.xlabel('Number of Samples')
    plt.ylabel('Suction Pressure (psi)')
    plt.title('Suction Pressure')
    pdf.savefig()
    plt.close()

    plt.figure(2)
    plt.plot(t,Pdis)
    plt.plot(t,P_d)
    plt.plot(t,P_d+0.375,'r')
    plt.plot(t,P_d-0.375,'r')
    plt.xlabel('Number of Samples')
    plt.ylabel('Discharge Pressure (psi)')
    plt.title('Discharge Pressure')
    pdf.savefig()
    plt.close()

    plt.figure(3)
    plt.plot(t,Tsuc)
    plt.plot(t,T_s)
    plt.plot(t,T_s+0.2,'r')
    plt.plot(t,T_s-0.2,'r')
    plt.xlabel('Number of Samples')
    plt.ylabel('Suction Temperature (F)')
    plt.title('Suction Temperature')
    pdf.savefig()
    plt.close()

    plt.figure(4)
    plt.plot(t,Tsuc)
    plt.plot(t,T_s)
    plt.plot(t,T_s+1.8,'r')
    plt.plot(t,T_s-1.8,'r')
    plt.xlabel('Number of Samples')
    plt.ylabel('Suction Temperature (F)')
```

```
plt.title('Suction Temperature with ASHRAE Standard')
pdf.savefig()
plt.close()

plt.figure(5)
plt.plot(t,Tdis)
plt.title('Discharge Temperature')
pdf.savefig()
plt.close()

plt.figure(6)
plt.plot(t,DT_sup)
plt.plot(t,DT_s)
plt.plot(t,DT_s+0.2,'r')
plt.plot(t,DT_s-0.2,'r')
plt.title('Superheat')
pdf.savefig()
plt.close()

plt.figure(7)
plt.plot(t,DT_sub)
plt.title('Subcooling')
pdf.savefig()

plt.figure(8)
plt.plot(t,w)
plt.title('Compressor Speed')
pdf.savefig()
plt.close()
```

APPENDIX B

Python Uncertainty Analysis for Scroll Compressor Tests

```
import pandas as pd
from pandas import ExcelWriter
import numpy as np
import matplotlib.pyplot as plt
import glob2
import os
import xlrd
from os.path import join
from glob2 import glob
import datetime as dt
import statistics as st
from matplotlib.backends.backend_pdf import PdfPages
from scipy.stats import ttest_ind
from sklearn.linear_model import LinearRegression
from mlxtend.plotting import plot_linear_regression

x,y,w,z=[[],[],[],[]]
y=[]
Pdis_uncert=[]
Psuc_uncert=[]
Tsuc_uncert=[]
Pdis_tot=[]
Psuc_tot=[]
Tsuc_tot=[]
Pdis_perc=[]
Psuc_perc=[]
Tsuc_perc=[]
T_cond=[]
BP=[]
WP=[]
Twi=[]
DT_sub=[]
T_evap=[]
SG=[]
SL=[]
MG=[]
ML=[]
```

```
writer = ExcelWriter('total_uncertainty.xlsx')
for name in glob2.glob('**/*'):
    if name.endswith((".csv")):
        #print(name)
        ##if "comp" in name:
        file1, ext=os.path.splitext(name)
        Filename=str(file1)+'.csv'
        df=pd.read_csv(Filename,
                       skiprows =
                       [0,1,2,3,4,5,6,7,8,9,11])
        #columns=df.dtypes.index
        #x.append(df.index)
        #y.append(np.array(df[columns[3]]))
        df1 = pd.DataFrame(df,
                           columns=
                           [u'Psuc', u'Tsuc', u'Pdis',
                            u'Twi', u'Twe',
                            u'Bypass_Position',
                            u'Water_Pump_Speed',
                            u'DT_sub', u'SG', u'SL',
                            u'MG', u'ML'])

        # Create variables for columns
        Psuc = df1[u'Psuc']
        Tsuc = df1[u'Tsuc']
        Pdis = df1[u'Pdis']
        Twi.append(df1[u'Twi'].mean())
        Twe = df1[u'Twe']
        BP.append(df1[u'Bypass_Position'].mean())
        WP.append(df1[u'Water_Pump_Speed'].mean())
        DT_sub.append(df1[u'DT_sub'].mean())
        SG.append(df1[u'SG'].mean())
        SL.append(df1[u'SL'].mean())
        MG.append(df1[u'MG'].mean())
        ML.append(df1[u'ML'].mean())

        if '70C' in name:
            T_cond.append(21.11)
        elif '80C' in name:
            T_cond.append(26.67)
        elif '90C' in name:
            T_cond.append(32.22)
        elif '100C' in name:
            T_cond.append(37.78)
        elif '110C' in name:
```

```
            T_cond.append(43.33)
        elif '120C' in name:
            T_cond.append(48.89)
        elif '130C' in name:
            T_cond.append(54.44)

        if '45E' in name:
            T_evap.append(7.22)
        elif '50E' in name:
            T_evap.append(10)
        elif '40E' in name:
            T_evap.append(4.44)
        elif '30E' in name:
            T_evap.append(-1.11)
        elif '20E' in name:
            T_evap.append(-6.67)
        elif '10E' in name:
            T_evap.append(-12.22)

        # Calculate averages for key variables
        Ps_avg = df1[u'Psuc'].mean()
        Ts_avg = df1[u'Tsuc'].mean()
        Pd_avg = df1[u'Pdis'].mean()
        N = len(df1[u'Psuc'])
        sumPs=0
        sumTs=0
        sumPd=0

        #calculate standard deviation
        for i in range(N):
            sumPs+=((Psuc[i]-Ps_avg)**2)/(N-1)
            sumTs+=((Tsuc[i]-Ts_avg)**2)/(N-1)
            sumPd+=((Pdis[i]-Pd_avg)**2)/(N-1)
        s_x_Psuc=np.sqrt(sumPs)
        s_x_Tsuc=np.sqrt(sumTs)
        s_x_Pdis=np.sqrt(sumPd)
##          print("s_x_Psuc=",s_x_Psuc)
##          print("s_x_Tsuc=",s_x_Tsuc)
##          print("s_x_Pdis=",s_x_Pdis)

        # Calculate random uncertainty
        s_Psuc=(s_x_Psuc/np.sqrt(N))*6.895
        s_Tsuc=s_x_Tsuc/np.sqrt(N)
        s_Pdis=(s_x_Pdis/np.sqrt(N))*6.895
        Psuc_uncert.append(s_Psuc)
```

```
            Tsuc_uncert.append(s_Tsuc)
            Pdis_uncert.append(s_Pdis)
##              print("s_Psuc=",s_Psuc)
##              print("s_Tsuc=",s_Tsuc)
##              print("s_Pdis=",s_Pdis)

            # Systematic uncertainty
            sigma_sys_Ps=0.1*6.895
            sigma_sys_Pd=0.375*6.895
            sigma_sys_T=0.2

            # total uncertainty
            u_Psuc=np.sqrt((s_Psuc**2)+(sigma_sys_Ps**2))
            u_Tsuc=np.sqrt((s_Tsuc**2)+(sigma_sys_T**2))
            u_Pdis=np.sqrt((s_Pdis**2)+(sigma_sys_Pd**2))

            # Calculate random uncertainty according to ASHRAE 23.1
            Psuc_tot.append((u_Psuc))
            Tsuc_tot.append(u_Tsuc)
            Pdis_tot.append((u_Pdis))

            #Calculate random uncertainty as a percentage of total
            #uncertainty
            Pdis_perc.append((s_Pdis/u_Pdis)*100)
            Psuc_perc.append((s_Psuc/u_Psuc)*100)
            Tsuc_perc.append((s_Tsuc/u_Tsuc)*100)

            print(Filename[:-4], 'total uncertainty')
            print('Psuc = ',Ps_avg,'\u00B1',u_Psuc)
            print('Tsuc = ',Ts_avg,'\u00B1',u_Tsuc)
            print('Pdis = ',Pd_avg,'\u00B1',u_Pdis)

            data = {'Random':[s_Psuc, s_Tsuc, s_Pdis],
                    'Total':[u_Psuc, u_Tsuc, u_Pdis]}
            d = pd.DataFrame(data,
                             index = ['Psuc', 'Tsuc', 'Pdis'],
                             columns=['Random', 'Total'])
            d.to_excel(writer, '%s'
                       % os.path.basename(Filename[:-4]))

writer.save()
print("")
print('Average total uncertainty across all measurements')
print('Suction Pressure—', 'Average:',
      np.mean(Psuc_tot),
```

```
        'Standard Deviation:', st.stdev(Psuc_tot))
print('Suction Temperature—', 'Average:',
        np.mean(Tsuc_tot),
        'Standard Deviation:', st.stdev(Tsuc_tot))
print('Discharge Pressure—', 'Average:',
        np.mean(Pdis_tot),
        'Standard Deviation:', st.stdev(Pdis_tot))

print("")
print('Average random uncertainty across all measurements')
print('Suction Pressure—', 'Average:',
        np.mean(Psuc_uncert),
        'Standard Deviation:', st.stdev(Psuc_uncert))
print('Suction Temperature—', 'Average:',
        np.mean(Tsuc_uncert),
        'Standard Deviation:', st.stdev(Tsuc_uncert))
print('Discharge Pressure—', 'Average:',
        np.mean(Pdis_uncert),
        'Standard Deviation:', st.stdev(Pdis_uncert))

print("")
print('Max uncertainty')
print('Suction Pressure—', 'Random:',
        np.max(Psuc_uncert),
        'Total:', np.max(Psuc_tot))
print('Discharge Pressure—', 'Random:',
        np.max(Pdis_uncert),
        'Total:',np.max(Pdis_tot))
print('Suction Temperature—', 'Random:',
        np.max(Tsuc_uncert),
        'Total:',np.max(Tsuc_tot))

print("")
print('Min uncertainty')
print('Suction Pressure—', 'Random:',
        np.min(Psuc_uncert),
        'Total:',np.min(Psuc_tot))
print('Discharge Pressure—', 'Random:',
        np.min(Pdis_uncert),
        'Total:',np.min(Pdis_tot))
print('Suction Temperature—', 'Random:',
        np.min(Tsuc_uncert),
        'Total:',np.min(Tsuc_tot))

T_cond1 = np.array([T_cond])
```

```
Pdis_uncert1 = np.array([Pdis_uncert])
print(T_cond1)
print(Pdis_uncert1)

with PdfPages('Condensing Temp v Pdis.pdf') as pdf:
    plt.figure(figsize=(10,8))
    plt.scatter(T_cond, Pdis_perc,
                label = 'Test Data')
    z = np.polyfit(T_cond, Pdis_perc, 1)
    p = np.poly1d(z)
    plt.plot(T_cond, p(T_cond), "r-",
             label = 'Linear Regression')
    plt.xlabel('Condensing Temperature (C)',
               fontsize = 22)
    plt.ylabel(' Discharge Pressure Random '
               'Uncertainty (% of total)',
               fontsize = 22)
    plt.xticks(Fontsize = 20)
    plt.yticks(fontsize = 20)
    plt.legend(fontsize = 16)
    pdf.savefig()
    plt.show()
    plt.close()

    plt.figure(figsize=(10,8))
    plt.scatter(T_cond, Psuc_perc,
                label = 'Test Data')
    z = np.polyfit(T_cond, Psuc_perc, 1)
    p = np.poly1d(z)
    plt.plot(T_cond, p(T_cond), "r-",
             label = 'Linear Regression')
    plt.xlabel('Condensing Temperature (C)',
               fontsize = 22)
    plt.ylabel(' Suction Pressure Random '
               'Uncertainty (% of total)',
               fontsize = 22)
    plt.xticks(Fontsize = 20)
    plt.yticks(fontsize = 20)
    plt.legend(fontsize = 16)
    pdf.savefig()
    plt.show()
    plt.close()

    plt.figure(3)
    plt.scatter(T_cond, Tsuc_perc)
```

```
    z = np.polyfit(T_cond, Tsuc_perc, 1)
    p = np.poly1d(z)
    plt.plot(T_cond, p(T_cond), "r-")
    plt.xlabel('Condensing Temperature [F]')
    plt.ylabel(' Suction Temperature Random '
               'Uncertainty (F)')
    pdf.savefig()
    plt.close()

with PdfPages('Evaporating Temp v Pdis.pdf') as pdf:
    plt.figure(figsize=(10,8))
    plt.scatter(T_evap, Pdis_perc,
                label = 'Test Data')
    z = np.polyfit(T_evap, Pdis_perc, 1)
    p = np.poly1d(z)
    plt.plot(T_evap, p(T_evap), "r-",
             label = 'Linear Regression')
    plt.xlabel('Evaporating Temperature (C)',
               fontsize = 22)
    plt.ylabel(' Discharge Pressure Random '
               'Uncertainty (% of total)',
               fontsize = 22)
    plt.xticks(Fontsize = 20)
    plt.yticks(fontsize = 20)
    plt.legend(fontsize = 16)
    pdf.savefig()
    plt.show()
    plt.close()

    plt.figure(figsize=(10,8))
    plt.scatter(T_evap, Psuc_perc,
                label = 'Test Data')
    z = np.polyfit(T_evap, Psuc_perc, 1)
    p = np.poly1d(z)
    plt.plot(T_evap, p(T_evap), "r-",
             label = 'Linear Regression')
    plt.xlabel('Evaporating Temperature (C)',
               fontsize = 22)
    plt.ylabel(' Suction Pressure Random '
               'Uncertainty (% of total)',
               fontsize = 22)
    plt.xticks(Fontsize = 20)
    plt.yticks(fontsize = 20)
    plt.legend(fontsize = 16)
    pdf.savefig()
```

```
    plt.show()
    plt.close()

    plt.figure(3)
    plt.scatter(T_evap, Tsuc_perc)
    z = np.polyfit(T_evap, Tsuc_perc, 1)
    p = np.poly1d(z)
    plt.plot(T_evap, p(T_evap), "r-")
    plt.xlabel('Evaporating Temperature [F]')
    plt.ylabel(' Suction Temperature Random '
               'Uncertainty (F)')
    pdf.savefig()
    plt.close()

with PdfPages('Bypass Valve Position.pdf') as pdf:
    plt.figure(1)
    plt.scatter(BP, Pdis_perc)
    z = np.polyfit(BP, Pdis_perc, 1)
    p = np.poly1d(z)
    plt.plot(BP, p(BP), "r-")
    plt.xlabel('Bypass Valve Position (%)')
    plt.ylabel(' Discharge Pressure Random '
               'Uncertainty (psi)')
    pdf.savefig()
    #plt.show()
    plt.close()

    plt.figure(2)
    plt.scatter(BP, Psuc_perc)
    z = np.polyfit(BP, Psuc_perc, 1)
    p = np.poly1d(z)
    plt.plot(BP, p(BP), "r-")
    plt.xlabel('Bypass Valve Position (%)')
    plt.ylabel(' Suction Pressure Random '
               'Uncertainty (psi)')
    pdf.savefig()
    #plt.show()
    plt.close()

    plt.figure(3)
    plt.scatter(BP, Tsuc_perc)
    z = np.polyfit(BP, Tsuc_perc, 1)
    p = np.poly1d(z)
    plt.plot(BP, p(BP), "r-")
    plt.xlabel('Bypass Valve Position (%)')
```

```
    plt.ylabel('␣Suction␣Temperature␣Random␣'
               'Uncertainty␣(F)')
    pdf.savefig()
    plt.close()

with PdfPages('Water␣Pump␣Speed.pdf') as pdf:
    plt.figure(1)
    plt.scatter(WP, Pdis_perc)
    z = np.polyfit(WP, Pdis_perc, 1)
    p = np.poly1d(z)
    plt.plot(WP, p(WP), "r-")
    plt.xlabel('Water␣Pump␣Speed␣(Hz)')
    plt.ylabel('␣Discharge␣Pressure␣Random␣'
               'Uncertainty␣(psi)')
    pdf.savefig()
    #plt.show()
    plt.close()

    plt.figure(2)
    plt.scatter(WP, Psuc_perc)
    z = np.polyfit(WP, Psuc_perc, 1)
    p = np.poly1d(z)
    plt.plot(WP, p(WP), "r-")
    plt.xlabel('Water␣Pump␣Speed␣(Hz)')
    plt.ylabel('␣Suction␣Pressure␣Random␣Uncertainty'
               '␣(psi)')
    pdf.savefig()
    #plt.show()
    plt.close()

    plt.figure(3)
    plt.scatter(WP, Tsuc_perc)
    z = np.polyfit(WP, Tsuc_perc, 1)
    p = np.poly1d(z)
    plt.plot(WP, p(WP), "r-")
    plt.xlabel('Water␣Pump␣Speed␣(Hz)')
    plt.ylabel('␣Suction␣Temperature␣Random␣Uncertainty'
               '␣(F)')
    pdf.savefig()
    plt.close()

with PdfPages('Inlet␣Water␣Temperature.pdf') as pdf:
    plt.figure(1)
    plt.scatter(Twi, Pdis_perc)
    z = np.polyfit(Twi, Pdis_perc, 1)
```

```
    p = np.poly1d(z)
    plt.plot(Twi, p(Twi), "r-")
    plt.xlabel('Inlet Water Temperature (F)')
    plt.ylabel(' Discharge Pressure Random Uncertainty '
               '(psi)')
    pdf.savefig()
    #plt.show()
    plt.close()

    plt.figure(2)
    plt.scatter(Twi, Psuc_perc)
    z = np.polyfit(Twi, Psuc_perc, 1)
    p = np.poly1d(z)
    plt.plot(Twi, p(Twi), "r-")
    plt.xlabel('Inlet Water Temperature (F)')
    plt.ylabel('Suction Pressure Random Uncertainty'
               ' (psi)')
    pdf.savefig()
    #plt.show()
    plt.close()

    plt.figure(3)
    plt.scatter(Twi, Tsuc_perc)
    z = np.polyfit(Twi, Tsuc_perc, 1)
    p = np.poly1d(z)
    plt.plot(Twi, p(Twi), "r-")
    plt.xlabel('Inlet Water Temperature (F)')
    plt.ylabel('Suction Temperature Random Uncertainty (F)')
    pdf.savefig()
    plt.close()

with PdfPages('Subcooling.pdf') as pdf:
    plt.figure(1)
    plt.scatter(DT_sub, Pdis_perc)
    z = np.polyfit(DT_sub, Pdis_perc, 1)
    p = np.poly1d(z)
    plt.plot(DT_sub, p(DT_sub), "r-")
    plt.xlabel('Subcooling (F)')
    plt.ylabel(' Discharge Pressure Random Uncertainty (psi)')
    pdf.savefig()
    #plt.show()
    plt.close()

    plt.figure(2)
    plt.scatter(DT_sub, Psuc_perc)
```

```
    z = np.polyfit(DT_sub, Psuc_perc, 1)
    p = np.poly1d(z)
    plt.plot(DT_sub, p(DT_sub), "r--")
    plt.xlabel('Subcooling (F)')
    plt.ylabel('Suction Pressure Random Uncertainty (psi)')

    pdf.savefig()
    plt.close()

    plt.figure(3)
    plt.scatter(DT_sub, Tsuc_perc)
    z = np.polyfit(DT_sub, Tsuc_perc, 1)
    p = np.poly1d(z)
    plt.plot(DT_sub, p(DT_sub), "r--")
    plt.xlabel('Subcooling (F)')
    plt.ylabel('Suction Temperature Random Uncertainty (F)')
    pdf.savefig()
    #plt.show()
    plt.close()


import statsmodels.api as sm
data = {'Discharge Pressure Uncertainty': Pdis_perc,
    'Suction Pressure Uncertainty': Psuc_perc,
    'Suction Temperature Uncertainty': Tsuc_perc,
    'Condensing Temperature': T_cond,
    'Water Pump Speed': WP, 'Bypass Valve Position': BP,
    'Condenser Water Inlet Temperature': Twi,
    'Evaporating Temperature': T_evap, 'Subcooling': DT_sub,
    'Small Gas Expansion Valve Position': SG,
    'Small Liquid Expansion Valve Position': SL,
    'Medium Gas Expansion Valve Position': MG,
    'Medium Liquid Expansion Valve Position': ML}
df2 = pd.DataFrame(data,
        columns=['Discharge Pressure Uncertainty',
            'Suction Pressure Uncertainty',
        'Suction Temperature Uncertainty',
            'Condensing Temperature',
        'Water Pump Speed',
            'Bypass Valve Position',
            'Condenser Water Inlet Temperature',
            'Evaporating Temperature', 'Subcooling',
            'Small Gas Expansion Valve Position',
            'Small Liquid Expansion Valve Position',
            'Medium Gas Expansion Valve Position',
```

```
            'Medium Liquid Expansion Valve Position'])
y = df2['Condensing Temperature']
x = df2['Discharge Pressure Uncertainty']*1000000
model = sm.OLS(x, y).fit()
predictions = model.predict(x)
print(model.summary())
stat, p = ttest_ind(y, x)
print('Statistics = %.3f, p = %.3f' % (stat, p))
alpha = 0.05
if p > alpha:
    print('Same distributions')
else:
    print('different distributions')

y1 = df2['Water Pump Speed']
x1 = df2['Discharge Pressure Uncertainty']
model1 = sm.OLS(x1, y1).fit()
predictions1 = model1.predict(x1)
print(model1.summary())

y10 = df2['Water Pump Speed']
x10 = df2['Suction Pressure Uncertainty']
model10 = sm.OLS(x10, y10).fit()
predictions10 = model10.predict(x10)
print(model10.summary())

y2 = df2['Bypass Valve Position']
x2 = df2['Discharge Pressure Uncertainty']
model2 = sm.OLS(x2, y2).fit()
predictions2 = model2.predict(x2)
print(model2.summary())

y9 = df2['Bypass Valve Position']
x9 = df2['Suction Pressure Uncertainty']
model9 = sm.OLS(x9, y9).fit()
predictions9 = model9.predict(x9)
print(model9.summary())

y3 = df2['Condenser Water Inlet Temperature']
x3 = df2['Discharge Pressure Uncertainty']
model3 = sm.OLS(x3, y3).fit()
predictions3 = model3.predict(x3)
print(model3.summary())
stat3, p3= ttest_ind(x3, y3)
print('Statistics = %.3f, p = %.3f' % (stat3, p3))
```

```
if p3 > alpha:
    print('Same distributions')
else:
    print('different distributions')

y4 = df2['Evaporating Temperature']
x4 = df2['Discharge Pressure Uncertainty']
model4 = sm.OLS(x4, y4).fit()
predictions4 = model4.predict(x4)
print(model4.summary())

y5 = df2['Evaporating Temperature']
x5 = df2['Suction Pressure Uncertainty']
model5 = sm.OLS(x5, y5).fit()
predictions5 = model5.predict(x5)
print(model5.summary())

y6 = df2['Condensing Temperature']
x6 = df2['Suction Pressure Uncertainty']
model6 = sm.OLS(x6, y6).fit()
predictions6 = model6.predict(x6)
print(model6.summary())

y7 = df2['Condenser Water Inlet Temperature']
x7 = df2['Suction Pressure Uncertainty']
model7 = sm.OLS(x7, y7).fit()
predictions7 = model7.predict(x7)
print(model7.summary())
stat7, p7 = ttest_ind(x7, y7)
print('Statistics = %.3f, p = %.3f' % (stat7, p7))
if p7 > alpha:
    print('Same distributions')
else:
    print('different distributions')

y8 = df2['Condenser Water Inlet Temperature']
x8 = df2['Suction Temperature Uncertainty']
model8 = sm.OLS(x8, y8).fit()
predictions8 = model8.predict(x8)
print(model8.summary())

y11 = df2['Subcooling']
x11 = df2['Suction Pressure Uncertainty']
model11 = sm.OLS(x11, y11).fit()
predictions11 = model11.predict(x11)
```

```
print(model11.summary())

y12 = df2['Subcooling']
x12 = df2['Discharge Pressure Uncertainty']
model12 = sm.OLS(x12, y12).fit()
predictions12 = model12.predict(x12)
print(model12.summary())

y13 = df2['Small Gas Expansion Valve Position']
x13 = df2['Suction Pressure Uncertainty']
model13 = sm.OLS(x13, y13).fit()
predictions13 = model13.predict(x13)
print(model13.summary())

y14 = df2['Small Gas Expansion Valve Position']
x14 = df2['Discharge Pressure Uncertainty']
model14 = sm.OLS(x14, y14).fit()
predictions14 = model14.predict(x14)
print(model14.summary())

y15 = df2['Small Liquid Expansion Valve Position']
x15 = df2['Suction Pressure Uncertainty']
model15 = sm.OLS(x15, y15).fit()
predictions15 = model15.predict(x15)
print(model15.summary())

y16 = df2['Small Liquid Expansion Valve Position']
x16 = df2['Discharge Pressure Uncertainty']
model16 = sm.OLS(x16, y16).fit()
predictions16 = model16.predict(x16)
print(model16.summary())

y17 = df2['Medium Gas Expansion Valve Position']
x17 = df2['Suction Pressure Uncertainty']
model17 = sm.OLS(x17, y17).fit()
predictions17 = model17.predict(x17)
print(model17.summary())

y18 = df2['Medium Gas Expansion Valve Position']
x18 = df2['Discharge Pressure Uncertainty']
model18 = sm.OLS(x18, y18).fit()
predictions18 = model18.predict(x18)
print(model18.summary())

y19 = df2['Medium Liquid Expansion Valve Position']
```

```
x19 = df2['Suction Pressure Uncertainty']
model19 = sm.OLS(x19, y19).fit()
predictions19 = model19.predict(x19)
print(model19.summary())

y20 = df2['Medium Liquid Expansion Valve Position']
x20 = df2['Discharge Pressure Uncertainty']
model20 = sm.OLS(x20, y20).fit()
predictions20 = model20.predict(x20)
print(model20.summary())
```

APPENDIX C

LabVIEW Code

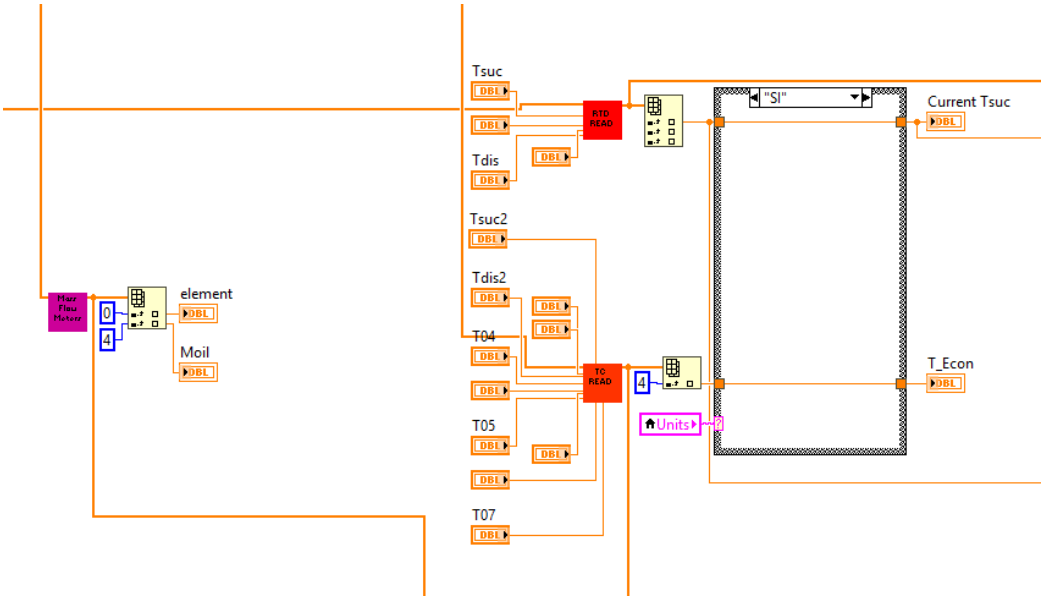

Figure C.1: Mass flow, thermocouple, and RTD blocks collecting raw data values

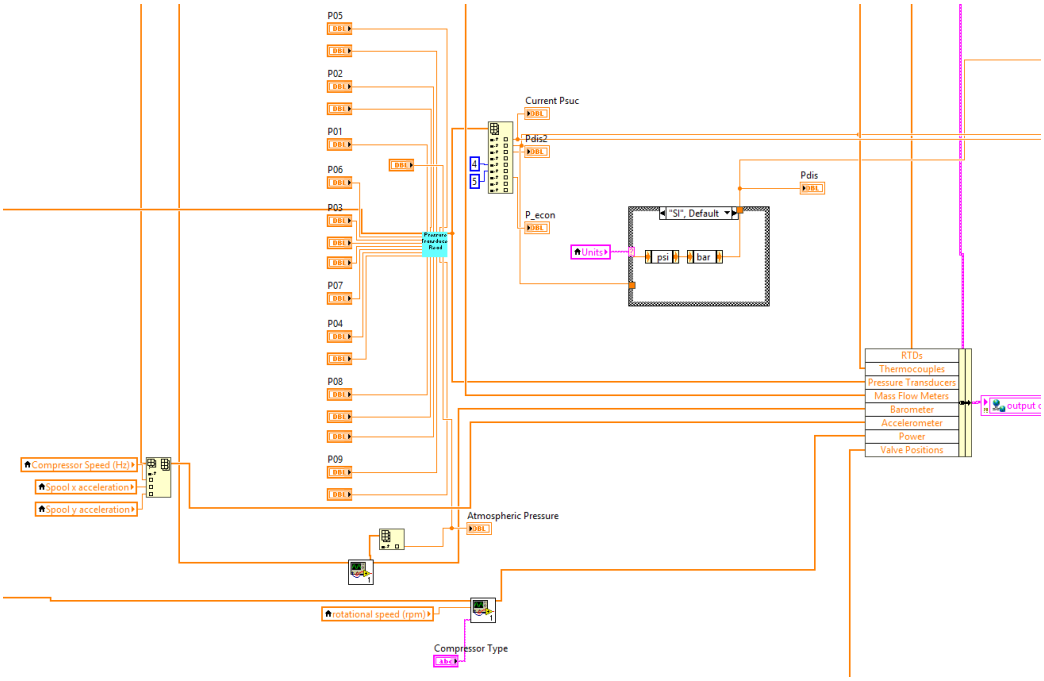

Figure C.2: Pressure transducer, barometer, power blocks reading raw data values

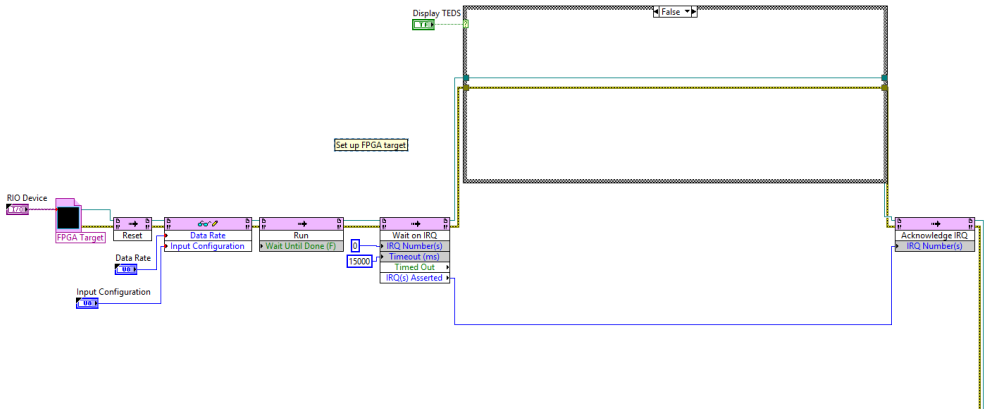

Figure C.3: Initialization of the FPGA target, which reads the accelerometer at a faster rate than the rest of the sensors

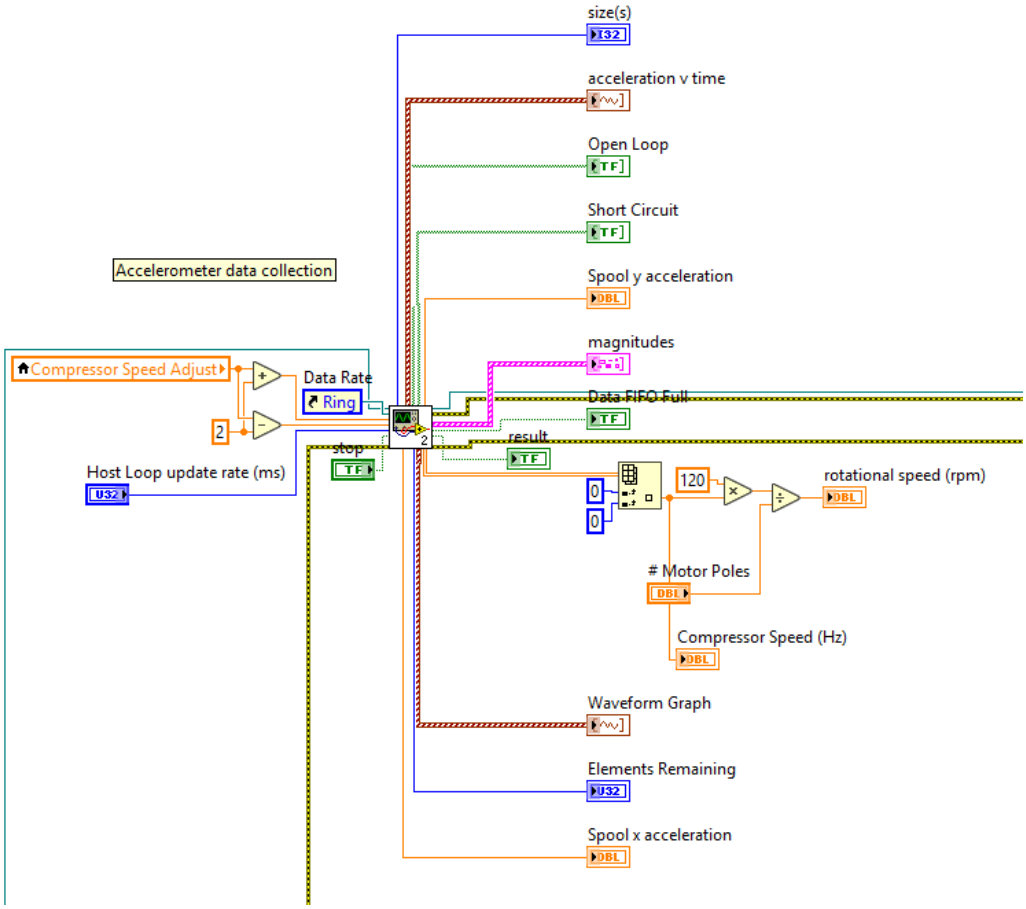

Figure C.4: Screen shot of VI that reads and outputs the accelerometer data

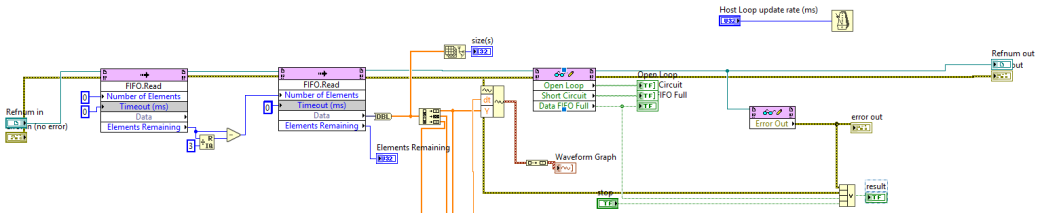

Figure C.5: Screenshot of the use of FIFOs (first in first out) to read the data that is captured by FPGA target

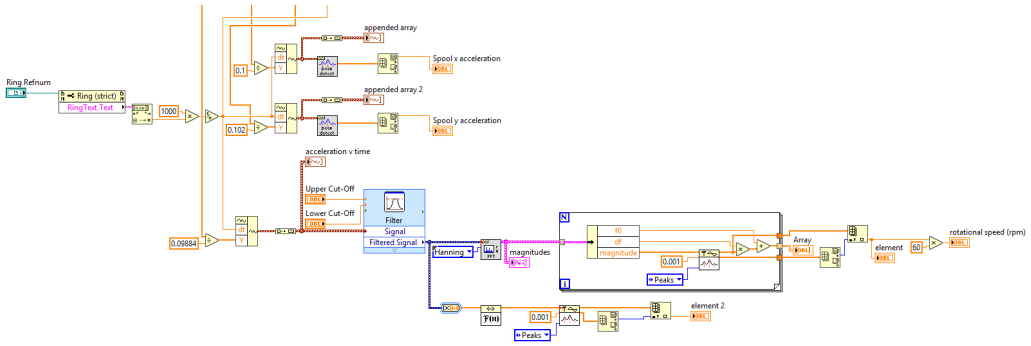

Figure C.6: Use of Fast Fourier Transforms to convert the accelerometer signal to frequency and rotational speed

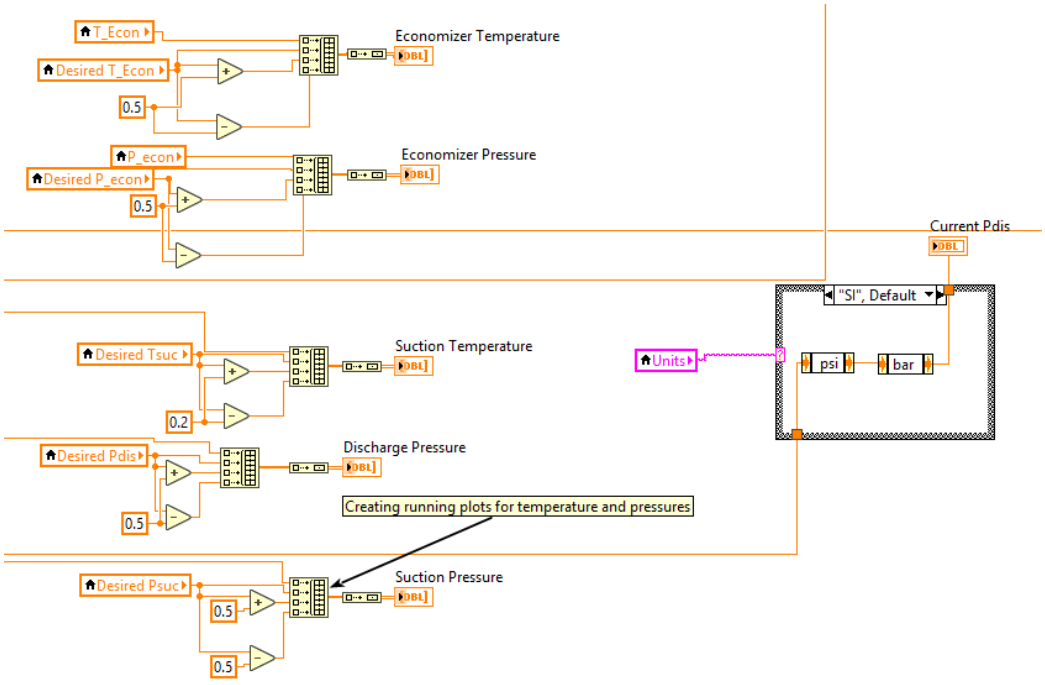

Figure C.7: Creation of running plots that are viewed on the Target VI

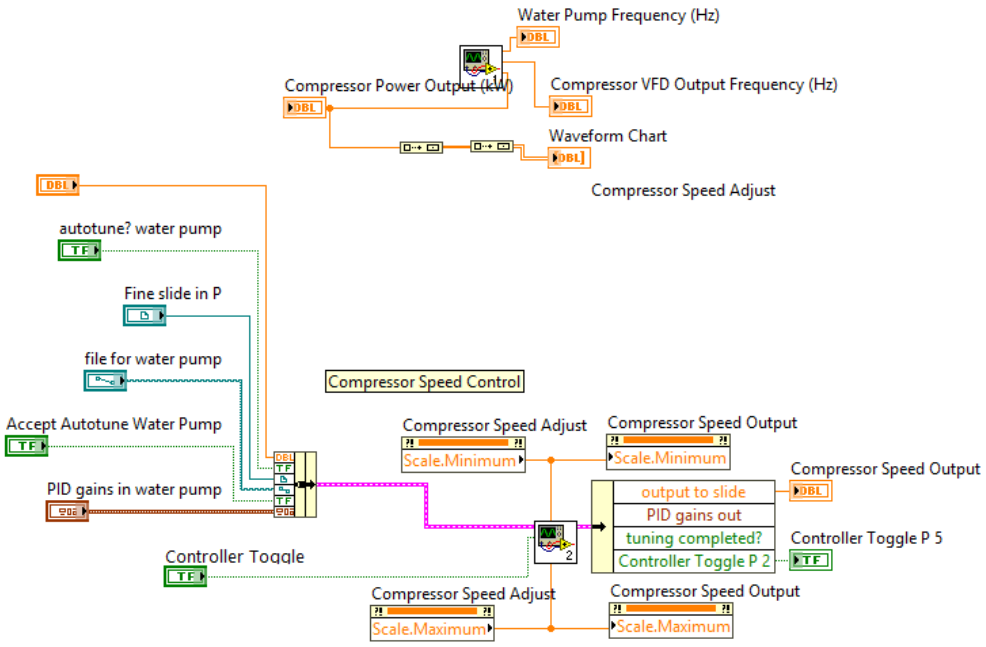

Figure C.8: Compressor speed adjust and VFD feedback blocks on Target VI

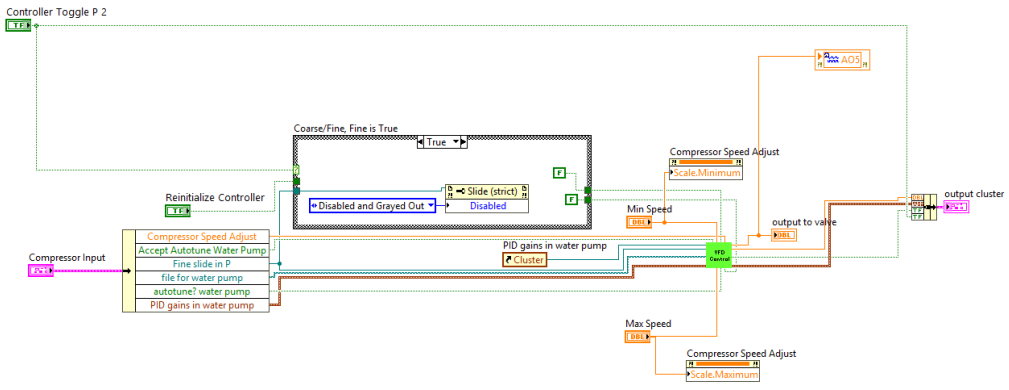

Figure C.9: VI which controls the compressor adjustment

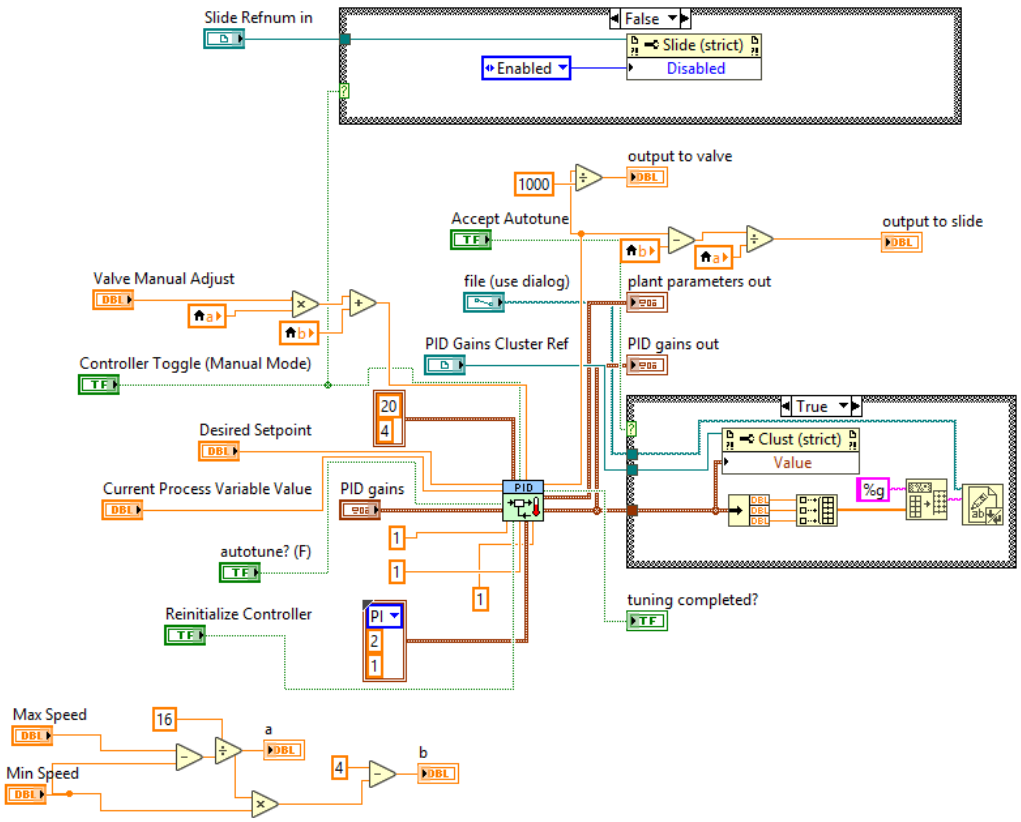

Figure C.10: Compressor VFD block which converts set speeds to output signals to the VFD

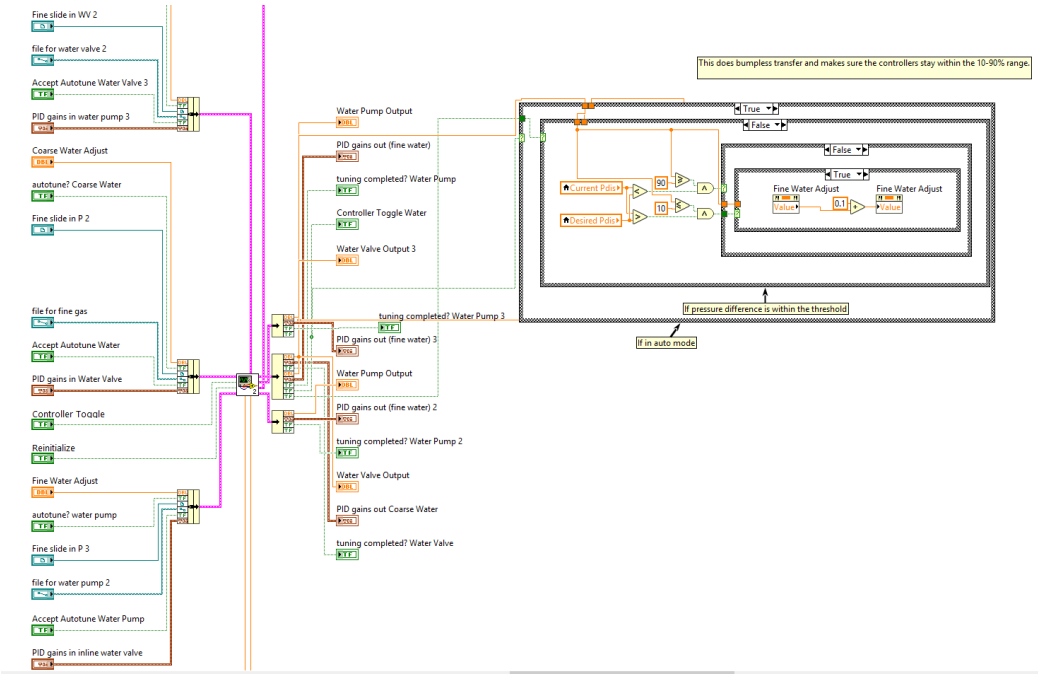

Figure C.11: Water control block showing inputs and outputs

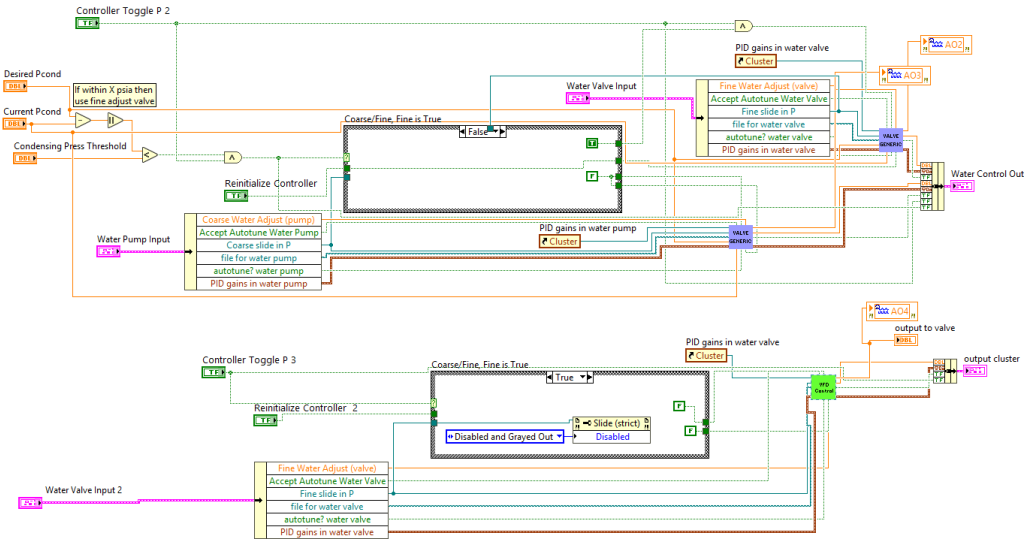

Figure C.12: Water valve selection block for automatic control

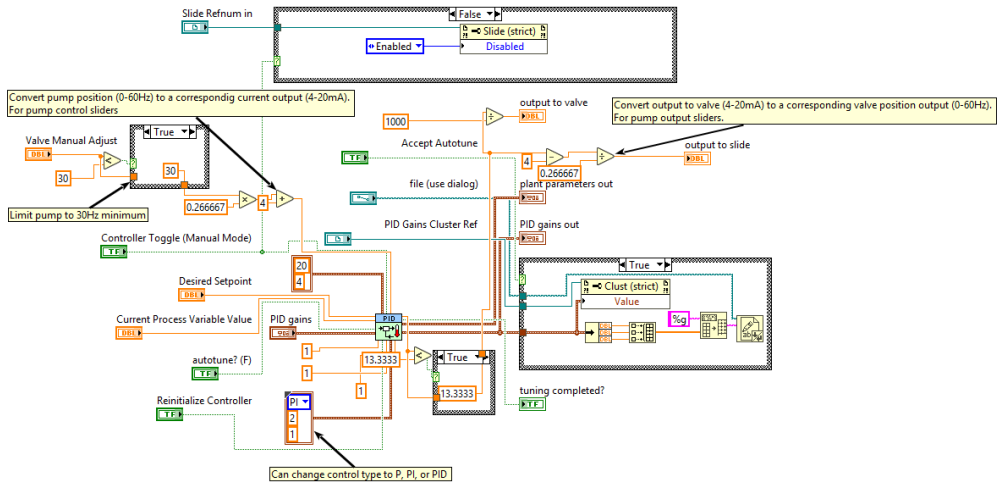

Figure C.13: Example of PID block for pump. Converts pump speed to a signal output

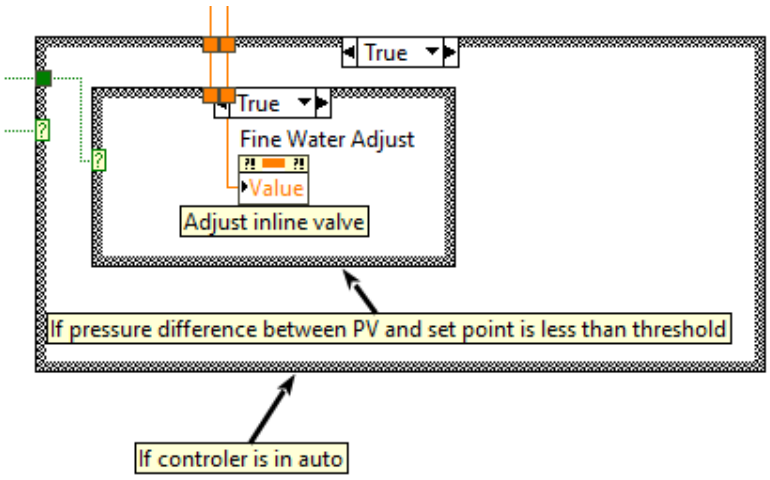

Figure C.14: Example of bumpless transfer on water line valves

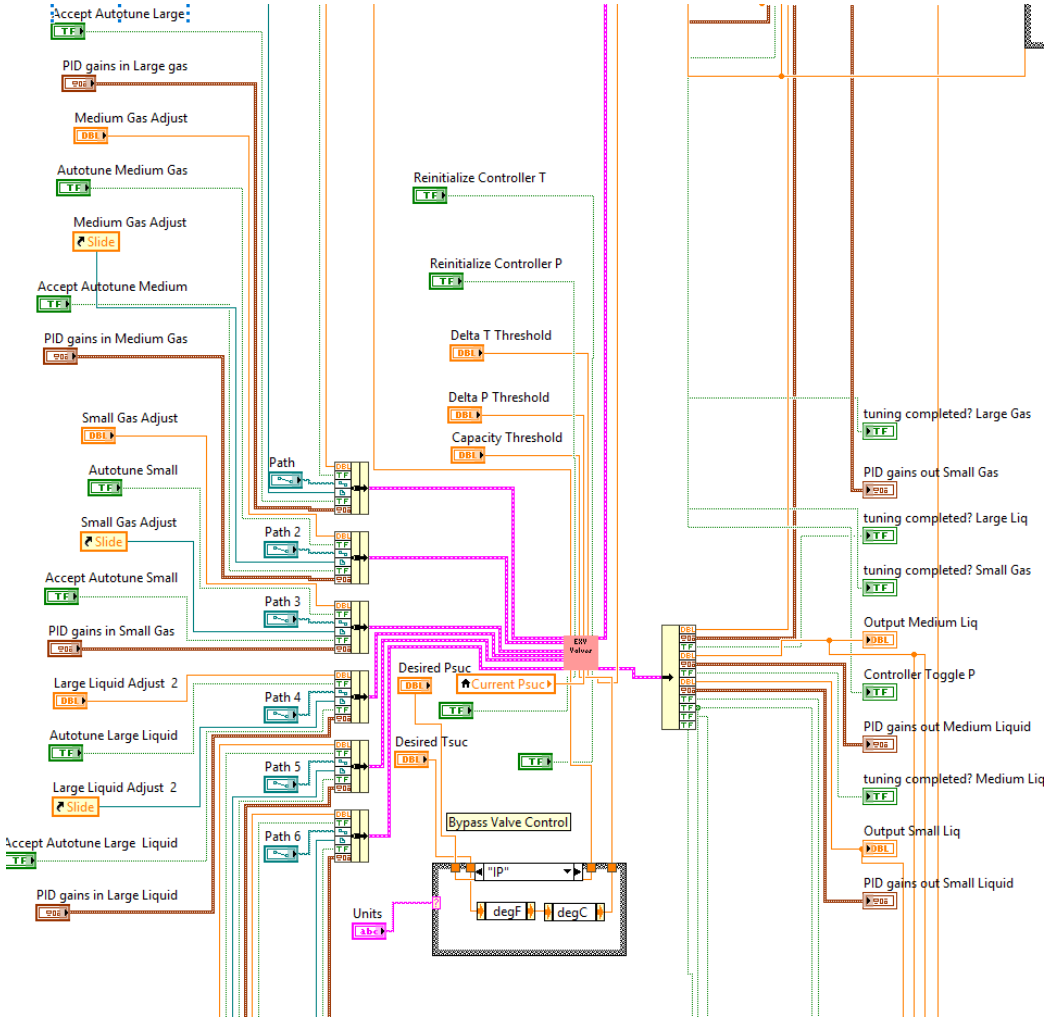

Figure C.15: Inputs and outputs of the suction temperature and pressure control block

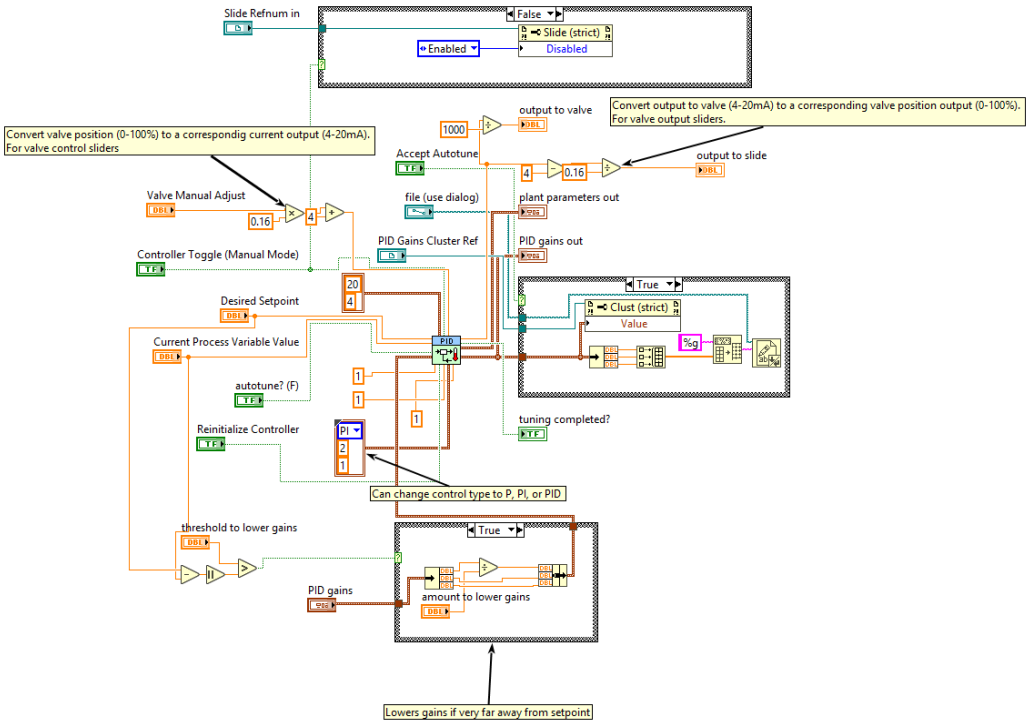

Figure C.16: Example of PID block used for valve. Coverts valve positions to an output signal

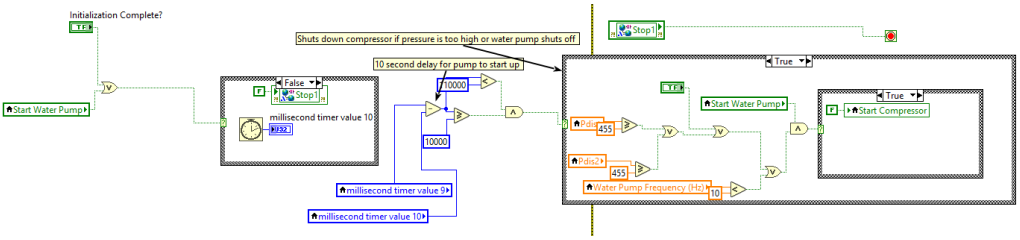

Figure C.17: Example of software shutdown implemented within LabVIEW

VITA

Jake M Singleton

Candidate for the Degree of

Master of Science

Thesis: Control and Commissioning of a Hot-Gas Bypass Compressor Load Stand for Testing Light-Commercial Compressors Using Low-GWP Refrigerants

Major Field: Mechanical Engineering

Biographical:

Education:

Received a Bachelors of Science in Mechanical Engineering at Oklahoma State University in May 2018.

Completed the requirements for the degree of Master of Science with a major in Mechanical Engineering at Oklahoma State University in July 2020.